

***NONLINEAR BEHAVIOR OF THE  
THERMO ACOUSTIC INSTABILITIES  
IN THE LIMOUSINE COMBUSTOR***

*Juan Carlos Román Casado*



NONLINEAR BEHAVIOR OF THE  
THERMOACOUSTIC INSTABILITIES IN THE  
LIMOUSINE COMBUSTOR

Juan Carlos Román Casado

# UNIVERSITY OF TWENTE.

*This research was financially supported by the European Commission in the Marie Curie Actions - Networks for Initial Training program, under call FP7-PEOPLE-2007-1-1-ITN, Project LIMOUSINE, with project number 214905.*

© Juan Carlos Roman Casado, Enschede, 2013

No part of this publication may be reproduced by print, photocopy or any other means without the permission of the copyright owner.

ISBN: 978-90-365-3554-0

DOI: 10.3990./1.9789036535540

Printed by: Ipskamp Drukkers, Enschede

Keywords: Thermo-acoustics, Combustion Instability, Limit cycle, Gas turbine, Frequency Doubling, Chaos Theory.

Revised 3<sup>rd</sup> June 2013

Cover: LIMOUSINE Flame combustor version 3 without the top liner.

NONLINEAR BEHAVIOR OF THE THERMOACOUSTIC  
INSTABILITIES IN THE LIMOUSINE COMBUSTOR

DISSERTATION

to obtain  
the degree of doctor at the University of Twente,  
on the authority of the rector magnificus,  
Prof. dr. H. Brinksma,  
on account of the decision of the graduation committee,  
to be publicly defended  
on Thursday 4<sup>th</sup> of July, 2013 at 14:45

by

Juan Carlos Román Casado

born on January 7<sup>th</sup>, 1984  
in Valladolid, Spain.

This dissertation has been approved by:

*The Promotor:* Prof. dr. ir. Th.H. van der Meer

*The Assistant Promotor:* Dr. ir. J.B.W. Kok



*Yoo!*

[

]

# Contents

Summary.....	xi
Introducción.....	xv
Samenvatting.....	xix
Publications.....	xxiii
Acknowledgments.....	xxv
Chapter 1 Introduction .....	1
Background.....	1
Lean Premixed Combustion.....	3
Thermoacoustics.....	4
Control of Thermoacoustics Instabilities.....	6
The LIMOUSINE Project and Thesis Objective.....	8
Thesis Outline .....	9
Chapter 2 Foundations of Thermoacoustics.....	11
Introduction.....	11
Acoustics.....	11
Combustion Noise & Combustion Instabilities.....	17
Chapter 3 Experimental Setup .....	23
Introduction.....	23
LIMOUSINE Version 1 .....	23
LIMOUSINE Version 2 .....	26
LIMOUSINE Version 3 .....	29
Auxiliary Equipment.....	31
Sensors.....	33
Data Acquisition System .....	37
Chapter 4 Limit Cycle Characterization.....	39
Introduction.....	39
Boundary Conditions & Acoustic Modes.....	39



Combustion Results .....	44
Structural Behavior .....	84
Emissions .....	87
Chapter 5 Non-linear effects and Chaos Analysis .....	89
Introduction to Bifurcation Analysis .....	89
Experimental Results .....	90
Non-linear Dynamics .....	95
Discussion .....	107
Chapter 6 Frequency Doubling .....	111
Introduction .....	111
Measured Results .....	112
Fitting Code Results .....	116
Discussion .....	119
Chapter 7 Coupling with the Structure .....	123
Introduction .....	123
Aero-Elastic Integration .....	123
Combustion Results .....	129
Wall Vibration .....	134
Discussion .....	136
Chapter 8 Conclusions .....	141
Observed Flame Instability Behavior .....	141
Final Remarks .....	145
Bibliography .....	147
Appendix A Semi-infinite hoses .....	A-1
Introduction .....	A-1
Proposed Design Changes .....	A-1
Appendix B Impedance Tube .....	B-1
Introduction .....	B-1
Appendix C Green's Function Approach .....	C-1
Introduction .....	C-1
Experimental Implementation .....	C-2

Results.....	C-4
Appendix D FSI In A Thin Liner Combustor .....	D-1
Introduction.....	D-1
Experimental Investigation.....	D-1
Results.....	D-2
Appendix E Measurement Accuracy .....	E-1
Introduction.....	E-1
Relative Calibration.....	E-1



# Summary

The topic of this dissertation are the large amplitude pressure perturbations which are sometimes observed in gas turbine burners and boilers. The pressure oscillations are the result of unstable feedback between the combustion process and pressure waves. The amplitude of these oscillations reach such large amplitudes that the oscillation is limited by non-linear phenomena. This phenomenon is known as Limit Cycle Oscillation (LCO) of pressure and has a negative impact on the technical lifetime of the gas turbine engine. The LCO effects include enhanced crack formation and propagation in the liner, increased heat transfer to the walls and higher emission of pollutants in the flue gases. As part of the project is LIMOUSINE research on various aspects of the Limit Cycle Oscillation by a multidisciplinary team of European researchers from different universities and research institutes. LIMOUSINE The project is funded by the European Commission under the Marie Curie FP7 Initial Training Network, grant agreement number 214905.

The root cause of the oscillations is the strengthening of the flame perturbations by the acoustic disturbances which propagate through the burner. The oscillations only show the feedback mechanism in closed burners, in which the surrounding walls enclose the acoustic waves around the flame. The knowledge of the relationship between the characteristic acoustic period of the flow and combustion reaction is critical to the determination of the instability conditions and growth rates. The fulfillment of the Rayleigh criterion is a necessary (but not sufficient) condition for the occurrence of the instability.

These dynamic phenomena have been studied empirically with the aid of laboratory scale atmospheric combustion setups specifically designed for this project. These combustion chambers have rectangular cross-section and they use a wedge-shaped "bluff body" to stabilize the flame. In some studies, the length of the combustion chamber may be modified with the addition of a second liner module. The burner uses methane as fuel and the thermal power ranges between 30 and 70 kW. For these operational parameters, the turbulent intensity of the flame conditions is low to medium. The burner could operate in three different regimes, depending on the fuel and air flows and combustion chamber length. The first regime shows stable combustion situation characterized by long and

quiet flames. The second regime is characterized by the occurrence of Limit Cycle Oscillations (LCO). The characteristic of this regime are the very large pressure fluctuations and a very compact flame. The third regime exhibits properties from the other two regimes.

The frequency of the LCO is related to the acoustic resonance frequency of the combustion chamber, as can be seen from the sensitivity of the Helmholtz and Strouhal dimensionless numbers. The observed pressure profile in the combustion chamber is of a quarter-wave shape with the maximum oscillating pressure at the inlet of the burner, and a node in the exhaust.

Versions 1 and 2 of the burner share the same burner design, with relatively wide passages around the wedge. The difference between version 1 and version 2 is that version 1 has flexible walls and version 2 has much more rigid walls. The stability of the combustion depends on the ratio of the acoustic period and the time scale of the convective transport, which for this particular kind of burners, matches in lean combustion conditions. The LIMOUSINE version 3 combustor has narrow passages around the bluff body instead, which lead to accelerated mixing of methane and air and stronger recirculation zones in the wake of the wedge. The unstable regime in version 3 was observed at air / fuel ratios that are in the vicinity of stoichiometric mixtures. In this case, the instability is attributed to the favorable ratio of the characteristic time of the recirculation zone, and the acoustic period.

One of the features of the limit cycle is the non-linearity of the signal. The pressure spectrum shows regularly spaced secondary peaks which do not match any of the acoustic modes. The origin of these dynamics lies on the temporal waveform, which resembles a saw tooth instead of a sinusoidal signal. In order to describe the signal nonlinearity, quadratic terms are added to the flame transfer function at limit cycle conditions.

The characteristics of the limit cycle were investigated with methods that rely on properties of non-linear systems, such as the fractal dimension. The dimension of the attractor in phase space of the measured time series for the pressure and the heat release rate is high (4 to 5) on the situation of stable combustion and drops to 3 at the limit cycle. However, the signal of the wall vibrations shows identical characteristics in both the stable and the unstable regime with an embedded dimension of 2. This happens in spite of the fact that the amplitude of the signal

during the LCO a full order of magnitude higher than the stable regime. These values may be used for the development of advanced burner control systems.

Last but not least, the interaction between wall vibration and combustion induced oscillations was examined. This was done in the version 1 of the LIMOUSINE combustor, which is wider and longer than the subsequent versions. The liner material is also thinner and therefore large vibration levels were recorded during the unstable combustion. The coupling of the two physical systems is visible in this situation. The pressure spectrum during unstable combustion can capture the natural frequencies of the liner wall. Simultaneously, the measured signal of the Laser Doppler Vibrometer shows the a response of the liner wall to the acoustic field frequencies.



# Introducción

El objetivo de esta tesis doctoral es el estudio de las oscilaciones de la presión en calderas y cámaras de combustión de las turbinas de gas. Las oscilaciones de presión son el resultado de la interacción entre el proceso de combustión y el campo acústico. La magnitud de las oscilaciones crece hasta que se alcanza un equilibrio con fenómenos no lineales. Este fenómeno, conocido como Ciclo Límite, tiene como principal consecuencia la reducción de la vida útil de los diferentes elementos de la turbina. Los efectos del Ciclo Límite incluyen un aumento de la formación y propagación de grietas en la estructura, un aumento de la transferencia de calor a las paredes y una mayor emisión de contaminantes en los gases de escape. Esta tesis se encuadra dentro del proyecto de investigación LIMOUSINE, financiado por la beca número 214905 de la Comisión Europea y la iniciativa Marie Curie Actions.

El origen de las perturbaciones está en la interacción entre la combustión y las ondas de presión en el interior del quemador. Las oscilaciones son sólo posibles en quemadores cerrados, en los cuales las paredes que rodean a la llama pueden contener el campo acústico. En este caso, la relación entre el período acústico y el tiempo característico de la combustión es fundamental para la determinar las condiciones de inestabilidad y la tasa de crecimiento de la amplitud de la presión. El cumplimiento del criterio de Rayleigh es una condición necesaria (pero no suficiente) para la aparición de la inestabilidad.

Dichos fenómenos dinámicos han sido estudiados empíricamente con la ayuda de quemadores atmosféricos de pequeña escala diseñados específicamente para este proyecto. Los quemadores tienen sección transversal rectangular y utilizan un "cuerpo romo" en forma de cuña para estabilizar la llama. En ciertos casos, la longitud de la cámara de combustión puede ser modificada con la adición de un segundo módulo. El quemador utiliza gas metano como combustible, con una potencia variable entre 30 y 70 kW. En estas condiciones, la llama presenta niveles bajos o medios de turbulencia.

El quemador puede funcionar en tres regímenes diferentes, en función de los flujos de aire y combustible y la longitud de cámara de combustión. El primer régimen muestra una situación caracterizada por llamas largas y estables. El



segundo régimen se caracteriza por la presencia del ciclo límite de oscilaciones de la presión (CLO). Las características de este régimen incluyen grandes fluctuaciones periódicas en la presión y una llama compacta. El tercer régimen exhibe propiedades típicas de los otros dos regímenes.

La frecuencia de la CLO está relacionada con la frecuencia de resonancia acústica de la cámara de combustión, como se puede ver a partir de la evolución de los números adimensionales de Helmholtz y de Strouhal. El perfil de presión en la cámara de combustión se corresponde con un cuarto de onda. El máximo se sitúa en la entrada del quemador y existe un nodo en la sección de salida.

La primera y la segunda versión del quemador comparten el mismo diseño básico, con amplios pasajes alrededor del prisma triangular. La diferencia entre la versión número 1 y la número 2 es que las paredes de la versión 1 son más flexibles y las de la versión son más rígidas. La estabilidad de la combustión depende de la relación entre el período acústico y el retraso convectivo de la llama, que para este tipo de quemadores ocurre con mezclas de combustible y aire pobres.

La versión número 3 del quemador LIMOUSINE tiene pasajes estrechos alrededor de la cuña, que producen una aceleración de la mezcla y una zona de recirculación de mayor intensidad. En la versión 3, el régimen de combustión inestable aparece para mezclas de aire y combustible cercanas al valor estequiométrico. En este caso, la inestabilidad se debe a una relación adecuada entre tiempo característico de la zona de recirculación y el período acústico.

Una de las características del ciclo límite es la no linealidad de la señal. El espectro de la presión muestra picos secundarios regularmente espaciados que no coinciden con ninguno de los modos acústicos del sistema. El origen de dichas dinámicas se encuentra en la forma de onda, que se parece más a un diente de sierra que a una señal sinusoidal. Para describir la no linealidad de la señal, se han añadido términos cuadráticos a la función de transferencia de la llama en las condiciones de ciclo límite.

Las características del ciclo límite han sido investigadas con métodos que se basan en las propiedades de los sistemas no lineales, tales como la dimensión fractal. La dimensión del atractor en el espacio fásico para la presión y la tasa de liberación de calor es alta (valores de 4 a 5) en el régimen estable de combustión y cae a 3 para el Ciclo Límite. Sin embargo, las vibraciones estructurales de la pared

muestran las mismas características en los dos régimen, con una dimensión de empotrada de 2 y esto ocurre a pesar del hecho de que la amplitud de la señal durante el CLO sea un orden de magnitud mayor que durante el régimen estable. Dichos valores pueden ser usados para el desarrollo de sistemas avanzados de control.

Por último, pero no menos importante, se analiza la interacción entre la vibración de la pared y los oscilaciones de la combustión Esta investigación se llevó a cabo en la primera versión del quemador LIMOUSINE, que es más ancha y larga que las versiones posteriores. Las paredes de esta versión son también más delgadas y por lo tanto, se registraron los niveles de vibración grandes durante el Ciclo Límite. El acoplamiento entre la llama y la vibración estructural es posible en esta situación. El espectro de la presión durante la combustión inestable puede capturar las frecuencias naturales de la pared. Al mismo tiempo, la señal medida con el vibrómetro láser muestra la respuesta de la estructura a las frecuencias del campo acústicas.



# Samenvatting

Het onderwerp van dit proefschrift is de studie van druk oscillaties met hoge amplitude, zoals die kunnen worden waargenomen in gasturbine verbrandingskamers, branders en luchtkanalen. De druk oscillaties zijn het gevolg van een instabiele terugkoppeling tussen het verbrandingsproces en drukgolven, waarbij de amplitude is gegroeid tot zulke hoge waarden, dat de oscillatie begrensd is door niet-lineaire verschijnselen. Dit fenomeen staat bekend als Limit Cycle Oscillation (LCO) van de druk en heeft een negatieve invloed op de technische levensduur van de gas turbine motor. De LCO kan leiden tot versnelde scheurgroei en scheurvoortplanting in de liner, verhoogde warmteoverdracht naar de wanden en hogere emissies van verontreinigende stoffen in de rookgassen. In het kader van het project LIMOUSINE is onderzoek verricht aan verschillende aspecten van de Limit Cycle Oscillation door een multidisciplinair team van Europese onderzoekers van verschillende universiteiten en onderzoeksinstituten. Het LIMOUSINE project is gefinancierd door de Europese Commissie in het kader van het Marie Curie FP7 Training Network, grant agreement number 214905.

De oorzaak van de druk en verbrandingsoscillaties is de (versterking van de) geluidsproductie door een vlam en de gevoeligheid van een vlam voor akoestische verstoringen die zich door de brander voortplanten. De oscillaties vertonen alleen terugkoppelingsverschijnselen in akoestisch gesloten branders, waarbij de omringende wanden de akoestische golven opsluiten rond de vlam. Kennis van de relaties tussen de karakteristieke tijdschalen van de akoestiek, stromingsdynamica en verbrandingsverschijnselen is cruciaal voor de bepaling van de condities van instabiliteit en groeisnelheden van de instabiliteiten van het multifysische systeem. De vervulling van het Rayleigh criterium is een noodzakelijke (maar niet voldoende) voorwaarde voor het optreden van de instabiliteit.

Deze dynamische verschijnselen werden empirisch onderzocht met behulp van een aantal ontwerp variaties van een specifiek voor dit project ontworpen atmosferische verbrandingskamer op laboratoriumschaal. Drie verschillende ontwerpversies werden getest. Deze verbrandingskamers zijn cilindrisch met een rechthoekige doorsnede en ze gebruiken een wigvormige “bluff body” om de vlam te stabiliseren. In sommige studies werd de lengte van de

verbrandingskamer gewijzigd met de toevoeging van een tweede liner module. De brander gebruikt methaan als brandstof en het gebruikte thermische vermogen varieerde tussen 30 en 70 kW. Bij deze vermogens opereerde de vlam in een laag tot medium turbulente stromingstoestand. De brander kon in drie verschillende regimes opereren, afhankelijk van: de brandstof- en luchtdebieten en de verbrandingskamerlengte. Het eerste regime toont een stabiele verbranding gekenmerkt door lange vlammen en de afwezigheid van druk dynamiek. Het tweede regime is gekenmerkt door het optreden van Limit Cycle Oscillations (LCO). Hier treden zeer grote drukschommelingen op en de vlam is zeer compact. Het derde regime kan beide vorige situaties vertonen, afhankelijk van de operationele historie.

De frequentie van de LCO is gerelateerd aan de akoestische eigenfrequenties van de verbrandingskamer, zoals blijkt uit de gevoeligheid voor variaties van de Helmholtz en Strouhal getallen. Het waargenomen drukprofiel in de verbrandingskamer is een kwart golf van vorm met de maximale oscillerende druk bij de inlaat van de brander en een drukknop in de uitlaat.

Versies 1 en 2 van de brander hebben hetzelfde brander design, met relatief wijde passages rond de wig die de vlampositie stabiliseert. Het voornaamste verschil tussen versie 1 en 2 is dat versie 1 een flexibele wand heeft en versie 2 een zeer rigide wand. De stabiliteit van de verbranding is afhankelijk van de verhouding van de akoestische periode en de tijdschaal van het convectieve transport. De LIMOUSINE versie 3 heeft nauwere stromingspassages rond de wig, die leiden tot versnelde menging van methaan en lucht en sterkere recirculatie zones in het zog van de wig. Het instabiele regime wordt in versie 3 waargenomen bij lucht/brandstofverhoudingen die in de buurt komen van stoichiometrische mengsels. In dit geval wordt de instabiliteit verklaard door de gunstige verhouding van de karakteristieke tijd van de recirculatie-zone en de akoestieke periode.

Een van de kenmerken van de limiet cyclus is de niet-lineariteit van het signaal. Het drukspectrum toont op regelmatige afstanden secundaire pieken die niet overeenkomen met een van de akoestische modi. Deze pieken kunnen ook worden afgelezen uit de vorm van het tijdssignaal, wat op een zaagtand signaal lijkt. Om deze situatie te kunnen beschrijven met een overdrachtsfunctie, werden in een tijdsdomeinbeschrijving extra kwadratische termen toegevoegd aan de vlam transfer functie voor de respons op de limiet cyclus frequentie.

De kenmerken van de Limiet Cyclus werden onderzocht met methodieken die zich baseren op eigenschappen van niet-lineaire systemen, zoals de fractale dimensie. De dimensie in phase space van de attractor van de gemeten tijdseries voor de druk en de verbrandingssnelheid temporele is hoog (4 tot 5) voor de situatie van stabiele verbranding en daalt naar 3 tijdens de limiet cyclus. Echter, het signaal van de wand trillingen toont identieke eigenschappen tijdens zowel het stabiele en het instabiele regime met een ingebedde dimensie van 2. Dit gebeurt ondanks het feit dat de amplitude van het signaal gedurende de LCO een volledige orde van grootte hoger. Deze waarden kunnen worden gebruikt voor de ontwikkeling van geavanceerde branderbesturingssystemen.

Naast de stroming werden in het onderzoek ook de interactie tussen de wand trillingen en de verbranding onderzocht. Dit werd met name gedaan in de versie 1 brander, die breder en langer was dan de volgende versies. Het liner materiaal is ook dunner en daardoor werden grote vibraties geregistreerd tijdens de instabiele verbranding. De koppeling van de beide fysische systemen is zichtbaar in deze situatie. Het druk spectrum kan bij instabiele verbranding een respons vertonen op de natuurlijke frequenties van de liner wand. Omgekeerd, het gemeten signaal van de Laser Doppler Vibrometer toont de druk dynamiek als scherpe pieken die boven de achtergrondruis uitkomen.



# Publications

- [1] Roman Casado, J. C., Alemela, P. R., and Kok, J. B. W., 2010 "Combustion dynamics coupled to structural vibration," ICSV Cairo.
- [2] Roman Casado, J. C., Alemela, P. R., and Kok, J. B. W., 2011, "Experimental and numerical study of the effect of acoustic time delays on combustion stability " ICSV Rio de Janeiro.
- [3] Roman Casado, J. C., and Kok, J. B. W., 2012, "Flame describing function measurements for limit cycle characterization," ICSV Vilnius.
- [4] Roman Casado, J. C., and Kok, J. B. W., 2012, "Non-Linear Effects in a Lean Partially Premixed Combustor During Limit Cycle Operation " ASME Turbo ExpoCopenhagen.
- [5] Roman Casado, J. C., Tufano, S., Stopford, P., and Kok, J. B. W., 2012, "Modelling Flame-Generated Noise in a Partially Premixed, Bluff Body Stabilized Model Combustor " ASME Turbo ExpoCopenhagen.
- [6] Hernández, I., Staffelbach, G., Poinsot, T., Román Casado, J. C., and Kok, J. B. W., 2013, "LES and acoustic analysis of thermo-acoustic instabilities in a partially premixed model combustor," *Comptes Rendus Mecanique*, 341(1–2), pp. 121-130.
- [7] Alemela, P., Casado, J., Kumar, S., and Kok, J., 2013, "Thermoacoustic analysis of the dynamic pressure inside a model combustor during limit cycle oscillations," *International Journal of Spray and Combustion Dynamics*, 5(1), pp. 25-48
- [8] Shahi, M., Kok, J. B. W., Roman Casado, J. C., and Sponfeldner, T., 2013, "Sensitivity of the numerical prediction of flow in the LIMOUSINE combustor on the chosen mesh and turbulent combustion model," ASME Turbo ExpoSan Antonio, TX.
- [9] Roman Casado, J. C., and Kok, J. B. W. Linear, nonlinear and chaotic observed behaviour during combustion. In preparation.
- [10] Flame and structure interaction in a thin liner combustor during unstable combustion. In preparation.
- [11] Frequency doubling during limit cycle of pressure oscillation. In preparation.





# Acknowledgments

In the first place I want to thank my advisor Jim Kok for offering to me the opportunity to work in the University of Twente and in the LIMOUSINE project. I do believe that I could not have made it without his help and dedication. Of course, Jim was not alone. I have always counted with Genie for advice and support with the laboratory equipment and Arthur to answer my questions. Working for the ThW group has been a pleasure. As chair of the department, Theo leads a dynamic group and has created a working atmosphere that encourages collaboration between all the members. On the one hand there are the people working in combustion, thermoacoustics or heat transfer: Anton Verbeek, Marc, Simon Bühler, Joris, Shang Long, Nikola, Uros and Taha; and on the hand there is the part of the department dedicated to future fuels, with Jerry, Jan, Nick, Lixian, Miladin, Joost, Eddy and Gerrit. I appreciate the interaction with the COPA-GT fellows Simon and Virginia, and my best wishes in their path to their doctoral degree. I must include a special mention to Sally and Ceciel, that were the best secretaries one can ask for.

The other LIMOUSINE fellows have been a very important part of the project. In France, Ignacio and Basti. In the UK, Patrick, Bela, Sebastian and Thomas. Germany was base for Harmen, Roel, Simone and Antonio. I have to include Lukas (Czech Republic), Salvo (Belgium) and Sebastian Lipari (Spain). I will always remember the workshops and dinners shared in Enschede, Toulouse, Keele, Munich, Zaragoza, Brno, London and Stuttgart and I hope to cross roads again with you in the future.

I also thank Bert and Axel from the TM department. With their help, the research done in PhD can be truly consider multiphysics.

The University of Twente also gave me two activities to relax from everyday research. The first one is climbing. Thanks to TSAC and its members, I discover the pleasure of rock climbing in a country with no mountains. The second one is P-NUT, the PhD Network of the University of Twente. I am happy and proud to witness how P-NUT transformed from a small and informal association to a professional organization with more than 180 PhD members. But I am happier to had done it with Bjorn, Amiee, Sergio, Josine, Shashank, Raja, Giovane, Nicole,

Bijoy, Juan, Victor, Silja (as VP), Rong, Jonathan, Rense, Joana, Anja, Mihaela, Janne, Adithya, Burcu, Febriyani, Nana and Mohammadreza. My work as P-NUT treasurer was much easier thanks to my predecessor Sergio, my colleague Harmen and my successor David. It was a pleasure to be involved with people that want to make a difference.

La gente de España ha sido y es una parte imprescindible de esta tesis doctoral: Myriam, Cristina, Nacho, Javier, Estela, Rebeca, Esmeralda, Sergio y Susana, Miguel Peña y Carles. Todos ellos están presentes aquí conmigo, aunque vivan lejos. No me olvido de Alberto (ni de su esposa Zhutian), que tiene parte de culpa de que empezara mi segunda aventura fuera de España.

For these four years, Enschede has been home to a collection of people that made me feel like never before. My home mates at Macandra, Roberto, Xiao, Alessandro, Andrea, Hasti and Joel, Desi, Roland, Laura, Cristina, Edit, Damla, Trajce and Paula. Other notable inhabitants of Enschede included Peter, my guitar teacher Pablo and Olga.

My officemates have been the persons I have spent the largest amount of time of the PhD with. Thanks to Winnie and Anne, Riza and Anton Bijl. They have made a pleasure going to work every morning. I have important words for the LIMOUSINE project members at Twente. Without the constant discussion and knowledge exchange between us, the LIMOUSINE combustor behavior would have remained unexplained. Reddy for his wise guidance, Can with his distinctive approach from outside the combustion science side and Santosh and Mina for all the time shared in the office and away. I have enjoyed every second.

Y gracias a toda mi familia en Valladolid: mis padres, mis tíos y mis abuelos. Desde que se inventó el Skype, es casi como si nunca me hubiera ido.

I have appreciated all the time I had with Mirjam and her family in Enschede. Definitely, one of the best things ever happened to me. My last words are for my two paranymphs, which are the supports I have used to assemble this book. Thanks Mehmet for enlighten me in so many occasions and thanks Yuri for making me a wiser man.

# Chapter 1 Introduction

## Background

Gas turbines are efficient machines for the production of mechanical power and electricity. They are often used in the range between 20 and 200 MWe and they are the most common engine of airplanes and helicopters. Nowadays, turbine engines can power naval ships or some land vehicles. With the development of mini and micro gas turbine technology, they also have become a solution for combined heat and power of households [1]. Turbine engines offer multiple advantages, such as fuel flexibility, low maintenance requirements and high specific power. The waste heat in the exhaust gases is at high temperature, which allows the combination of the gas turbine engine with steam turbines to increase the joint efficiency of the system above 60% [2].

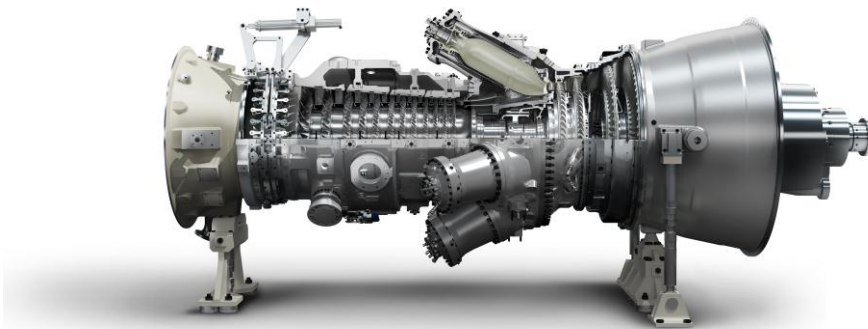


**Figure 1-1: Siemens SGT-750 Gas turbine<sup>1</sup>.**

As an example of a turbine engine, the model SGT-750 from Siemens Energy is shown in figure 1-1. The air pressure is increased in an axial compressor. Next, the air is mixed with fuel and burnt in the combustion chambers. Finally, mechanical work is extracted in the turbine blades from the exhaust gases. Therefore, the working fluid follows a 3 steps open Brayton cycle. The extracted energy is used to drive the air compressor and the electric generator.

---

<sup>1</sup> Copyright Siemens AG. Used with permission.

Due to increased awareness of the public opinion on environmental issues, the amount of pollutant species in the flue gases is strictly limited by law. In the case of The Netherlands, the emissions from combustion installations are regulated by the '*Besluit emissie-eisen stookinstallaties milieubeheer A*' act, which is the dutch implementation of the European Directive for Large Combustion Plants (2001/80/EC) [3]. It regulates the emission in the fume gases of NOX, SO<sub>2</sub>, ammonia and volatile hydrocarbons, which cause damage to vegetation, reduction of bio-diversity and damage to materials, artworks and monuments. In addition, the pollutants have harmful effects on human health due to fine dust and ozone formation. Measured levels of NOX in the flue gases (at 3% O<sub>2</sub>) must be lower than 75 mg/Nm<sup>3</sup> for gas turbines that use natural gas in combined cycle power plants. However, other countries or regions may establish more severe limits.

Until the flame temperature reaches 1500 °C, NOX emissions are not significant. Once this threshold is surpassed, any further rise in temperature causes a quick increase in the thermal NOX formation rate due to the Zeldovich mechanism. During the years, a variety of solutions have been developed to avoid hot spots and reduce the maximum flame temperature.

Injection of water or steam into the combustion chamber was one of the early solutions. The thermal inertia of the steam drastically reduces the flame temperature at the cost of increased engine complexity and expensive water consumption. The introduction of the can and the annular combustor design, that replaced the previous silo combustor models, reduced the amount of cooling and leakage flow and enabled the possibility of smart air management and lean combustion. The elimination of the diffusion pilot flame, intended to stabilize the flame, further helped to reduce locally high temperature. Finally, premixing the air and fuel streams before they enter combustion chamber prevented the formation of hot spots. However, lean premixed flames are prone to the development of unstable combustion and to the rise of high amplitude pressure perturbations (for example, figure 1-2). As consequence of the increased solicitations, cracks and structural damage will appear in the liner elements or the transition pieces [4-6]. Engines that develop unstable combustion suffer of shorter overhaul intervals, have higher operative costs and they may fail catastrophically.

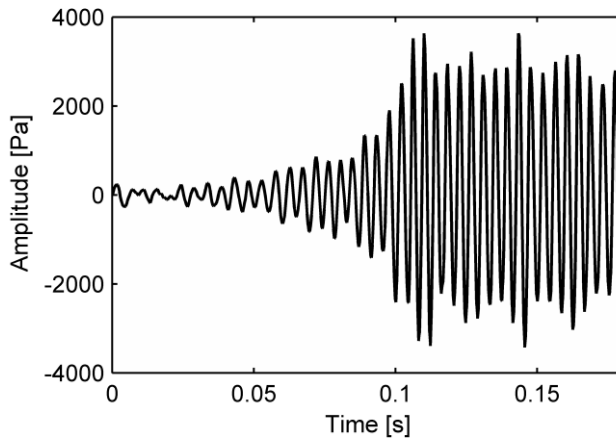


**Figure 1-2: Measured development of pressure Limit Cycle Oscillations in a laboratory scale combustor.**

## Lean Premixed Combustion

The combustion reaction may be classified based on whether the fuel and air are mixed before they enter the combustion chamber or if they are mixed in the flame itself. In premixed combustion, the flame front propagates into the coming stream of reactants. This makes these flames dangerous, because the flame front can travel upstream into the swirling vanes and other parts of the engine that are not designed to bear high temperatures. To achieve a perfect mixture, large residence times and volumes are necessary, which can burn explosively. Thus, due to safety reasons, perfectly premixed combustion is not common in industrial machines and limits the application of this concept to research combustors. Gas turbine manufacturers use a partially premixed approach instead, in which fuel and air are right mixed before the combustion chamber. The result is a uniform mixture with small variations in the air to fuel equivalence ratio  $\lambda$ . The premixed flames have long response times, since the fluctuations are related to the convective speed of the flame. This is the reason because premixed flames are likely to couple with the low frequency acoustic eigenfrequencies of the combustion chamber.

On the contrary, transport and mixing processes are simultaneous in diffusion type flames. Due to the limited available time from the injection until the start of combustion, the air to fuel ratio is not uniform and can range from very poor to

very rich mixtures. These local rich and hot spots are the source NOX production. Diffusion flames do not show unstable behavior, because the time delays within the flame are small and the high temperatures have a stabilizing effect.

## Thermoacoustics

Music, sound, speech and noise are all transient perturbations of the air pressure above and below the mean atmospheric value and can be perceived by humans with the hearing sense. Usually known as sound waves, they travel through physical media transporting energy without net transfer of mass, by means of particle-to-particle interaction. In the wave, as one fluid particle is displaced from its equilibrium position, it applies a push or a pull on its nearest neighbors and creates successive locations of compression and rarefaction. This particle interaction continues in all directions throughout the entire medium. The amplitude range of the acoustic waves is very large. The hearing threshold for a healthy young human is  $2 \cdot 10^{-6}$  Pascal while the amplitude of the noise from a jet engine exhaust 30 meters away rises up to 200 Pascal [7] (8 orders of magnitude!). Even in this last example, the amplitude of the waves is smaller than the 101325 Pascal of the mean atmospheric pressure. In the jet exhaust example, the maximum velocity at which the fluid particles vibrate is around 0.4 meter per second, which is more than enough to interact with other kind of fluid perturbations.

The interaction between combustion and acoustic waves has been reported for more than 160 years. For example, the LeConte described in 1858 how the musical tones from different instruments provoked changes in the height of the flames lighting the room. In his own words, '*a deaf man might have seen the harmony*' [8]. During the 19<sup>th</sup> century, further research in thermoacoustics was carried out. In 1850 Sondhauss studied the sound heard by glass workers while they blew molten glass bulbs at the end of narrow tubes [9, 10]. Almost one century later it was discovered that hollow tubes with one end chilled to cryogenic temperatures also produce a similar sound [11].

Contemporary to Sondhauss, professor Rijke of the University of Leiden in The Netherlands studied what would become the most typical example of a thermoacoustic experiment: the Rijke tube, sketched in figure 1-3. It consists of a vertical open tube that has a heating element in its interior [6, 12]. As long as the

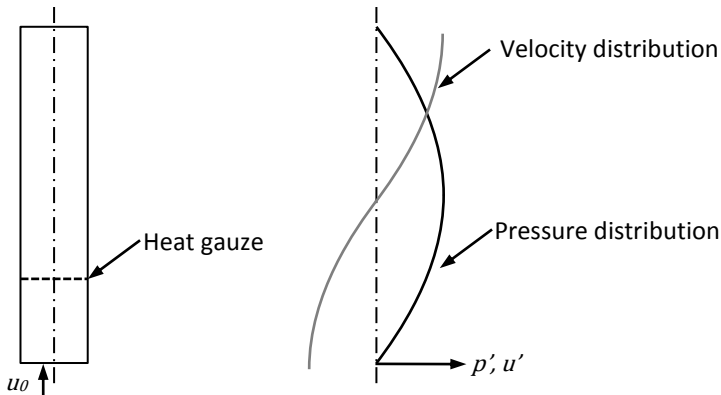


**Figure 1-3: Rijke Tube.**

gauze is placed in the bottom half of the pipe, the tube emits a very loud sound after the heating is switched off.

The heat source of a Rijke tube is wire gauze, which is heated with a candle or by an electric current. If the gauze temperature is high enough, it is possible to maintain standing pressure waves inside the pipe. The instability in the Rijke tube requires the presence of a mean flow through the pipe, which can be either natural convection in vertical tubes or forced flow. The frequency of the sound is related to one of the acoustic eigenmodes of the tube.

The instability driving mechanism lies in the unsteadiness of the heat transfer from and to the gauze [13]. During the first half of the perturbation cycle, the combined effect of the mean flow and the acoustic velocity pushes the cold gases through the wire mesh, where they are heated. The hot gases expand and change their density, becoming an acoustic source. For the remaining half cycle, the acoustic velocity is reversed, and the previously heated gases travel upstream into the mesh. The smaller temperature difference during this half period reduces the effective heat transfer to the fluid and cools the fluid parcel on top of the gauze.

The phenomenon was explained by Lord Rayleigh [14], which states that the amplitude of the perturbation will increase as long as the acoustic pressure and the heat release are in phase and the amount of energy in the acoustic field is sufficient to overcome the losses. Thermoacoustics oscillations have been observed in other devices, like ramjets, rocket engines [15, 16], furnaces [17] and of course, gas turbines combustor [4, 18, 19].



## Control of Thermoacoustics Instabilities

The goal of the gas turbine designer is to avoid the dangerous effects of the thermoacoustic instabilities in the hardware and to develop the most reliable machine possible. Fortunately, they have some of tools in its arsenal to address this problem. The best way to avoid the negative effects of the thermo acoustic oscillations is to prevent their appearance in the first place. Designers can use mathematical models of the thermoacoustic instability and scaling rules to predict the presence and characteristics of the unstable combustion. With this rules at hand, the designer can start an iterative design process until a stable combustor is produced.

The different describing models have different origins. One possible option are models built from empirical data. Large scale test of turbine engines is very expensive, complex and time consuming, so the data availability is very limited and often restricted or classified. The compressor, combustion chamber and turbine are tested separately during their development and complete units are only tested during the commissioning phase. On the contrary, the characterization of small or medium scale laboratory flames is much simpler. Therefore, most of the flame models for industrial burners are based in analytical or numerical calculations.

Nowadays, the most common modeling approach uses the combination of a 1D acoustic elements network that represents the burner geometry and a flame model [20, 21] to represent the combustion with simple equations. The frequency and other oscillation characteristics are predicted from the solution of the model equations, using the Finite Element Method (FEM) or an analytical approach. Either way, these kind of problems can be solved within minutes on a personal computer.

### Flame Models

Numerical flame models can be classified by accuracy or by computational cost. Better representations of the flame can be achieved with increasingly larger computer calculation time, so it is important to choose the optimal solution for the particular case under study.

The most computationally expensive models are based on the direct numerical simulation (DNS) of the conservation and energy equations in the combustor

volume. These equations are usually complex and must be solved in fine grids, which results in considerable numerical efforts. With state of the art clusters of supercomputers, laboratory test cases can be solved [22] but full size industrial turbine combustors are way too large to simulate.

By simplifying some of the terms in the governing equations, less expensive models can be realized, such as Large Eddy Simulations or LES. The large structures of the flow are solved directly with the equations, but smaller (and more expensive to solve) scales rely on approximations. This approach requires coarser meshes and it is considerably faster than DNS. With large clusters of processors, the simulation of laboratory combustors or industrial burners is possible [23, 24]. This is one of the currently preferred methods by industry and academia alike.

The least expensive and least accurate method uses Reynolds Averaged Navier Stokes equations (RANS) of the fluid. The turbulence and chemistry are solved with a set of simplified terms and parameters, which results in the least CPU intensive method. RANS models offer less accuracy in the results, but after experimental validation of a test case, they can be confidently used in the design or the upgrade of combustors.

## Passive Solutions

With the gathered information from the models or the gas turbine operators experience, the burner and combustion chamber can be designed (or modified) to prevent the occurrence of instability at certain fixed frequencies. For example, Helmholtz resonators or cavities may be installed in the combustor to damp specific flame dynamics. Passive control systems are simple, cheap and robust, but they may not be sufficient to ensure stable combustion over all the operational conditions [25-29].

A different kind of passive solutions use the tuning of the air or fuel flows to change the characteristic times associated with the flame and prevent the coupling with the acoustic field. A control strategy can be the modification of the location or the properties of the cooling holes and passages. In gas turbine engines with more than one fuel injection port, the flame characteristic delays can be modified with an uneven fuel distribution over the injectors.

## Active Systems

Active control systems use sensors, controllers and actuators in a closed or open control loop to prevent the growth of the instability amplitude. The sensor usually measures the instantaneous pressure of the combustion chamber and sends a signal to the controller. The controller operates an actuator, which typically modulates the fuel flow, to break the feedback loop. Gas turbine manufacturers do not favor active control systems in their engines because of their complexity, cost and risk of damage in the event of failure [30-36].

## The LIMOUSINE Project and Thesis Objective

The previous sections showed that the path to clean combustion needs the concurrent effort of scientists and engineers from different fields. The LIMOUSINE<sup>2</sup> project is an initiative of the European Commission to strengthen the fundamental scientific work in the field of thermo-acoustic instabilities in combustion systems. The network comprises 12 partner institutions across Europe that focus on a variety of fields such as mathematics, computational modeling, structural mechanics, acoustics, fluid mechanics, experimental combustion techniques, material science and control systems theory. The exchange of knowledge between the fellows was achieved by a program of meetings, courses, workshops and internships.

The work presented in this dissertation is based on one particular work package (3.1) of the LIMOUSINE project. The scope of the research is the development and characterization of a generic combustor in which thermo acoustic instabilities may occur. For this research, not one but up to three different versions of the combustor were built. The LIMOUSINE combustor may seem different from industrial gas turbine burners, but the limit cycle phenomenon under study is essentially identical. The generated data can be used in the subsequent investigation of flame characteristics or validation of numerical models.

As pointed out in the thesis' title, the main focus lies on the analysis with non-linear tools of the pressure perturbations during limit cycle oscillation in a laboratory scale combustor (LIMOUSINE). The observed flame behavior is characterized with dimensionless parameters for a clear understating of the root cause of the perturbation. Afterwards, the consequences of these oscillations are

---

<sup>2</sup> LIMOUSINE: *Limit Cycles of Thermoacoustic Oscillations in gas turbine combustor. Marie Curie Initial Training Network under the Framework 7, project 214905.*

studied, with special attention to frequency doubling effects and the coupling of wall vibrations to the acoustic field. The understanding of these flame dynamics is necessary for the design of robust burners and control systems.

The thesis tries to address the following research questions.

From the flame dynamics: What are the characteristics of the limit cycle? What is the cause of the frequency doubling effect observed in the pressure spectra and where it comes from? What are the dynamics of the flame and what influence do they have in the implementation of control system?

From the structural point of view: Can the limit cycle oscillations couple with the natural vibration of the structural elements? What are the effects in the fluid flow and what are the effects in the life prediction of the material?

## **Thesis Outline**

The Introduction chapter is followed by the Foundations of Thermoacoustics chapter, where the most important concepts about acoustics and combustion are presented.

Chapter 3 describes the three versions of the LIMOUSINE combustor used during this research. This chapter also includes information about the used sensors, data acquisition systems and experimental techniques.

Chapter 4 describes the general results measured in the LIMOUSINE setup version 2 and version 3. It describes the observed flame regimes and their characteristics, such as amplitude and frequency of the oscillation.

Chapter 5 uses non-linear tools to characterize the Limit Cycle Oscillations.

Chapter 6 studies the observed non-linear frequency doubling effect, which leads to relatively large oscillations at multiple times the thermoacoustic instability frequency.

Chapter 7 of the dissertation explores Fluid Structure Interaction for large amplitude perturbations on the prototype LIMOUSINE version 1 combustor.



# Chapter 2 Foundations of Thermoacoustics

## Introduction

Thermoacoustic phenomena have received much attention from the scientific community in the last half century, proved by the large number of scientific journal articles, publications, and books on the topic. Thermoacoustic effects appear in a wide range of applications and includes refrigerators, Stirling engines [37], mixture separators and of course, combustion related devices. The aim of this present chapter is not to extensively review all the research on the field, but to provide to the reader the tools and the mathematical theory that will be used in the rest of the dissertation. This chapter is divided in two subsections. The first part covers the essential acoustics concepts and the second part introduces the basics of the combustion process from an acoustic point of view.

## Acoustics

The understanding of the acoustics field is key to predict the characteristics of the combustion induced instability, since they are closely linked together. The introduction chapter already pointed out that acoustic waves are the unsteady perturbations of the pressure  $p$  above and below the mean level. Usually, the amplitude of the perturbations is much smaller than the variable mean value. This allows splitting the variable into two components: a mean value ( $\bar{p}$ ), which is constant in time and space, and its fluctuation ( $p'$ ), as in equation (2.1).

$$p(\mathbf{x}, t) = \bar{p} + p'(\mathbf{x}, t) \quad (2.1)$$

The splitting approach is valid as long as the fluctuating amplitudes are small with respect to the mean value ( $p' \ll \bar{p}$ ) and the second order derivatives can be neglected. Evaluating the conservation laws for mass, momentum and energy and the equation of state of a fluid particle, it is possible to obtain the wave equation that describes the pressure field in a certain domain.

$$\frac{\partial^2 p'}{\partial t^2} - c^2 \frac{\partial^2 p'}{\partial x^2} = 0 \quad (2.2)$$

Equation (2.2) assumes a one-dimensional domain with a quiescent and homogenous medium [38]. In this case, the speed of sound  $c$  is only a function of the temperature  $T$ , the gas constant  $R$ , and the ratio of specific heats  $\gamma$  ( $c_p/c_v$ ).

$$c^2 = \gamma RT \quad (2.3)$$

The solution to equation (2.2) is the combination of two traveling waves  $F$  and  $G$  (2.4).

$$p' = A * F(x - ct) + B * G(x + ct) \quad (2.4)$$

These waves can adopt any waveform and both travel at the same speed of sound  $c$ . While the wave  $F$  travels in the direction of increasing  $x$  values, the wave  $G$  travels in the opposite direction. Values  $A$  and  $B$  are two (complex) constants that depend on the boundary conditions of the problem under study. Using the conservation of momentum, the relation between pressure and velocity fluctuations is described by equation (2.5).

$$\bar{\rho} \frac{\partial u'}{\partial t} + \frac{\partial p'}{\partial x} = 0 \quad (2.5)$$

With expressions (2.4) and (2.5), it is also possible to write the wave equation in terms of the acoustic velocity  $u'$  (see (2.6)). The expression describes the physical acoustic velocity of a fluid particle as it moves back and forth in the sound wave travel direction. Particle velocity should not be confused with the speed of the wave as it passes through the medium  $c$ .

$$u' = \frac{1}{\rho c} (A * F(x - ct) - B * G(x + ct)) \quad (2.6)$$

The specific acoustic impedance  $Z$  is defined by expression (2.7):

$$Z = \frac{p'}{u'} \quad (2.7)$$

Impedance is defined as the ratio between the fluctuations of pressure and particle velocity at a certain fluid location. Comparing equations (2.4) and (2.6), it follows  $Z = \bar{\rho}c$ . The presented solution of the wave equation can be extended to

account for the mean flow effects and dissipation at the boundaries. Interaction or coupling of the modes is a second-order phenomenon and therefore it is not considered in the linear regime.

## The Wave Equation in the Frequency Domain

The wave equation can also be expressed in the frequency domain by the application of mathematical manipulations and Laplace transformations. Assuming the harmonic time dependence  $e^{i\omega t} = \cos(\omega t) + i \sin(\omega t)$  and introducing the wave number  $k$  (2.8) for waves at frequency  $f$  [Hz].

$$k = \frac{\omega}{c} = \frac{2\pi f}{c} \quad (2.8)$$

The acoustic field can be described with equation (2.9):

$$\frac{\partial^2 p(\omega, x)}{\partial x^2} + k^2 p(\omega, x) = 0 \quad (2.9)$$

Equation (2.9) is a second order ordinary differential equation of only one independent variable ( $x$ ) instead of the two variables ( $x, t$ ) of a partial differential equation (2.2). The solution to the Helmholtz equation is once more a combination of two traveling waves in opposite directions. The equations (2.10) and (2.11) are the solution to the pressure and velocity fields respectively.

$$p' = e^{i\omega t} (p_A e^{-ikx} + p_B e^{ikx}) \quad (2.10)$$

$$u' = \frac{e^{i\omega t}}{\rho c} (p_A e^{-ikx} - p_B e^{ikx}) \quad (2.11)$$

The complex values  $p_A$  and  $p_B$  are often referred as *Riemann Invariants* and they depend on the boundary conditions of the problem.

## Acoustic Boundary Conditions

In acoustic problems, boundary conditions describe the response to an incoming acoustic wave when the wave reaches a discontinuity of the medium properties. Examples of discontinuities are temperature gradients (linked to the speed of sound  $c$ ), changes in the cross sectional area or interaction with rigid surfaces. Figure 2-1 shows how incoming wave  $p^+$  splits at the boundary into a reflected wave  $p^-$  and a transmitted wave  $p^{tr}$ . Mathematically, the discontinuity is



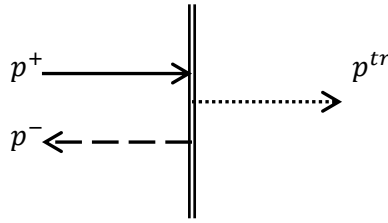


**Figure 2-1: Incoming wave (solid arrow), transmitted wave (dotted arrow) and reflected wave (slashed arrow) in at boundary of the acoustic domain.**

characterized by the complex reflection coefficient  $R$  and the transmission coefficient  $T$ . The coefficient  $R$  definition is the ratio between the reflected and the incoming sound wave amplitudes.

$$R = \frac{p^-}{p^+} \quad (2.12)$$

Similarly, the transmission coefficient  $T$  is the ratio between the transmitted wave and the incoming wave amplitude.

$$T = \frac{p^{tr}}{p^+} \quad (2.13)$$

And in a lossless transition, due to the conservation of energy.

$$R + T = 1 \quad (2.14)$$

Different boundary conditions result in different combinations of  $R$  and  $T$  values. However, there are three special conditions that are worth to describe.

### ***Open End ( $R = 1 \angle \pi$ , $T = 0$ )***

Open end termination or soft boundary condition is characterized by the presence of a pressure node at the boundary interface. Acoustic velocity is maximum in a open end termination. This conditions are found at the opening of cavities to an open larger space, for example the bell of musical instruments. The reflected wave has the same amplitude as the incoming one, but these two waves are out of phase.

### ***Perfect Match ( $R = 0, T = 1 \angle 0$ )***

In this case, the wave travels from the first medium to the second medium without any distortion or energy dissipation and no waves are reflected into the first medium.

### ***Closed End ( $R = 1 \angle 0, T = 0$ )***

The closed end condition is the opposite situation to the open end condition. It is characterized by a velocity node at the interface. The reflected wave has the same magnitude as the upcoming wave, but contrary to the open end termination, it does not show a phase shift. Closed end conditions are also called hard conditions, because this condition is characteristic of rigid surfaces.

## **Reflection Coefficient Determination**

There are a few experimental approaches to measure the reflection coefficient of the boundaries of the combustor, all of them based on the direct or indirect determination of the Riemann invariants. In the one dimensional case, there are two Riemann invariants and therefore two data points are needed. The proposed techniques to gather and process the data led to the derivation of a family of algorithms called the *Two Microphone Method* [39-41]. These algorithms are often applied in experimental devices named *Impedance Tubes*, which are rigid tubes with a speaker at one end and the sample of interest at the opposite end. The microphones measure the system response to the speaker sound and thereby, the reflection coefficient can be found. For more information about impedance tubes, check appendix B.

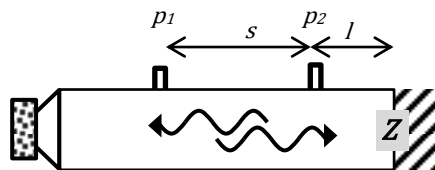


**Figure 2-2: Impedance tube.**

In this study, the followed approach was proposed by Munjal and Doige [42]. Instead of the absolute value of the pressure measurements, they used the relative (complex) pressure ratio between two microphones (2.15).

$$H_{21} = \frac{p_2}{p_1} \quad (2.15)$$

If mean flow and dissipation effects are neglected, the reflection coefficient  $R$  at one frequency  $\omega$  is obtained from equation (2.16). The results of the method are accurate as long as the sound field is 1 dimensional (dimension of the wavelength is larger than the transversal dimensions of the domain).

$$R(\omega) = \left\{ \frac{H_{21} - e^{-iks}}{e^{iks} - H_{21}} \right\} e^{2ikl} \quad (2.16)$$

The *Multi-Microphone Method* “MMM” [29, 43, 44] can be considered as the extension of the two microphone method. The method finds the complex amplitudes of the forward and backward traveling waves from the measured values of three (or more) microphones. In this case, the system of equations is overdetermined because the number of equations (3 or more) is larger than the number of unknowns (2) and cannot be solved by the application of traditional techniques. The Riemann invariants have to be calculated with optimization algorithms that search for the best fit of the predicted pressure field to the observed data.

## Acoustic Eigenmodes

The Helmholtz equation eigenmodes describe the resonance frequencies of a system. The oscillation amplitudes of an acoustic system can grow very quickly if the oscillating frequency matches with one of these modes. The eigenfrequencies and eigenmodes correspond to the eigenvalues and eigenvectors of the wave equation in matrix form  $A_{ij}$  with boundary conditions  $BC_i$ .

$$A_{ij}(\omega) \begin{pmatrix} p_i \\ u_i \end{pmatrix} = BC_i \quad (2.17)$$

Acoustic systems have an infinite number of resonances, but the modes with the lower frequency are the most interesting. The expression of the frequency of the successive eigenmodes can be calculated analytically for some simple geometry domains. The  $n^{th}$  resonance for the open-open and open-closed conditions in a 1D isothermal and quiescent domain of length  $L$  and speed of sound  $c$  adopt the familiar formulas in table 2-1.

**Table 2-1: Formulation of the eigenfrequencies for a 1D isothermal quiescent domain.**

OPEN-OPEN	OPEN-CLOSED
$f_n = n * \frac{c}{2L}$	$f_n = (2n - 1) * \frac{c}{4L}$
$n \in \mathbb{N}$	

In these two ideal situations, the resonances are located at constant intervals in the frequency domain. This is not the general behavior and the intervals between modes become irregular with geometry or speed of sound gradients. Two or more 1-dimensional elements can be linked to each other to describe the effects of the temperature or the area changes. Every extra element adds two more unknowns  $p_i$  and  $u_i$  to the network and increases the size of the matrix  $A_{ij}$  by four, but at the same time, two new boundary conditions ( $BC_i$ ) can be incorporated if the transport equations (mass and momentum) are evaluated at the joints. In these matrices, the search of the eigenfrequencies is done numerically.

## Combustion Noise & Combustion Instabilities

In gas turbine engines, fuel and pressurized air from the compressor are mixed and burnt in the combustion chamber. The reaction of the fuel molecules with the oxygen of the air produces heat, light emission, carbon dioxide and water. The released heat forces the flue gases to a fast and sudden expansion that results in the generation of powerful acoustic waves as well. The contained energy in the acoustic waves is only a small fraction of the flame thermal energy, around  $10^{-5}$  to  $10^{-8}$  of the rated engine power [19]. This sound is called ‘*combustion roar*’ and it is a broadband noise whose frequencies are usually located in the 100 to 2000 Hz range. In a 200 MW combustor, the sound pressure level of the roar is around 143 dB (reference SPL level  $10^{-12}$  Pa) [19, 45], but the roar itself is not a problem for the constructive elements as long as it does not couple with any of the structural eigenmodes.

External factors, such as the flow oscillations from the compressor outlet, local inhomogeneity in the fuel and air mixture or even the *combustion roar* itself may produce an uneven heat release in time and space. The consequence is the production of periodic pressure waves that travel through the combustion chamber and are reflected at the domain boundaries. These reflected waves

reach the burner upstream end and the plenum chamber, where they are able to modify the aerodynamics of the upstream side of the combustor. Once the perturbations are convected downstream through the burner to the combustion chamber, they become the source for the unsteady heat release and they encourage the start of the following cycle of the feedback loop. This instability mechanism has already been described by many researchers [13, 46-48] and it is shown in figure 2-3.

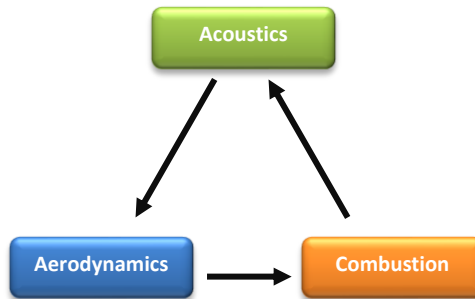


**Figure 2-3: Thermo acoustic loop.**

Growth of the instability amplitude is only possible if the three participating elements can efficiently exchange energy with each other. Mathematically, it can be expressed with equation (2.18), which describes the energy transfer rate between the flame and the pressure field and relates it to the acoustic energy losses. The equation is also known as the Rayleigh criterion [49].

$$\frac{\gamma - 1}{\gamma \bar{p}} \int_V \int_T p'(x,t) Q'(x,t) dt dV \geq \int_A \int_T p'(x,t) u'(x,t) dt dA \quad (2.18)$$

The Rayleigh criterion is a tool to examine the stability of a system. If the energy flux from the flame to the acoustic field is greater than the losses, the amplitude of the pressure oscillations will grow every cycle until the two quantities are in balance [50-52]. At this point, the amplitude remains constant over time and this unstable regime is called Limit Cycle of pressure Oscillations (LCO). This is presented in figure 2-4.

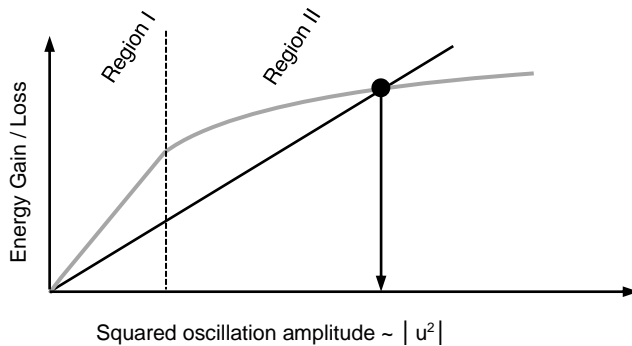


**Figure 2-4: Energy gain (gray) and loss (black) as a function of the acoustic velocity. Adapted from [51, 52].**

The acoustic losses of combustions systems are linearly dependent on  $|u^2|$  [53], assuming that acoustic impedance at the boundaries is independent of the oscillation amplitude. The energy gain of the flame has two regimes. For small amplitude perturbations, the energy gain is proportional to the velocity perturbation. After certain point, the perturbation growth rate decreases as it gets closer to the mean velocity [53-55]. The final limit cycle amplitude is the corresponding to the intersection of the two curves.

### Frequency Transfer Function

The description of the flame instability growth in figure 2-4 is not yet complete, because it lacks the important variations due to the transient oscillations. The combustion process, as every other process in nature, has its own associated time delays. Leaving flames aside for a moment, a simple pendulum is an excellent example of the importance of the temporal relationships. The pendulum natural frequency (or natural period) depends on its mass and length. If a person gives regular impulses to a pendulum at a frequency close its natural frequency, the amplitude of each swing increases rapidly. If the frequency of the impulses is far from the characteristic frequency, the amplitude of the pendulum swing remains low, even with strong impulses. This argument can be transferred to the combustion field, with the velocity perturbations in the upstream of the flame as the input parameter and the heat release rate as the output. The relationship between them is called *Flame Transfer Function*.

$$FTF(\omega) = \frac{\frac{Q'(\omega)}{\overline{Q}}}{\frac{u'(\omega)}{\overline{u}}} \quad (2.19)$$

From the FTF point of view, the flame is a black box with one input and one output. The practical interest of the FTF lies in its use, as a building block, for the network models used to predict combustion behavior. In the last years, there have been many reports of FTF for a variety of geometries [4, 21, 56-64], obtained from either practical or numerical experimentation. A slightly different approach to characterize the flame is the Transfer Matrix by [65, 66] that uses the acoustic field as the output variable. This allows measuring the flame response at the upstream and downstream ends.

The FTF only describes the behavior in the (low amplitude) linear regime, as shown in figure 2-4, where the heat release perturbations are proportional to the velocity perturbations at the inlet. For the correct modeling of the high amplitude regime, where non-linear effects are important, the function must include the amplitude of inlet perturbation. The function is called *Flame Describing Function*.

$$FDF(\omega, |u'|) = \frac{\frac{Q'(\omega)}{\overline{Q}}}{\frac{u'(\omega)}{\overline{u}}} \quad (2.20)$$

Like the FTF, the FDF has been studied for a variety of flame holder geometries: bluff body flames [54, 67], perforated plates [13, 68] and swirling flames [24, 51, 69-71].

To measure the FTF or FDF, the fluid needs to be externally excited, usually with a loudspeaker or a siren unit. In self-excited systems, which develop the Limit Cycle spontaneously, it is not possible to retrieve a FTF for a range of frequencies, since the oscillations only contain one single frequency  $\omega$ . The study of self-excited systems focuses on nonlinear and non-normal effects [72], non-linear heat rate transfer [33] and the description of the frequency with the observed flame dynamics with flame imaging techniques [61, 73-75].

## Research in Bluff Body Combustors

To sustain the combustion process, the mixture of air and fuel needs to be heated above the auto ignition temperature. For the turbulent flame explored here, this is done by mixing the fresh reactants and the hot burnt gases in a recirculation zone of turbulent eddies and vortex structures. Swirling combustors are the most common solution in boilers and gas turbine combustors, but bluff body burners have been used in industrial burners, propulsion engines and scientific reactors as well. Over the years, researchers have studied many different geometrical configurations and bluff body shapes, including tulip shaped bluff bodies [54, 76-79], cylinder prisms [80], wires [81] or bullet shaped [82] inserts. In some of the cases, the fuel was injected, at least partially, from the bluff body itself, which resulted in jet flames [83].

Triangular bluff bodies have also been widely used in experimental and analytical studies. The triangular bluff body used by Sjunnesson et al in their experimental research [84] has been used since for validation of many numerical studies [85-88] and scaling laws [89]. For a similar bluff body, Soteriu et al [90] studied the influence of the reactants temperature and Swetaprovo et al [91] investigated the blow off mechanisms. Most of the mentioned studies report a stable combustion regime where the only observed oscillations came from aerodynamic instabilities.

The von Karman instability for non-reacting flows is characterized by large scale, asymmetric shedding of vortices with a frequency determined by the Strouhal number  $St$  [90, 92] defined by (2.21).

$$St = \frac{D}{U} f_{VK} \quad (2.21)$$

Here  $D$  is the characteristic size of the body and  $U$  is the upstream fluid flow velocity. In triangular bodies pointing upstream the reported  $St$  number values at which vortex shedding may typically occur is 0.13 for low Reynolds numbers [93] or about 0.2 for high Reynolds numbers [94, 95]. Given a sufficiently long recirculation zone length, the separated shear layer evolves into shear layer rollup and creates the Kelvin–Helmholtz instability [96].

$$f_{KH} = 0.0235 f_{VK} Re^{0.67} \quad (2.22)$$



In reacting cases, the combustion released heat greatly influences the flow field after the bluff body, breakings down the vortices and other coherent structures and preventing the rise of these type of instabilities [97, 98].

Most of the presented studies in the literature have low blockage ratios and stable flames, with only few of them showing an unstable regime of high amplitude oscillations. For example, the observations of Sivakumar and Chakravarthy [99] showed the unstable flame regime in a similar combustor to LIMOUSINE that uses partially premixed mixture and a V gutter instead of the solid bluff body flame holder. They performed a systematic variation of the controlling parameters of the flame and were able to identify two combustion regimes. The onset of combustion instability is observed to be due to the natural acoustic mode locking on to the vortex shedding frequency. In the study by Yu et al [100] the same characteristic is also observed for a partially premixed dump combustor.

The unstable regime is also shown in the study by Rogers and Marble [101]. Their flame is stabilized in the wake of a triangular bluff body with a high blockage ratio, which resulted in a large Mach numbers at the burner tips. In this combustor, screech modes were recorded at high frequency, usually 3800 Hz. They also reported low frequency oscillations for relatively rich mixtures ( $\lambda < 1.10$ ), whose frequency roughly corresponds to the acoustic longitudinal eigenfrequencies of the chamber.

# Chapter 3 **Experimental Setup**

## **Introduction**

The results of the present thesis were obtained from an experimental setup specially optimized for the study of the Limit Cycle oscillations in lean combustion conditions. The main feature of the combustor is its multidisciplinary approach, which allows the study of flame dynamics, acoustic field and structural vibrations simultaneously. Unlike other research combustors and burner setups, that are specially built for a single laboratory and the available measuring techniques, the LIMOUSINE combustor was prepared to be used by many independent researchers in different countries, allowing each individual fellow to focus in his or hers areas of expertise. For that reason, the combustor was optimized to maximize the number of experimental techniques that can be used. The final design required the agreement of the partners of the LIMOUSINE project on the constructive details, such as the maximum dimensions of the combustor or the location of the supports. The functional parameters were also debated by the fellows, e.g., the maximum allowed pressure drop in the feeding lines or the nominal operational conditions.

## **LIMOUSINE Version 1**

The basic design was derived from an existing laboratory combustor that was developed in the Laboratory of Thermal Engineering of the University of Twente prior to the start of the project and was renamed LIMOUSINE version 1.

The main characteristic of the setup is that the length and depth of the combustor are larger than the width. For this reason, the flame can be considered two dimensional in nature, at least in regions that are far from left and right edges, where 3 dimensional effects are important. This is a sensible advantage for the numerical analysis of the flame, as the combustion may be captured using only a periodically repeated slice of the combustor. The flame is stabilized due to the presence of a bluff body inserted in the fluid path and not due to swirling vanes.



**Figure 3-1: LIMOUSINE version 1 combustor.**

There is still one extra advantage of this geometry: the side walls of the combustor have high length to width ratios. The liner duct is less stiff than a square or circular liner section with the same perimeter, and interaction between fluid and structure is encouraged.

The LIMOUSINE version 1 combustor walls are 1 mm thick plates steel plates welded in a rectangular shape. It is in a vertical position and the upstream end is the closest to the ground while hot gases leave the combustor at the top to the chimney. The combustor consists of two sections bolted together at the flame holder location. The upstream section includes the plenum chamber and the flame holder/fuel injector. The air is fed from PVC hoses into the upstream end and passes through a perforated plate. The downstream section just consists of a rectangular liner duct.

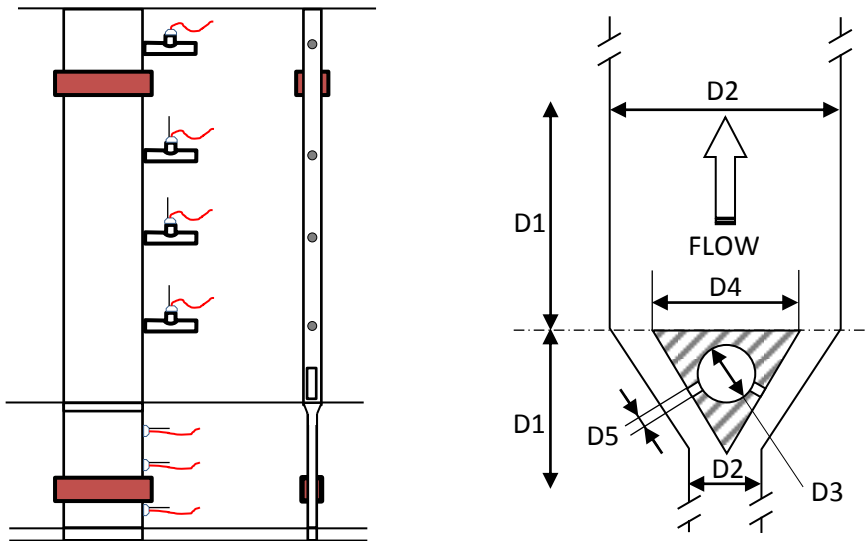


**Figure 3-2: LIMOUSINE version 1 main dimensions (LHS) and burner sketch (RHS). Dimensions are in table 3-1.**

**Table 3-1: LIMOUSINE version 1 main dimensions.**

D1	Height up/downstream [mm]	322/1106	Number of gas injection holes	78
	Width of the combustor [mm]	220	Designed combustor power [kW]	40
D2	Depth up/downstream [mm]	25/50	Designed air excess ratio [ ]	1.4
D3	Diameter of distributor hole [mm]	5	Upstream air velocity [ $\text{m s}^{-1}$ ]	3,17
D4	Wedge side dimension [mm]	21.2	Gas injection velocity [ $\text{m s}^{-1}$ ]	17,45
D5	Diameter injector holes [mm]	1	Cold flow Reynolds Number	4500

As seen in the left hand side of figure 3-2, the downstream part has a wider cross section than the plenum (50 mm compared to 25 mm). To observe the flame, the combustor has a rectangular quartz window in each short sided wall. The flame holder is an equilateral triangular prism made from brass, facing upstream. This body is hollow and has holes in its lateral faces to inject the fuel. The most important dimensions are listed in table 3-1.

The combustor is connected to a supportive frame by two clamps. Each clamp consists of two parallel metal strips over the wide faces that are bolted to each

other, but not bolted or welded to the combustion liner wall. This version of the combustor has 7 ports at the 50 mm face to measure the internal pressure. Three of them are located in the upstream plenum and four in the downstream side. The pressure transducers in the upstream plenum are screwed in the lateral wall, so the tip of the transducer is flush mounted to the internal face of the duct. The ones on the downstream side cannot use this solution, because of the high temperatures during the experiment. They are mounted in semi-infinite side tubes connected to the lateral wall of the combustor.

## **LIMOUSINE Version 2**

The LIMOUSINE version 1 was a prototype to learn about the limit cycle and its characteristics, but it presents few drawbacks. For example, the support plates were not rigid enough and allowed large wall displacements. Based on this original design but considering the requirements of the different project fellows, a second version was produced by the University of Twente. This newer version is smaller and shorter, so it can be installed in every partner's research facility. The material was upgraded to high quality stainless steel, to ensure consistent and reliable operation for longer periods. The newer design also includes a large optical section for advanced imaging techniques. Due to the modular design, the combustor parts can be removed or modified by the fellows. The resulting combustor is named LIMOUSINE version 2 in figure 3-3.

The depth of the version 2 combustor is 50 mm for the combustion chamber and 25 mm for the plenum, but width is reduced to 150 mm. The wall thickness is 4 mm, to limit the effect of the structure in the flame and the acoustic field. The piece that has evolved the most from version 1 to version 2 is the flame holder triangular prism. Despite the fact that the two bluff body prism's size remains in 22 millimeters, other characteristics dimensions do change greatly.

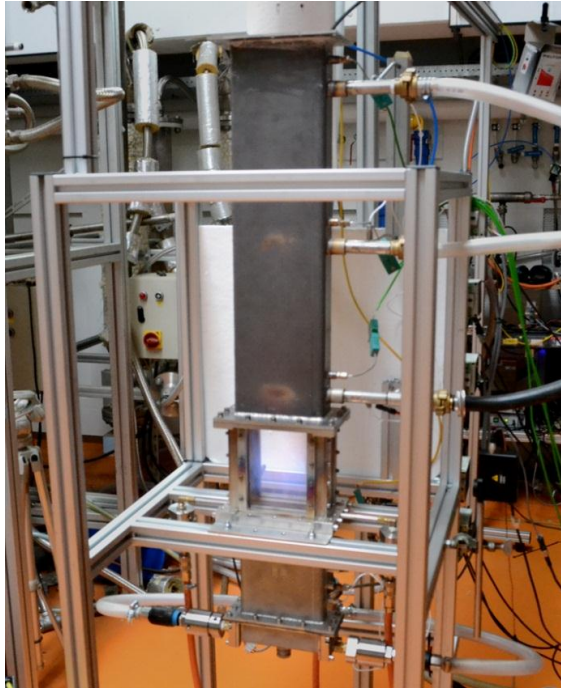


**Figure 3-3: LIMOUSINE version 2 and version 3 combustor.**

The diameter of the internal distributor hole was increased to the maximum diameter possible to provide a better fuel distribution over the injection holes and simultaneously reduce the fuel line pressure losses. At the same time, the distribution hole center is displaced towards the upstream edge to accommodate the quartz windows of the optical section. In total, it presents 62, 1 mm diameter holes separated by a 4 mm gap. The holes were not placed in the middle of the lateral faces, like in LIMOUSINE version 1, but at 6 mm from the triangle tip. The new location allows longer nozzle and an improved fuel/air mixing process.

Figure 3-4 shows the wedges from versions 1 and version 2 in the same sketch. The left hand side is the previous version 1 design and the right hand side is the version 2 wedge. The burner inlet is located at 275 mm from the top of the wedge and the combustion chamber is 780 mm long. The combustor features large quartz glass windows in the 4 sides to allow full optical access to the first 150 mm of the flame. The total length of the combustor is 1050 mm, including the airbox. The outlet of the combustor was modified with the installation of a flange to easily add more liner ducts and change the length of the combustion chamber..

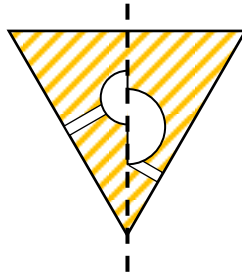


**Figure 3-4: LIMOUSINE wedge cut-out version 1 (LHS) and versions 2 and 3 (RHS).**

The blocks and pieces that compose the burner assembly, as well as the top liner, are made from heat resistant stainless steel SS310 specification. The airbox assembly and plenum are made of SS316, because the expected thermal load of these pieces is smaller. The wedge was made out of brass for precise and easy machining. Between the different components and between the glass plates and the metal pieces mica gaskets were used to prevent gas leakage

The air distribution system on the upstream end was designed to achieve three main goals simultaneously. It has to deliver a constant and uniform flow of air over the cross sectional area, it must behave as an acoustically closed end condition and it must accomplish the previous two goals with the least pressure drop possible. This is indeed a difficult optimization problem, as the goals are counteracting: for a uniform flow distribution, a large number of injection nozzles are desirable while to reach acoustically closed boundary conditions, the flow through the orifices should be choked. These goals can be achieved if the pressure of the feeding flow is high, but that is unpractical and expensive. The feeding system ran through several design iterations that converged in the following design. The incoming air flow is split in two, and each flow is sent to a pipe in the upstream end of the combustor. The pipes pass through one lateral wall and they are blind at the other end. Each pipe has 22 drills of 2 mm diameter. In this design, the holes in one of the pipes do not directly face the holes in the opposite pipe. The air flow in these small injection holes is not sufficiently high to reach choked conditions. Mach numbers are in the order of 0.1 to 0.5, depending on the flow parameters, but it seems enough to decouple the system. An advantage of this design is the absence of flow straighteners or perforated plates that can modify the acoustic field. The upstream end counts with one extra inlet port to connect a loudspeaker for acoustic excitation.

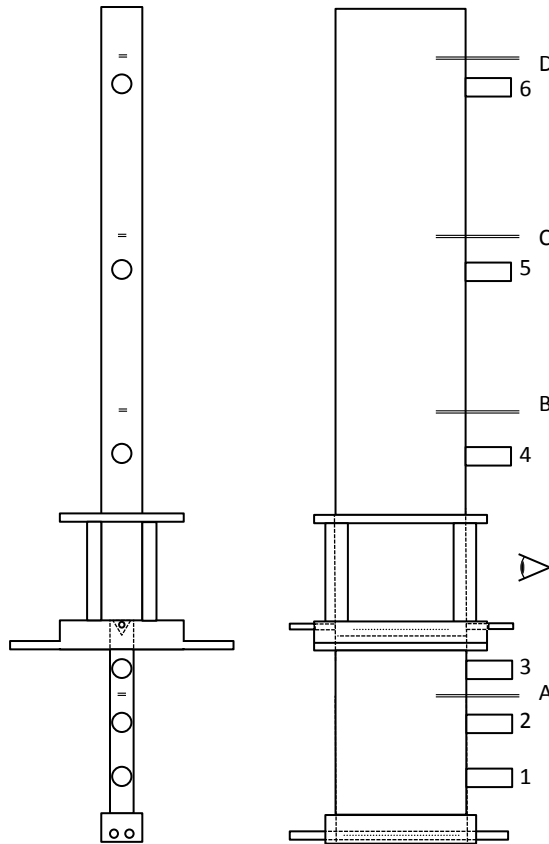


**Figure 3-5: LIMOUSINE version 2 and version 3 sketch showing the location of pressure sensors (1 to 6), temperature sensors (A, B, C, D), PMT and ICCD cameras (eye).**

### LIMOUSINE Version 3

During the experimental characterization of the LIMOUSINE version 2 combustor, it was discovered that the LCO oscillations were only possible if an extra liner was mounted on top of the original liner. The length of this combustor assembly with two liners was well above 1 meter and therefore, it was not a feasible solution to export to other laboratories. The long and thin observed flames hinted at the necessary improvement of the air/fuel mixing rate. Therefore the first modification was to increasing the momentum of the fuel jets with a new wedge design at the cost of greater pressure losses. The number of drilled holes in the body was reduced, from 62 to 26 holes while other dimensions remained unaltered. The injector drill size was also reduced from 1 to 0.8 mm in diameter.



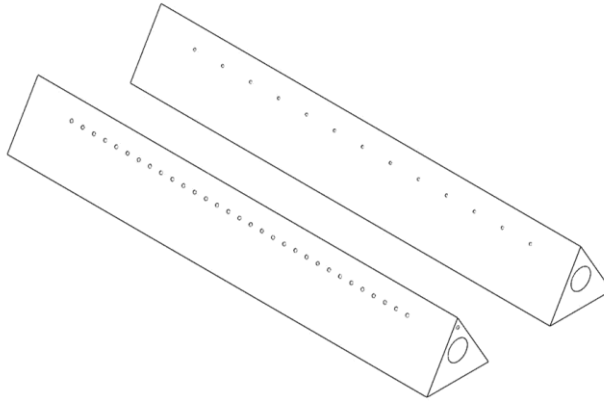


**Figure 3-6: LIMOUSINE version 2 standard wedge and wedge with smaller holes.**

Combustion testing was conducted for this configuration without ever reaching unstable flame dynamics and, in the end, the whole idea was discarded. A new approach was the modification of the blocks flanking the wedge to reduce the cross sectional area in the burner. The blocks side wall is collinear with the upstream duct internal wall instead of parallel with the triangular body face. The gap between the wedge and the block is sufficient to keep the velocity of the fluid below 20 meter per second in the nominal design point to use PIV techniques. The new block design includes two extensions on its sides to fix the orientation and position of the wedge.

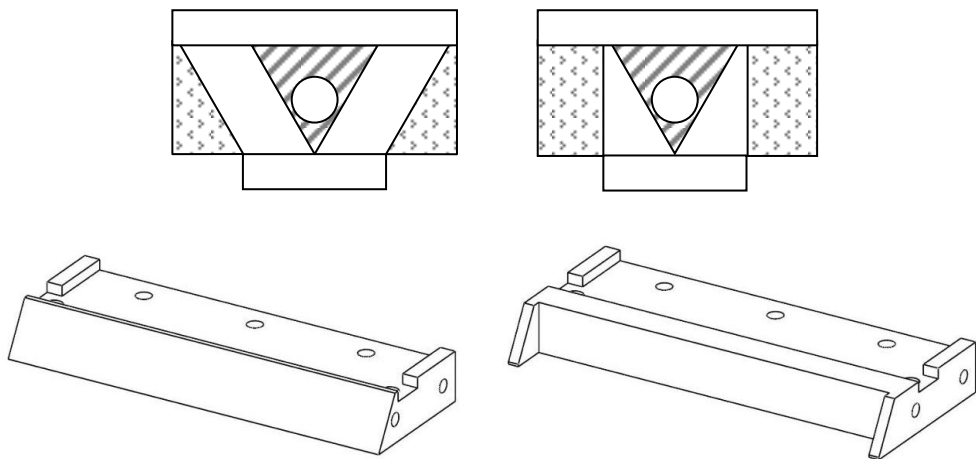


**Figure 3-7: LIMOUSINE version 2 (LHS) and version 3 (RHS) lateral cut out section and constructive blocks isometric view.**

These modifications were successful and the combination of the new side blocks and the old 62 holes wedge resulted in unstable combustion for certain air and fuel conditions. This design is named LIMOUSINE version 3 combustor and is the most frequently used version through the research.

## Auxiliary Equipment

Auxiliary equipment is as important as the main test rig to successfully run the experiments. In this subsection, the fuel and air delivery systems are described. The combustor fuel is pure methane,  $\text{CH}_4$ , stored in high pressure bottles. Their rated pressure is 200 bar and it is reduced with a valve to 4 bar in the fuel supply lines. Due to the high pressure, methane can be injected without the need of a gas compressor. The air source is the laboratory compressed air supply line at 6 bar. The igniter system is a conventional spark plug connected to an electrical transformer. The spark plug is only used during the ignition and operated remotely with a computer.

Fuel and air flows are controlled by mass flow controller valves. The methane mass flow controller has a maximum capacity of 100 slm while the two air controllers connected in parallel can reach up to 1000 slm each. During the Flame Transfer Function measurements, an additional mass flow controller valve was used to split some of the air to the siren unit. A desktop PC with a backup power supply (UPS) controls the valves via FIELD-POINT data acquisition cards from National Instruments.

While testing LIMOUSINE version 1 combustor, it was discovered that the flame dynamics were sometimes related to perturbations of the flow in the control valves and the feeding pipes. For that reason, calibrated orifices were placed in the inlet of the fuel and air ports to acoustically decouple the combustor from the auxiliary equipment by a means of a shockwave. To work out the diameter of the pipe, the mass flow  $\dot{m}$  through an orifice of area  $A$  was calculated, assuming ideal gas and isentropic process (adiabatic and reversible).

$$\dot{m} = \frac{Ap_t}{\sqrt{T_t}} \sqrt{\frac{\gamma}{R}} M \left( 1 + \frac{\gamma - 1}{2} M^2 \right)^{-\frac{\gamma+1}{2(\gamma-1)}} \quad (3.1)$$

In the expression (3.1), the gas in the upstream side has a total pressure and total temperature  $p_t$  and  $T_t$  respectively. An orifice is choked when the velocity of the

flow is equal to the speed of sound in the fluid,  $M = 1.0$ , and therefore, a shock wave appears in its throat. The orifices are choked at the nominal design point of 40 kW power and air factor  $\lambda = 1.40$ . Therefore, the area of the nozzle throat is the only unknown in equation (3.2). For the air flow, the upstream pressure was set to 1.5 bar. In the gas nozzles, the upstream pressure design point is also 1.5 bar. The hoses that connect the control valves and the combustor are long and not insulated, with results in the temperature of the gas phase to be the room temperature 20 °C.

$$\dot{m} = \frac{Ap_t}{\sqrt{T_t}} \sqrt{\frac{\gamma}{R}} \left( \frac{\gamma + 1}{2} \right)^{-\frac{\gamma+1}{2(\gamma-1)}} \quad (3.2)$$

In the air supply hoses, the orifices have a diameter of 6.14 mm while orifices installed in the fuel line have 1.47 mm diameter hole. The orifices were drilled on a brass disc placed in a strong stainless steel casing. Both orifices were calibrated using a source of compressed air, showing a linear behavior in all the range of working pressure.

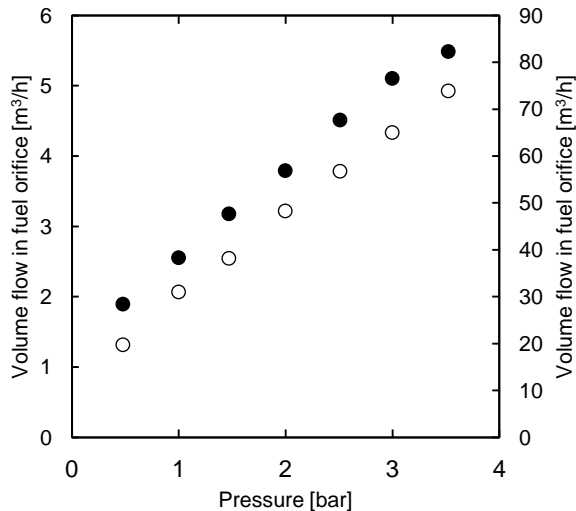


**Figure 3-8: Calibration of the gas nozzle ○ and air nozzle ●.**

## Acoustic drivers

In many occasions during this research, an acoustic driver unit was needed for acoustic excitation. The combination of a 10 inch Infinity loudspeaker and an audio amplifier is usually enough for the characterization of the acoustic behavior of the setup without combustion. However, to achieve very large perturbation amplitudes, a siren unit is used. The siren consists of a perforated rotating disc inside a metallic casing that intermittently obstructs the fluid path. In this way, perturbations up to 100% of the mean flow are possible. To minimize the amount of energy lost towards the feeding pipe, a chamber was placed on the upstream side of the casing.

## Sensors

### Pressure

The pressure perturbations are measured at 6 different locations (version 2 and version 3) with piezoelectric pressure transducers from Kulite, model XTE 190M. The pressure range of the transducer is 0.35 bar, enough to record in the high amplitude regimes. The full scale output signal is 100 mV, so they were connected to a calibrated voltage amplifier that increases the voltage range to 10 Volt. Due to its small size, the Kulite's natural frequency is around 150 kHz. Despite there were other (and cheaper) pressure sensor alternatives in the market, this model is very robust. It can be used in harsh environments with high vibration levels, up to 100 g, and temperatures of 175 °C, making them ideal for thermoacoustic applications.

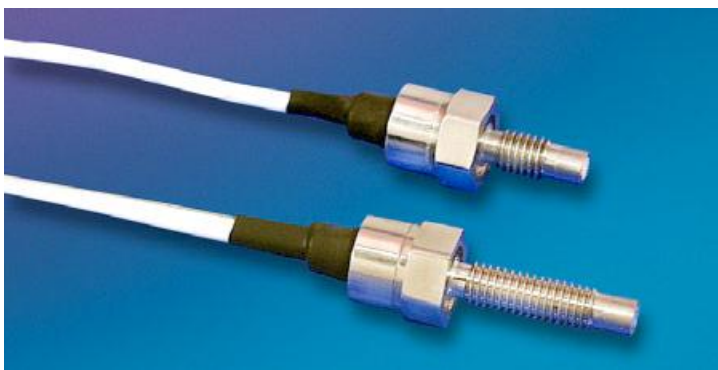
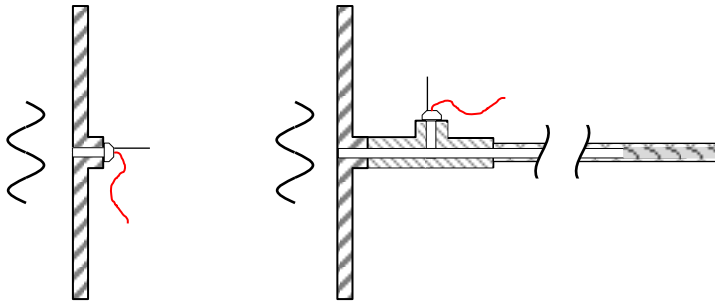


Figure 3-9: Kulite pressure transducer.



**Figure 3-10: Pressure transducer flush mounted (LHS) and in semi-infinite hose mounted (RHS).**

The three pressure transducers of the plenum are flush mounted in the wall (at 60, 120 and 180 mm upstream of the wedge top face) and the remaining 3 are mounted in side tubes of the combustion chamber.

Installing the pressure transducers in side tubes protects them from high temperatures and avoids the need for complex liquid cooling systems (figure 3-10). The side tubes are connect to long hoses closed at the other end with sound absorbing material that does not allow any flow through. The piezoelectric transducers have a secondary inlet port to measure differential pressure. To avoid any interference of the external sound waves, a thin and open (0.8 mm internal diameter) plastic tube hose was connected to this port. The locations of the downstream pressure transducers are at 200, 450 and 700 mm using the burner top plane as reference. More information about the semi-infinite hoses can be found in Appendix A of this dissertation.

## Heat Release

The flame heat release is measured using a *Photo Multiplier Tube* or PMT. It is a device that provides an output voltage proportional to the incident intensity of the received light. The measuring principle is based on photocathodes that release electrons and create an electrical current by a dynode chain after the detection of a photon. A band pass filter is placed in front of the sensor, to record only the flame emission at the required wavelength. The bands are centered around 430 nm or 306 nm, which are the wavelengths of the spontaneous emission of the chemical radicals  $\text{CH}^*$  or  $\text{OH}^*$ . These radicals are only produced and consumed in

the flame front and are commonly used to quantify the flame heat release rate. The PMT is located at one of the combustor sides with an OH\* filter installed.

### **High Speed Imaging**

Sometimes measuring the flame total light emissions is not enough. A picture of the flame front can reveal important details, such as flame length or instantaneous shape. During the research, two cameras were used to capture pictures of the flame. The first camera of the two is a high speed camera able to record up to 1000 frames per second. This camera has a separate image intensifier unit and both are controlled with a pulse / time delay generator. The second camera has only a maximum rate of 10 fps, but has the image intensifier integrated in the same body. Both cameras have a narrow band filter for CH\* or OH\* emission.

### **Fluid Velocity**

The velocity of the fluid is measured in the burner passage next to the wedge tip with a constant temperature anemometry system. The sensor is a very fine wire heated above the ambient temperature, which why this technique is sometimes called hot wire anemometry. Due to the small size of the wire, it can capture very fast changes in the velocity of the fluid but it is very fragile and it can snap if the velocity increases too much. The hot wire should be calibrated before each measurement, using a 5<sup>th</sup> order polynomial function. This technique is used only in experiments without combustion.

### **Temperature**

The flue gases temperature is measured with thermocouple sensors in the combustion chamber and plenum. The thermocouples are K type protected with an Inconel sheath of 3 mm in diameter. There are 3 thermocouples in the combustion chamber at 240, 500 and 750 mm from the wedge and one in the upstream duct, at 150 mm. The thermocouple tip is located 40 mm inside the combustor measured from the interior side of the wall. The liner wall temperature is more challenging to measure. Unlike other burners, the motion of the liner is crucial and its vibration level is measured in every experiment. Additional elements, such as insulation layers or the thermocouple sensors, would add solicitations to the structure and modify its behavior, which is not acceptable. Other possibilities, such as using ceramic paste to hold a small thermocouple have not succeed because they detach from the hot surface after some minutes of

operation. The only realistic possibility to measure wall temperature are optical techniques. An infrared sensitive camera is used to record temperatures at selected points. In several occasions an optical pyrometer is used.

## Wall Vibration

The response of the structural elements is measured with a Laser Doppler Vibrometer (LDV). The LDV is a non-contact laser technique that measures the Doppler shift of a laser beam reflected by the surface under study. The interference patterns of the beam and its reflection can be related to the velocity of vibration of the surface. The output of an LDV is a signal proportional to velocity component along the direction of the laser beam that is very precise and does not require calibration. This technique is useful in surfaces that are too hot to place a conventional accelerometer and does not add extra mass to the structure. The wall vibration was also measured in cold conditions (without combustion), but employing more conventional techniques.

To provide excitation to the structural system, an impact hammer is used. It is an instrumented hammer with a force cell in its tip to register the impact. The system response is recorded with small piezoelectric accelerometers. Both sensors produce small currents and need a signal conditioner/amplifier.

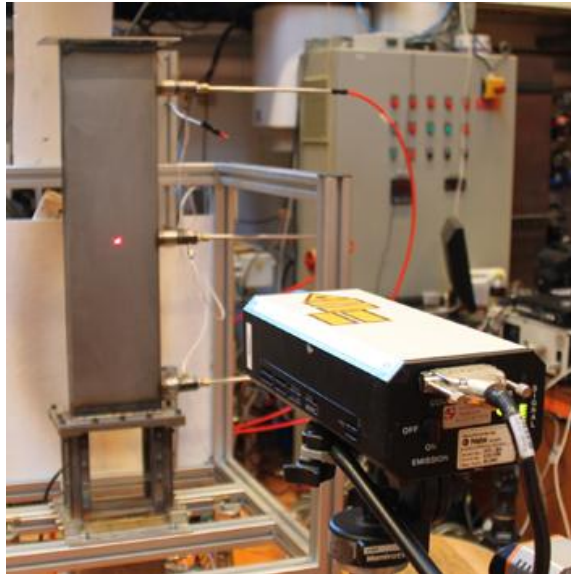


**Figure 3-11: Laser Doppler Vibrometer in operation.**

## Emissions

The composition of the exhaust gases is measured with a portable gas analyzer model RBR-Ecom KD. It can measure the amount of NO, CO, CO<sub>2</sub> and SO species.



**Figure 3-12: Portable gas analyzer.**

## Data Acquisition System

The signals are measured with a DAQ system linked to a laptop. In the beginning, one or more Siglab 20-42 units were used. Each Siglab unit can record up to 4 channels, but several units could be interconnected to increase the number of inputs channels. Data was usually recorded at a rate of 2560 samples per second simultaneously from all channels during 3.2 seconds (8192 samples). To minimize the error, the sets were linearly averaged. The Siglab unit had also two output channels that could produce different kinds of signals: sine, triangular or square waves and random signals. The Siglab units were used in version 1 measurements, the structural tests and the acoustic Green's function experiment.

The Siglab system was later replaced by a combination of different DAQ cards from National Instruments. The final configuration has three data acquisition cards NI 9239, offering 12 input channels. They can read  $\pm 10V$  signals at a maximum rate of 50000 samples per second simultaneously in all input channels. A module NI 9263 can produce 4 output channels to drive the speaker or the PMT gain control. The output channels are also used to produce a TTL step signal that can remotely trigger the CCD cameras. The thermocouple signals are read using a dedicated NI 9211 module. These cards are connected to a NI 9188 chassis linked to the computer via (wired) Ethernet. The system is monitored using a custom



Labview script. To achieve good resolution in the spectral measurements and save disk space, it uses an averaging algorithm for the signals. In this way, the software creates files with the measured time trace, but also files with the averaged FFT, auto spectrum, and even the frequency response functions using one designated channel as the stimulus input. The system allows automatic file naming, which prevents mistakes during the experiments. The Labview sampling rate is 3125 samples per second, recording a total of 10000 samples in 3.2 seconds.

The accuracy of the measuring chain is described in appendix E.

# Chapter 4 **Limit Cycle Characterization**

## **Introduction**

This chapter presents and discusses the measured results in the laboratory about the Limit Cycle Oscillations. The results of the acoustic characterization for version 2 or 3 of the LIMOUSINE setup are shown in the first place because the knowledge of the acoustic modes is key for the prediction of the instability frequency. Next, the discussion of the combustion measurements are presented for the four configurations under study: version 2 single and double liner, followed by the version 3 single and double liner. The final part of the chapter includes the results from the structural elements and the pollutants emission of the flame.

## **Boundary Conditions & Acoustic Modes**

The combustor was first studied from the acoustic point of view, without combustion, to accurately characterize the nature of its boundary conditions. From the point of view of flame stability and limit cycle development, the low frequency waves are the most important ones. Such waves have a wavelength comparable to the combustor length, but much longer than its width or depth. Therefore, the analysis can be limited to plane waves in a 1 dimensional field.

The characteristics of the inlet upstream end and the combustor exit were investigated on the LIMOUSINE version 3 combustor. The reflection coefficient was measured at room temperature without mean flow. The multi microphone method was used to capture the reflection coefficient, with the speaker to produce the stimulus signal. To avoid mechanical contact between the main components and to reduce the amount of noise picked up by the transducers, the speaker was suspended on rope straps from the aluminum frame. When connected to the upstream end, the interface was metal funnel and a PVC reinforced hose.

The speaker was tuned to single tone signals from 50 Hz to 400 Hz in steps of 10 Hz. This range is limited in the high end because it is very challenging to transfer the acoustic energy from the speaker to the interior of the combustor, resulting in low signal to noise ratio and poor accuracy. The acoustic characteristics of the boundaries are independent of the installed burner or the combustion chamber length. This means that version 2 and version 3 have identical acoustic properties.

### Acoustic Reflection Coefficient

In LIMOUSINE version 2 and version 3, the outlet end is open to the ambient and fitted with a rectangular flange. Due to its simplicity, it is expected to behave like an open end. The upstream inlet end is apparently acoustically a hard boundary condition, but the presence of the feeding pipes may change the actual reflection coefficient value. Figure 4-1 shows a sketch of the locations of the speaker and pressure transducers.

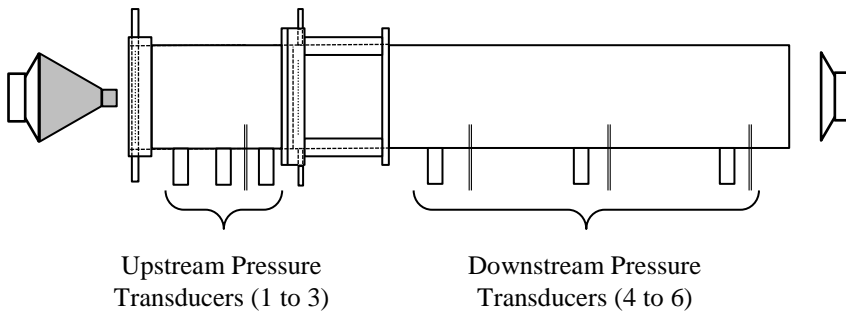


**Figure 4-1: Lay-out of the setup and loudspeaker location.**

The reflection coefficient of the upstream termination, shown in figure 4-2 (top), resembles a closed end. The magnitude is 1 for the full frequency range and its corresponding phase is very close to 0 radians, with a slight roll down from -0.1 to -0.4 radians. This confirms that the effect of the air distribution system is negligible and does not have any influence on the acoustic behavior of the combustor. Figure 4-2 (bottom) shows magnitude and phase of the reflection coefficient at the downstream end. The magnitude of the reflection coefficient is almost constant and varies from 1 to 0.9 in the studied 400 Hz range. At higher frequencies, the magnitude suddenly drops at 400 Hz because of the cut off

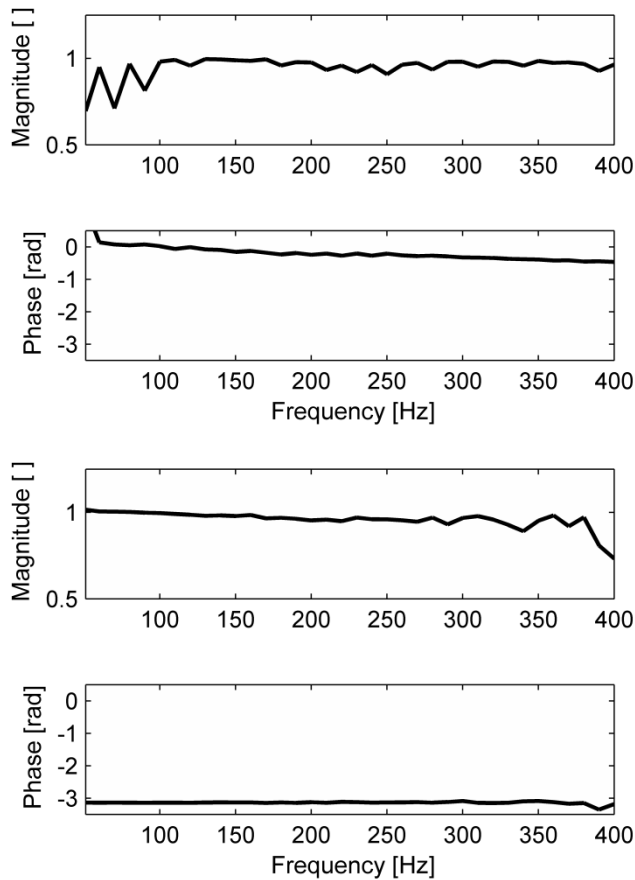


**Figure 4-2: Upstream end (top) and downstream end (bottom) reflection coefficient.**

frequency of the funnel. The reflection coefficient phase is flat at  $-3.1$  radian. These measured values allow classifying the upstream end as an open end termination. Contrary to the results from the LIMOUSINE version 1, the observed acoustic behavior of both ends agrees well with the predicted behavior.

## Calculations

The acoustic eigenfrequencies and eigenmodes can be calculated by means of the wave equation and the experimentally measured boundary conditions. This is not a trivial problem, but there is more than one strategy to find the solution. In the first approach, more straightforward, a FEM discretization and a solver software script are used to calculate the eigenfrequencies and eigenmodes of the system.

In this way, it is even possible to solve high eigenfrequencies related to three dimensional modes. The second strategy uses an analytical approach that solves the wave equation in a linear acoustic network of one dimensional elements.

## FEM Approach

The acoustic modes for a given configuration can be found with help of numerical techniques. While the basic working principle of the computational tools is relatively simple, developing an efficient and reliable code can be complicated and expensive. In this case, the best solution is to choose one of the many commercially available codes, such as COMSOL MULTIPHYSICS v4.1 or ANSYS APDL software.

The LIMOUSINE combustor geometry was modeled and meshed with the built in tools of COMSOL MULTIPHYSICS. The working fluid was air and the code allows choosing different temperatures to the different subdomains. To mimic the thermal gradients of the combustion, the air inlet, plenum and burner were set to 25 °C while the combustion chamber was set to 1250 °C.

Mach numbers inside the combustor were small and the effects of mean flow could be neglected for this calculation. The mesh had about 11000 unstructured tetrahedral cells with a maximum size of 0.0845 m. This size is enough to fit 10 elements in an 800 Hz wave, which is sufficient to model all the frequencies of interest. Boundary conditions were set to closed end (acoustic hard condition) in every interface except the outlet of the combustor, which was characterized as open end (acoustic soft condition). An length end correction was added [102] to account for the virtual extra length in the open end termination.

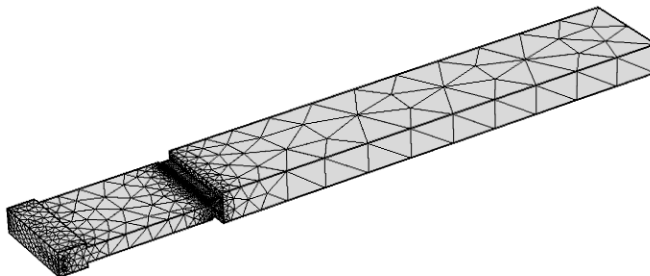


Figure 4-3: Combustor mesh used in COMSOL.

## Validation of the Acoustic Codes

The predicted results from the three codes were validated with the experimental results recorded at room temperature without combustion. In addition to the usual approach, the acoustic modes were measured with the Green's function approach, as described in appendix C. In this set of experiments, neither methane nor air was injected through the wedge holes. Table 4-1 shows the predicted frequency of the acoustic modes, the FEM predicted frequency and the predicted Green's function values. The agreement between the values is very good in this case. The predicted frequencies at room temperature with FEM and the analytical MATLAB script in the double liner case are shown in table 4-2.

**Table 4-1: Predicted single liner eigenfrequencies at room temperature.**

Mode	Analytical Frequency [Hz]	Analytical FEM [Hz]	Experimental Green [Hz]
1	87.2	91.1	88.75
2	236.4	252.6	253.1
3	374.4	380.6	356

**Table 4-2: Predicted double liner eigenfrequencies at room temperature.**

Mode	Analytical Frequency [Hz]	Analytical FEM [Hz]
1	53.15	56.1
2	159.1	164.7
3	249.3	265.6

The first three predicted eigenfrequencies in the presence of the temperature gradient are 189.4, 337.4 and 721.8 Hz. It is interesting to notice that these modes and the cold acoustic eigenmodes are not equally spaced in frequency, like the ideal duct case. One of the advances of the FEM method is that it is possible to examine three dimensional modes. The first 3D mode at room temperature is the fifth mode (at 1188 Hz) and therefore, the application of the 1 dimensional approximation is possible without loss of generality.

## Combustion Results

The combustion results are presented in the following section for all possible LIMOUSINE combustor configurations. The result reporting starts with LIMOUSINE version 2 burner, which is only capable of unstable combustion if an additional liner is installed. They are followed by version 3 burner configuration results with one liner and the last are the results corresponding to version 3 and two liners.

### LIMOUSINE version 2 Single Liner

The combustor version 2 was fired in the laboratory as an upgrade of version 1 combustor and the flames stabilized at each side of the triangular body. The flames were stable, stretched and thin, with larger size than the height of the optical section. Unfortunately, these flames did not present any significant dynamics even for the highest possible flows allowed by the mass flow controllers. The spectrum for 40 kW power and air factor  $\lambda = 1.40$ , which are the nominal operational conditions, is shown in figure 4-4. It presents the most interesting dynamics at 57, 175 and 340 Hz. Large noise levels between the 57 Hz frequency, which is vortex shedding and the 175 Hz, which is the first acoustic mode, creates a broadband oscillatory dynamics. The second acoustic mode of the combustor is seen at 340 Hz. The other dynamics, at 605 Hz and 805 Hz are effects of the combustion chamber vibrations, as will be shown at the chapter end. The temperature in the downstream duct is 1060 °C, measured from the thermocouple sensors after applying a correction for radiation losses.

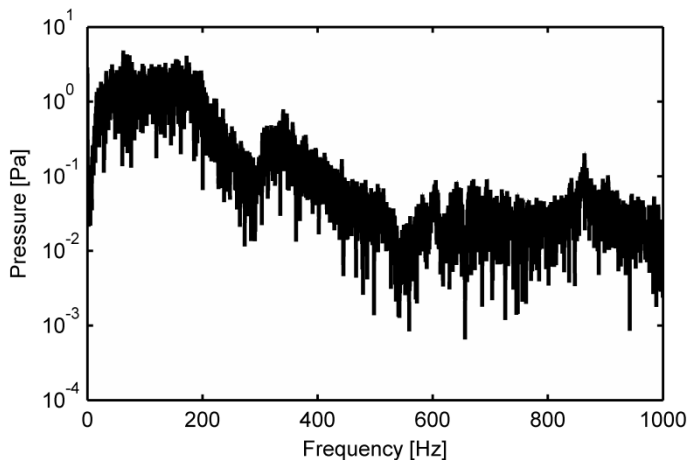


**Figure 4-4: LIMOUSINE version 2 single liner PT 4 pressure spectrum for 40 kW and  $\lambda = 1.40$ .**

With the analytical acoustic network model (2.17), the acoustic modes and their corresponding shapes can be predicted. The acoustic eigenmodes are found at 175, 325 and 694 Hz and plotted in figure 4-5. Because the modes do not depend in the internal burner geometry, version 2 and version 3 share the same frequencies. In the case shown above, there was good agreement between the first two acoustic eigenmodes and the first two recorded dynamics, which identifies them as acoustic modes.

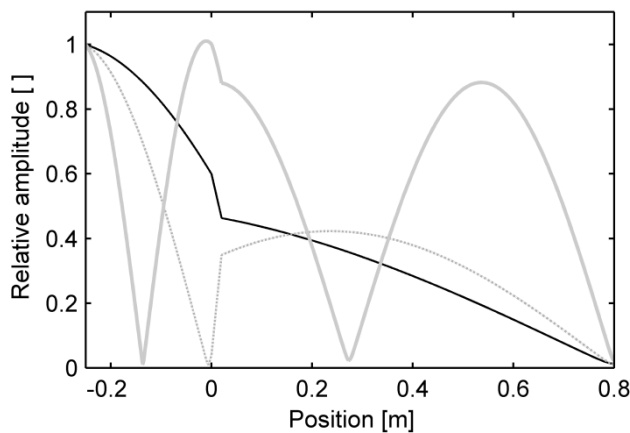


**Figure 4-5: Modal shapes in the single liner configuration. Modes are at 175 (thick black), 325 (solid gray) and 695 Hz (dotted gray).**

## LIMOUSINE version 2 Double Liner

LIMOUSINE combustor version 2 with a single liner did not show any interesting combustion dynamics or Limit Cycle Oscillations within the reachable operational conditions. Hence, some new designs were tested in order to develop an unstable combustor. The addition of a flange in the exit of the combustion duct made possible to investigate alternative configurations, with longer combustion chambers. This was, nonetheless, a provisional solution, because the requirements of the final design limited the maximum length of the combustor to 1 meter (agreed with the other project fellows). With the extra liner installed, the total length of the combustor was increased by 0.61 m, for a total of 1.61 meters from the bottom of the airbox to the top edge (figure 5-6). The addition of the liner does not only modify the frequency of the emitted sound, but for certain





**Figure 4-6 LIMOUSINE version 2 with double liner.**

combination of fuel and air flows the combustor enters in a Limit Cycle of pressure Oscillations.

In figure 4-7, the results are classified into three categories. The flames with rich fuel mixture ( $\lambda < 1.40$ ) or low inlet air velocity do not develop to unstable combustion regime. The limit cycle only manifest for lean mixtures and high burner inlet velocities. The points between the regimes are boundary points that can be in either regime, depending on the used path to reach them.

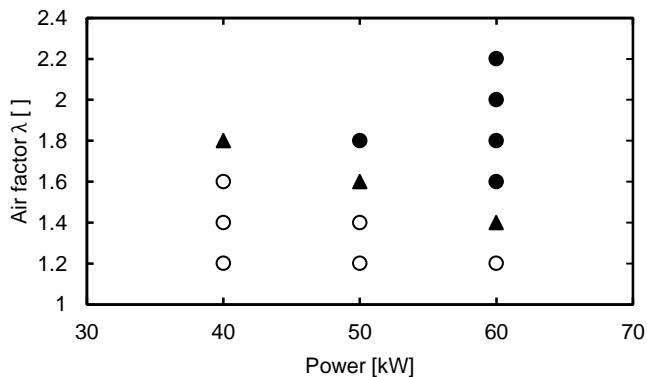


**Figure 4-7: LIMOUSINE version 2 double liner stability map: ○ Stable combustion, ▲ Boundary point, ● unstable combustion.**

### *Stable Regime*

The analysis for stable flame starts with figure 4-8 and the pressure spectrum for a stable point, such as 40 kW power and air factor  $\lambda = 1.40$ , measured in the pressure transducer PT 4. It shows that the main peaks at 100 Hz and the second peak at 390 Hz seem related to acoustic eigenmodes of this geometry. Additionally, the perturbations at 600 Hz can be linked to the vibrations of the structural elements. For this case, the combustion produces a rumble sound with amplitudes in the order of tens of Pascal.

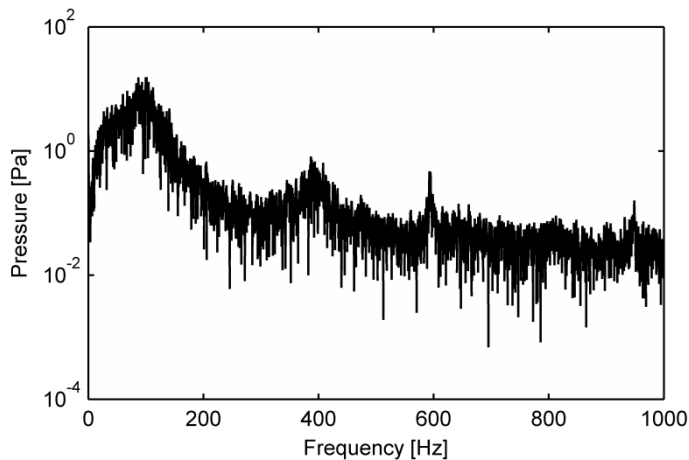


**Figure 4-8: LIMOUSINE version 2 double liner PT 4 pressure spectrum for 40 kW and  $\lambda = 1.40$ . Stable regime.**

### *Unstable Regime*

However, as the regime swapped from stable to Limit Cycle, the amplitude of the sound level in the combustion chamber increased some orders of magnitude. The noise level in the surroundings of the combustor also increased accordingly, with measured values at 1 meter from the combustor of 100 dB (A weighting) Sound Pressure Level.

The spectrum of pressure for the 60 kW and air factor  $\lambda = 1.80$  flame in figure 4-9 presents all the typical characteristics of the unstable regime. The general baseline and the acoustic modes are identical to the stable case, but the large thermoacoustic perturbations appear as thin and narrow peaks that rise high above the spectrum background. These dynamics are located in the range from 100 to 110 Hz, depending on the particular operational parameters. Other

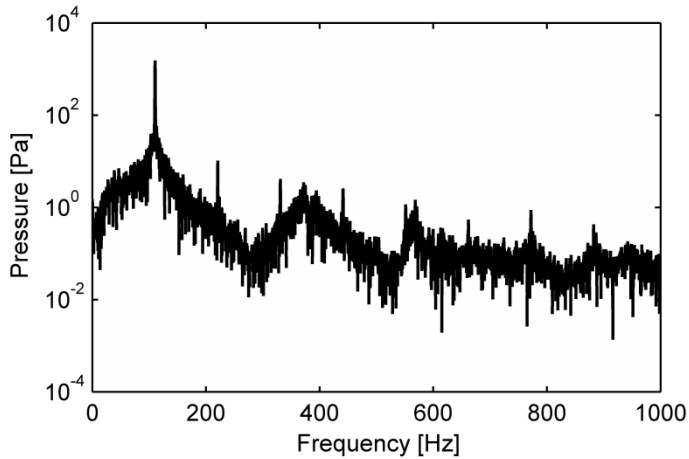


**Figure 4-9: LIMOUSINE version 2 double liner PT 4 pressure spectrum for 40 kW and  $\lambda = 1.80$ . Unstable regime.**

important characteristics of the limit cycle are the non-linear dynamics. These dynamics show up as sharp peaks located at multiple times the main peak frequency and do not correspond to any acoustic mode. In the 60 kW and air factor  $\lambda = 1.80$  particular case, the main perturbation appears at 110.3 Hz and the non-linear oscillations have frequencies at 220, 331 and 441 Hz (2, 3 and 4 times the original instability frequency). The second acoustic mode shows up as a wider peak at 371 Hz (see figure 4-5) and structural dynamics are recorded at 585 Hz. The measured flue gas temperature is 1003 °C in the combustion chamber.

The frequency of the predicted acoustic modes was calculated analytically with the same procedure of the previous section. The first three modes are predicted, for 1000 degrees °C at 110, 259 and 407 Hz and shown in figure 4-10. The first acoustic mode agrees well with the results, while the third mode is slightly overestimated by 7 % in the frequency. The second mode, at 259 Hz, does not show up in the pressure spectrum because there is a node (minimum pressure oscillation) close to the location of the pressure transducer, at 0.22 meter from the burner plane.

Table 4-3 gathers the results from all the measurements in the double liner geometry. It can be noted that the peak frequency (4<sup>th</sup> column) is weakly dependent on the flow rates. The frequency increases with thermal power and air excess factor, represented by Reynolds number ( $Re$ ) based on the upstream duct dimension.

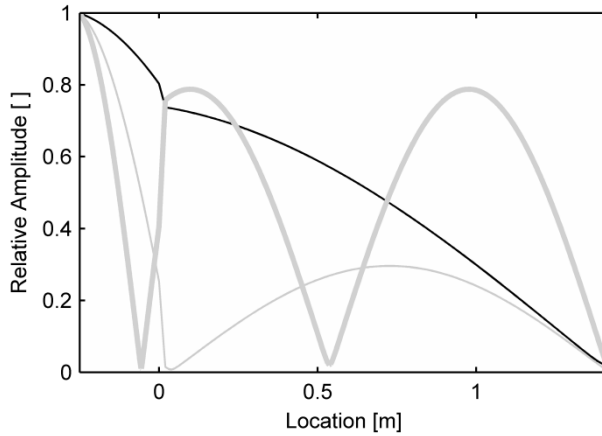


**Figure 4-10: Modal shapes in the double liner configuration. Modes are at 110 (thick black), 259 (thick gray) and 407 Hz (thin gray).**

**Table 4-3: LIMOUSINE version 2 double liner results.**

Th. Power [kW]	Air factor $\lambda$ [-]	Re [-]	Peak Freq. [Hz]	PT 4 Amp. [Pa]	PT 1 Amp. [Pa]	Temp. in Comb. [°C]
40	1.40	7093	102.650	15.534	18.933	942
40	1.60	8106	100.465	26.727	32.632	1074
50	1.40	8866	102.345	35.643	42.369	1100
50	1.60	10133	104.745	64.409	77.924	1070
60	1.40	10640	102.050	62.055	74.919	1196
60	1.60	12160	109.545	1171.100	1384.890	1076
60	1.80	13680	110.005	1552.700	1830.790	1003
60	2.00	15200	110.310	1415.000	1671.020	1003
60	2.20	16720	110.310	1393.500	1643.330	1003

This trend can be attributed to different magnitude of heat transfer losses at for the different operational points, which influence the average flue gas temperature and the speed of sound inside the combustor. The measured peak amplitude is strongly influenced by the mean flow field and will be discussed in the follow-up sections.

## Stability Analysis of LIMOUSINE Version 2

The previous analyses are verified with the mode shape of the pressure profile in the combustor, acquired from the data of the pressure transducers at the successive axial locations (figure 4-11). To adequately compare between the different operational conditions, all magnitudes (top) and phases (bottom) values are normalized with the measured pressure of sensor PT 1, which is the closest to the air inlet. The color of the different profile lines depends on the Reynolds number, with darker lines for higher  $Re$  numbers. Inlet, burner and exit planes are shown with dotted vertical lines in the graph. The measured mode shape is characteristic of a quarter wave mode, similar to the first analytically calculated profile on figure 4-10. The pressure has maximum amplitude in the inlet, (anti-node) and decreases the minimum value towards the open end (node).

The phase is constant in all the length of the combustor, which is a characteristic of standing waves. The overlapping profiles evidence that this setup behavior is reproducible at several operational points and even for large differences in the amplitude of the oscillations. From the experimental observations with the CCD cameras, it was understood that the long flames are a consequence of the poor quality of the fuel and air mixture. Also it can be argued that the  $OH^*$ -chemiluminescence signal captured by the intensified camera may not be representative of the maximum heat release location (flame length  $X_{OH^* max}$ ), since flame is not perfectly premixed. However for a qualitative treatment these measurements would be sufficient to characterize the flame and its stabilization behavior [103].

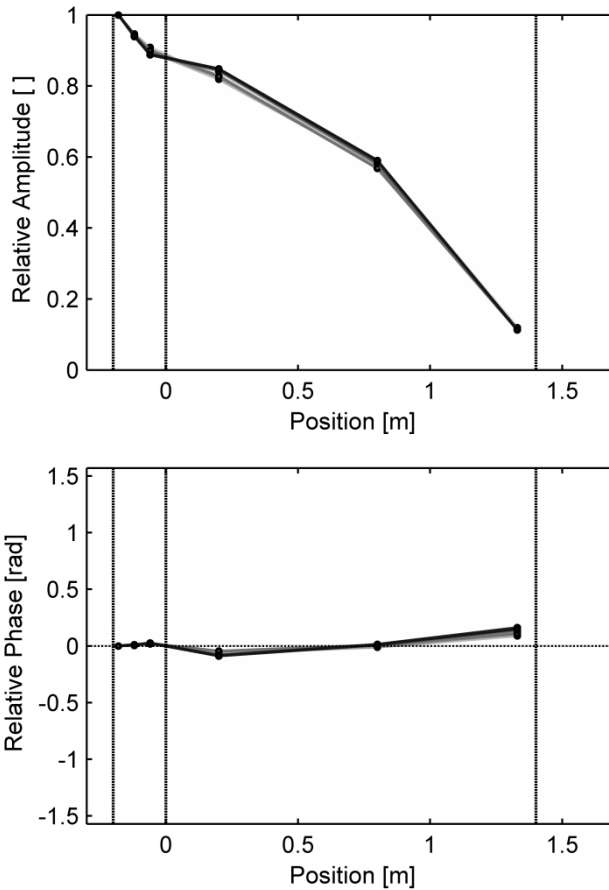


**Figure 4-11: LIMOUSINE version 2 double liner relative magnitude and relative phase of the pressure profile. Darker lines correspond to higher Re numbers.**

The convective time scale  $\tau_{conv}$  is defined as the delay time required for any perturbation in the flow at the point of fuel injection to travel to the location of the flame  $X_{OH^*max}$  with effective mean convective speed  $U_{eff}$  [66]. This can be presented mathematically as

$$\tau_{conv} \sim X_{OH^*max} / U_{eff} \quad (4.1)$$

For the case of 60 kW and air factor  $\lambda = 1.80$ , the  $U_{eff}$  is equal to 9 m/s and  $X_{OH^*max} \sim 100$  mm, thus the time delay  $\tau_{conv}$  results in 11.1 millisecond. The first eigenmode frequency  $f_1$  for the simple length liner is 175 Hz, which has an acoustic time period  $T = 1/f_1$  of 5.7 ms. Evaluating these two values, the period

of oscillation is small compared to the convective time scale obtained earlier. According to Lieuwen [18, 46] there can be an active feedback loop between the flame and acoustics whenever the convective time scales are of the same order of magnitude as of the acoustic time period. The relationship is represented mathematically with the expression (4.2).

$$C - \frac{1}{4} < n * \tau_{conv} / T < C + \frac{1}{4} \quad (4.2)$$

where  $C \sim 1$  is a constant that depends on the type of boundary/fuel conditions and  $n$  number. Although from figure 4-8 a modest amplitude maximum can be observed in the pressure spectrum plot around 175 Hz ( $T = 5.71$  ms), the feedback is not strong enough to bring the combustor into LCO. From the expression (4.2),  $\tau \sim 9$  millisecond and therefore it can be concluded that significant feedback between the pressure and flame was not possible and a LCO was not achieved. The characteristic times of the two dynamics is so different that it actually prevents any kind of interaction between acoustic and flame.

In the double liner case with an unmodified burner and the same operational parameters (60 kW power and  $\lambda = 1.60$ ) the flame stabilization time remained at  $\tau_{conv} \sim 11.1$  millisecond. However, the acoustic time period  $T$  increased to 9.1 ms ( $f_1 = 110$  Hz) in this configuration. In this current situation  $\tau_{conv} \sim 1.22 T$ , which closely satisfies the relationship (4.1) and the flame is able to provide significant coupling between combustion and acoustics. Thus the LCO and the feedback loop are expected to develop in the double liner configuration and this was indeed the observed case. The LCO was more prominent at higher flow rates, as this reduces the convective time scales further and  $\tau_{conv}$  becomes closer to the order of  $T$ . Flow rates have a negligible influence on the frequency of the LCO, but increase dramatically its amplitude. The results based on the expression (4.2) should be only valid for one of the many feedback processes that can produce the instability (figure 7-1) and other feedback mechanisms should be investigated to ensure the combustion stability. It is also very important that the accumulated acoustic energy due to the feedback process must be greater than the total acoustic losses to bring the system into an unstable regime. Once the system reaches the LCO, a non-linear saturation mechanism [53] will reduce the feedback rate and the oscillations reach constant and finite amplitude.

In the double liner configuration it can be concluded that there is a “match” of the convective time scales and the acoustic time period, which results in development of the LCO [104].

Further analysis is carried out to investigate the behavior of the unstable and stable points. As motivated from previous research [99, 105], the measured frequencies are represented by dimensionless quantities such as the Helmholtz (4.3) number and the Strouhal number. The Helmholtz ( $He$ ) number presented here is a modification of the classical definition  $He = fL/c$  to adapt it to systems where the speed of sound is not constant. The final speed of sound is the average of the speed of sound at each individual element weighted by its relative length. The formula may be used for as many elements as needed, but in the calculations the elements are limited to two:  $j = \text{upstream, downstream}$ .

$$He = f \frac{L}{c_{comp}} \quad (4.3)$$

$$c_{comp} = \frac{\sum L_j c_j}{\sum L_j} \quad (4.4)$$

The Strouhal ( $St$ ) number (4.5) is used to describe oscillating flow mechanisms, such as vortex shedding. The number is defined by the frequency  $f$  and ratio of the characteristic length  $h$  and the characteristic speed of the upstream fluid  $u$ .

$$St = f \frac{h}{u} \quad (4.5)$$

Helmholtz and Strouhal numbers can be used to characterize the origin of the LCO, based on their trends and distribution as function of the Reynolds number. In a limit cycle dominated by vortex shedding, the Strouhal number is constant with the Reynolds number while the Helmholtz number increases linearly. However, in an acoustically driven Limit Cycle, Helmholtz number is constant and Strouhal number varies hyperbolically with Reynolds number. The latter case is the observed behavior in the experiments, figure 4-12, confirming the limit cycle is indeed an acoustic phenomenon.



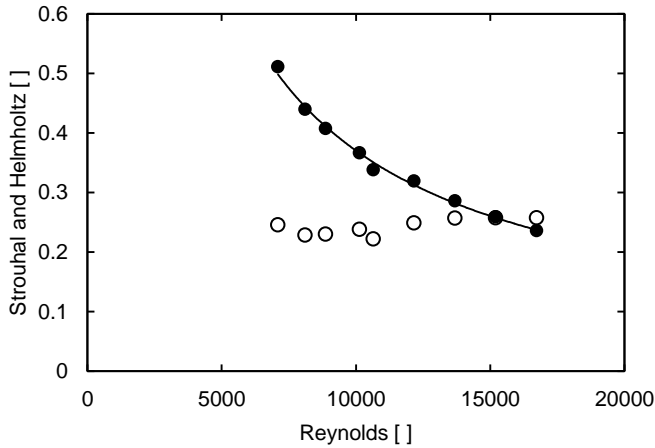


**Figure 4-12: LIMOUSINE version 2 double liner dimensionless numbers for all operating parameters. ○ Helmholtz number, ● Strouhal number.**

The Strouhal number follows a power law  $St = 1076.9 Re^{-0.866}$ , while the Helmholtz number is 0.25. Because the relationship between the wavelength and frequency is  $c = \lambda f$ , the Helmholtz number can be connected to the characteristic relative wavelength of the oscillation by (4.6).

$$\frac{1}{He} = \frac{c}{fL} = \frac{\lambda f}{fL} = \frac{\lambda}{L} \quad (4.6)$$

The measured value of  $He = 0.25$  corresponds to a wave length that is four times the combustor length and therefore the fundamental mode of an open-closed cavity. Hence, the system is now oscillating as a quarter wave resonator. To fully understand the thermoacoustic mechanism, figure 4-12 has to be observed together with corresponding heat release intensity from the Photo Multiplier Tube (PMT) in figure 4-13. The PMT intensity is considered directly proportional to the heat release rate fluctuations and it shows a strong correlation with the pressure fluctuations during LCO.

The phase delay between the PMT and pressure PT 4 is plotted in figure 4-14. The amplitude plot clearly shows a low amplitude regime sharply transforming around  $Re = 10000$  into a high amplitude unstable regime. A clear shift in phase delay values of 90 degrees can be observed at the bifurcation of the two combustion regimes. In the investigation performed by Sivakumar et al [99] in a similar combustor they were also able to identify the two flame regimes.

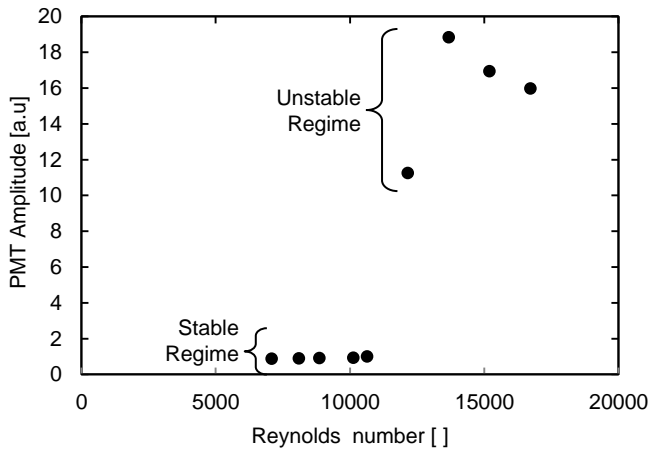


**Figure 4-13: LIMOUSINE version 2 double liner heat release rate.**

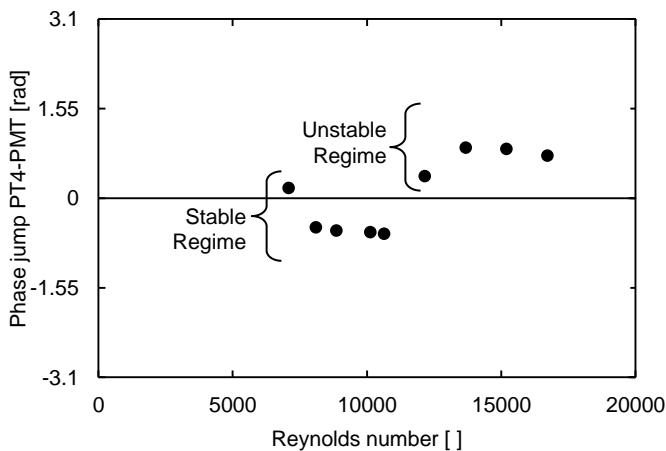


**Figure 4-14: LIMOUSINE version 2 double liner pressure – heat release phase jump.**

In the low frequency range ( $Re < 2.4 \cdot 10^4$ ), their work reported trends of Helmholtz and Strouhal similar to those presented above, but in their case, these oscillations are entirely linked to low amplitude perturbations. For their high Reynolds case, the trends of the dimensionless numbers  $He$  and  $St$  are different from the LIMOUSINE combustor. In their research, the Helmholtz number linearly increases with Reynolds and the Strouhal number is constant. The large amplitudes recorded in such regime suggest the presence of a flow-acoustic lock-on. Under these conditions, the sound excited by the vortex shedding is coupled with a strong acoustic feedback, but this is not the case seen in the research of the University of Twente.

The study of Chakravarthy et al [105] in a dump combustor showed similar results to LIMOUSINE. They also observed a flow/geometric regime that resulted in constant Helmholtz number and hyperbolically decreasing Strouhal number, which indicate the absence of flow-acoustic lock on. In the current investigation, the second process is applicable, where the flow-acoustic lock on is not promoted as pointed by the evolution Strouhal number not reaching constant values.

### **LIMOUSINE Version 3 Single Liner**

After the investigation with burner version 2, the new burner version 3 was installed and tested. The first tests were done in cold flow conditions without any acoustic excitation.

#### ***Cold Flow Observations***

Cold flow observation included acoustic characterization of the combustor without mean flow and the aerodynamic effects in the burner. For the latter, the pressure spectrum was measured for the same operating parameters that will be studied afterwards with combustion and external acoustic excitation was not used. The spectrum was measured with the pressure transducer PT 4, which is the closest to the burner in the downstream duct and result are in figure 4-15. The color of the lines is related to the different air mass flow rates supplied to the combustor. Higher mass flow rates correspond to darker lines.

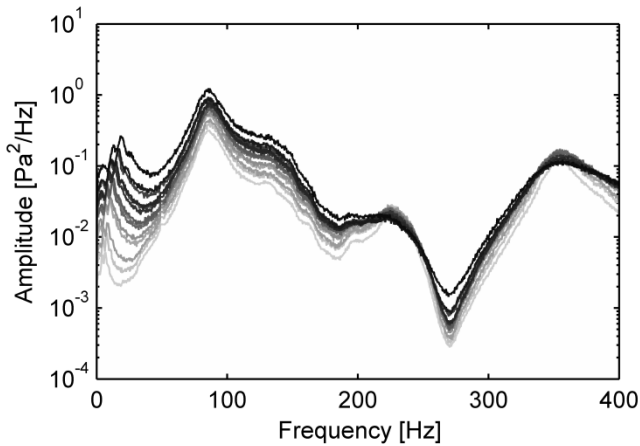


**Figure 4-15: LIMOUSINE version 3 single liner cold flow PT 4 pressure spectrum. Darker lines correspond to higher Re number.**

Figure 4-15 main peaks correspond to the acoustic modes at room temperature, already shown in the previously at 86, 223 and 353 Hz. The frequency of the eigenfrequency is independent of the mass flow rate, but higher mass flows result in larger amplitudes. In the very low frequency range, 5 to 25 Hz, the frequency shift of the successive lines seems to indicate the presence of a flow dependent perturbation. These perturbations are related to vortex shedding from the wedge or the edge of the side bodies and have a smaller magnitude than the acoustic oscillations.

### ***Combustion Experiments***

The upgrade from LIMOUSINE version 2 combustor to LIMOUSINE version 3 was successful and the version 3 combustor was finally able to operate in flames with large amplitude thermoacoustic oscillations. The flame behavior in version 3 was explored for the maximum range allowed by the air and fuel control valves, excluding very rich flames with mixture air factor lower than unity. All possible combinations of 4 thermal power and 4 mixture settings were tested, resulting in 16 different air and fuel conditions (figure 4-16). Experiments showed several well-defined flame regimes that depended on the air and fuel flows. Most of the cases were repeatable and always operate with the same combustion regime, but there was a small group of operating conditions that are able to sustain flames of either regime. The most important parameter for the combustor stability is the air factor. Overall, limit cycle is always present for flames of air factor  $\lambda = 1.60$  or

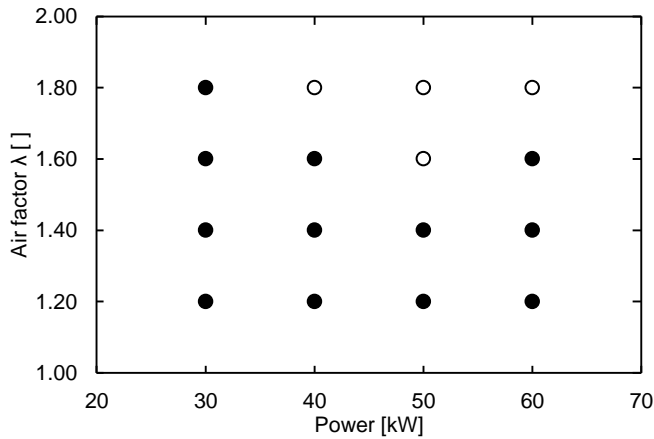


**Figure 4-16: LIMOUSINE burner version 3 single liner stability map: ○ stable combustion, ● unstable combustion.**

richer. For a given thermal power, the transition from unstable to stable flame behavior will happen at leaner values than the transition from stable to unstable flames.

### *Stable Regime*

The stable regime is characterized by a large flame and a relatively low amplitude combustion roar noise. The roar amplitude is constant in time and can be

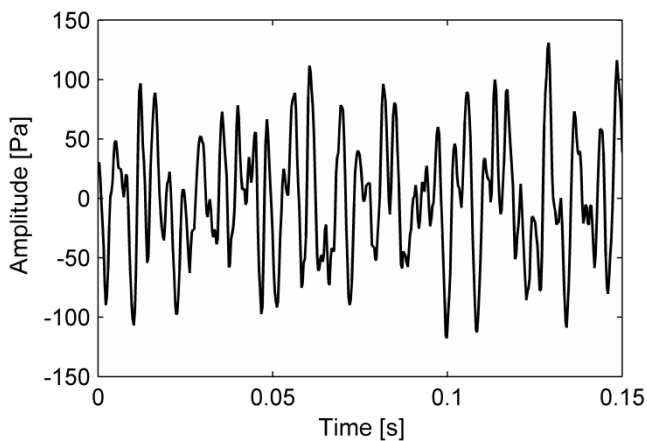


**Figure 4-17: LIMOUSINE version 3 single liner PT 4 pressure time trace for 40 kW and  $\lambda = 1.80$ . Stable regime.**

explained by the turbulent flow fluctuations combined with flame dynamics and damping the effect of the combustor acoustics. All the previous explain the chaotic and irregular measured time trace of figure 4-17. The amplitude of the signal is in the order of tenths of Pascal, but some perturbations reach up to 140 Pascal.

The corresponding pressure spectrum, in figure 4-18, reveals that the signal is mostly composed by three peaks very close to each other, giving the impression that there is only broadband dynamics in the 50 to 250 Hz range. The first peak is at 57 Hz, and it can be related to the periodic shedding of vortices as the fluid goes through the burner slits. There is yet another peak at around 175 Hz, which agrees well with the predicted first acoustic mode. The spectrum also shows some small perturbations at 250 Hz while the dynamics around 550 to 700 Hz are most probably related to the structural modes. The overall oscillation magnitude is very low.

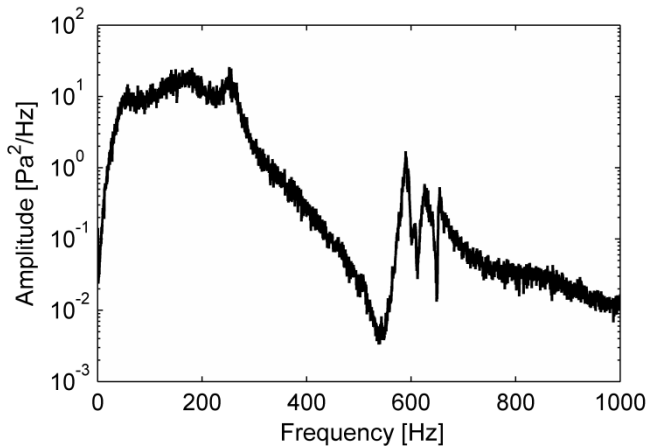


**Figure 4-18: LIMOUSINE version 3 single liner PT 4 pressure spectrum for 40 kW  $\lambda = 1.80$ . Stable regime.**

### ***Unstable Regime And Limit Cycle***

The stable combustion regime is often associated with lean combustion conditions. However, in the LIMOUSINE version 3 setup, the combustor enters into a high amplitude combustion regime as the mixture air factor is reduced. The roar noise from the stable regime transforms into a humming sound that can reach almost 4000 Pascal of amplitude in the upstream end for the most extreme

cases. Once this regime is fully developed, which takes less than one second, the amplitude of the oscillations remains regular over time. The 50 kW power and  $\lambda = 1.40$  flame, figure 4-19, is a perfect example of this behavior.

Figure 4-20 shows the derived power spectral density of the signal. The periodic dynamic of the signal in the time domain appears as a narrow and tall peak at 257 Hz surrounded by many secondary peaks, which are the non-linear dynamics. Non-linear dynamics always appear in the unstable combustion regimes and they

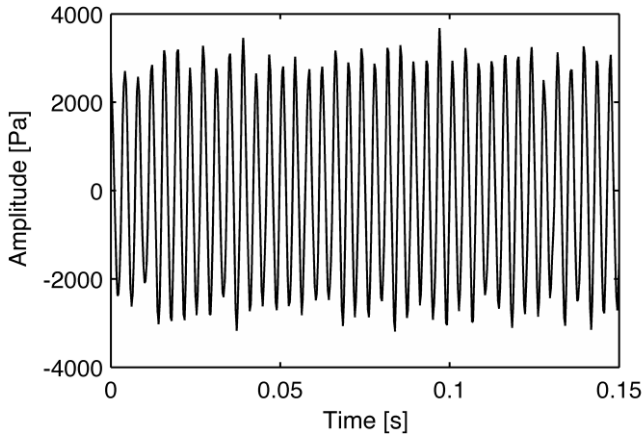


**Figure 4-19: LIMOUSINE version 3 single liner PT 4 time trace for 50 kW and  $\lambda = 1.40$ . Unstable regime.**

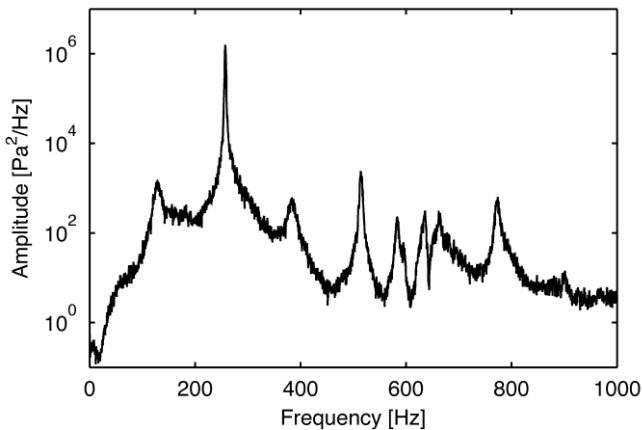


**Figure 4-20: LIMOUSINE version 3 single liner PT 4 pressure spectrum for 50 kW and  $\lambda = 1.40$ . Unstable regime.**

can be considered as a trademark of the LIMOUSINE combustor. Their characteristic frequencies at 128 Hz, 383 Hz and 541 Hz are half, one and half and two times the instability frequency. The peak at 774 Hz is, with good accuracy,  $3 \times 257$  Hz and it is therefore a non-linear dynamic related to the main peak. The structural modes shown in this figure are at around 600 Hz.

For the rest of the points, table 4-4 indicates the magnitude in the most upstream pressure transducer PT 1, magnitude in the pressure transducer closest to the flame (PT 4) and temperature in the combustion chamber. The Reynolds numbers of this combustor are moderately high, from 4560 to 13680. The measured flue gas temperatures downstream of the burner are lower than the expected adiabatic flame temperature, due to radiation losses through the optical section and from the liner walls.

**Table 4-4: LIMOUSINE version 3 single liner results.**

Th. Power [kW]	Air factor $\lambda$ [-]	Re [-]	Peak Freq. [Hz]	PT 4 Amp. [Pa]	PT 1 Amp. [Pa]	Temp. in Comb. [°C]
30	1.20	4560	245.625	801.646	2067.181	1203
30	1.40	5320	215.313	879.659	1964.668	1150
30	1.60	6080	197.500	990.271	2021.461	1101
30	1.80	6840	184.688	853.633	1646.973	1050
40	1.20	6080	261.563	1439.421	3289.729	1256
40	1.40	7093	234.063	801.086	1757.332	1200
40	1.60	8106	212.813	676.541	1410.824	1152
40	1.80	9120	252.188	4.920	10.089	1128
50	1.20	7600	267.813	2068.94	4031.266	1298
50	1.40	8866	257.188	1220.578	2208.811	1233
50	1.60	10133	191.563	10.671	18.627	1231
50	1.80	11400	224.380	6.464	10.801	1163
60	1.20	9120	271.880	2846.97	4825.205	1339
60	1.40	10640	267.500	2717.73	4081.029	1268
60	1.60	12160	245.000	1520.19	2417.731	1220
60	1.80	13680	227.188	14.690	319.738	1194



### ***Heat Release And Velocity Fields***

The flame of the LIMOUSINE combustor was also studied with advanced optical techniques. The spontaneous OH\* emission of the flame was recorded with a CCD camera aimed to the lateral side window. For every point, the flame is represented by the ensemble average of the movie frames. The flame is symmetric, so it is possible to compare the two regimes flame regimes by only showing half of the frame. In figure 4-21, the LHS corresponds to the unstable regime, while the right hand side is the stable burning regime. In the unstable regime, the flame stabilizes as a reacting mixture on top of the wedge. There is not any reaction recorded within one bluff body distance downstream of the burner and the flame length is limited to two to three times this characteristic length. In the stable regime, the flame has two flamelets, each of them anchored to the edges of the bluff body holder. Flames are thin, straight and symmetric, and its length is indeed much longer than the optical section. However, they are not as bright as the unstable flame.

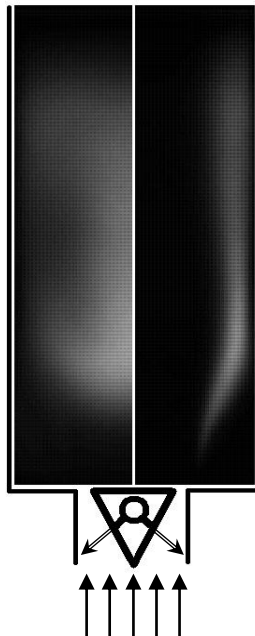


**Figure 4-21: LIMOUSINE version 3 single liner average OH\* emission. unstable regime (LHS) stable regime (RHS). Arrows indicate air and fuel flows.**

In addition to heat release and flame shape, the velocity field was measured using PIV. This technique was not available in the University of Twente, so measurements were done by the LIMOUSINE project fellow Thomas Sponfeldner in a twin unit of the version 3 single liner combustor at Imperial College. The vertical component of the velocity was measured once per regime. It was not possible to complete the measurements at Imperial College at the same experimental conditions studied by the University of Twente and the measurements were done at lower Reynolds number. Despite this fact, valuable information can still be obtained from the plots and figures. The left hand side of figure 4-22 shows the vertical velocity contours in the middle plane of the combustor for an unstable regime point (35 kW and air factor  $\lambda = 1.30$ ) and the right hand side show the stable point corresponding to 25 kW and air factor  $\lambda = 1.45$ . As expected from the burner design, velocity profiles are symmetric.

The main feature of the contour plot for the unstable flame is the presence of a strong recirculation zone on top of the wedge, approximately at 40 mm downstream of the wedge, where a velocity of 10 m/s in the upstream direction

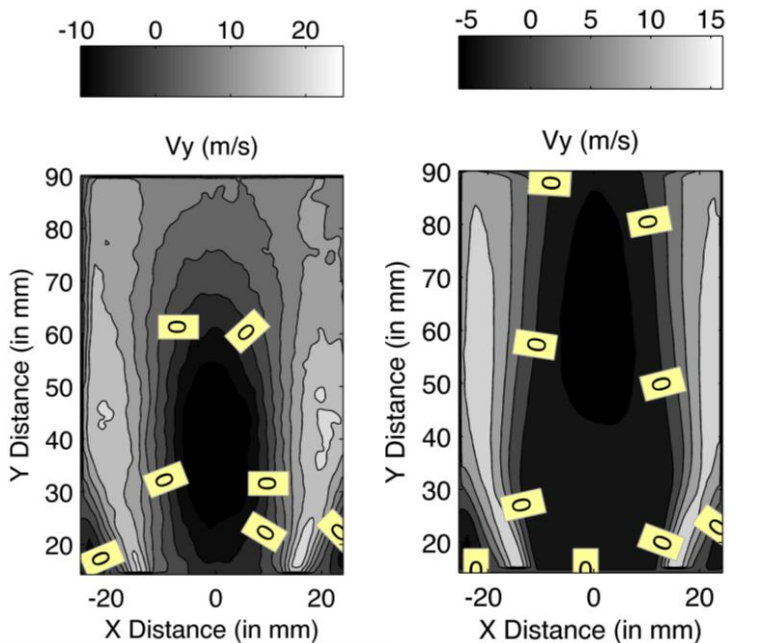


**Figure 4-22: LIMOUSINE version 3 single liner vertical velocity contours for unstable regime (LHS) and stable regime (RHS). Data from Imperial College London, with permission.**

can be found. Two small recirculation zones develop as well in the bottom corners of the combustor. Between the two zones, there are the large jets from the burner slits with velocities of the order of 20 meters per second. Large turbulence levels of the flame and the pressure perturbations cause the rough profiles, while the stable regime shows smoother contour edges. The size of the recirculation area is bigger in the unstable case but the point with the maximum negative speed is located at 60 mm downstream of the wedge.

### *Discussion Of Results*

The behavior of LIMOUSINE combustor version 3 is very different from the version 2 observed behavior. To compare between the two cases, the pressure

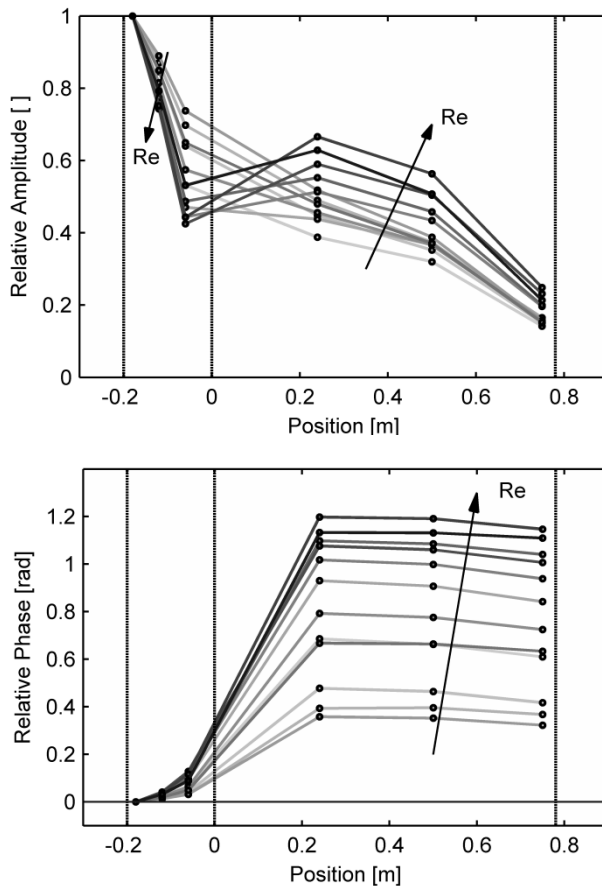


**Figure 4-23: LIMOUSINE version 3 single liner relative magnitude and relative phase of the pressure profile. Unstable regime.**

profiles along the combustor are used. Following the same approach of the previous section, magnitude and phase were normalized using the maximum of the pressure sensor PT 1 measurement. To avoid confusion to the reader, stable and unstable regimes are plotted in different charts.

The unstable profiles are plotted in figure 4-23, in which vertical lines show the inlet, wedge and exit of the combustor. The line color indicates the measured Reynolds number in the upstream end. Darker gray shade means higher Reynolds number. Within the unstable regime, two trends can be identified. From the magnitude point of view, for low Reynolds numbers, the pressure oscillation has a quarter wave mode shape, with the maximum pressure amplitude located in the entrance of the combustor and the minimum at the exit (top panel). The lower panel shows that the pressure phase is constant in the two chambers and the jump across the burner is small. However, as the Reynolds number increases the pressure profile shape shows larger discontinuity between the two ducts. In the most extreme cases, the pressure amplitude just upstream the burner is even lower than the pressure amplitude after it. Velocity in the burner slits may be momentarily reversed during the limit cycle, and together with the measured phase difference, it points to a partial decoupling of the pressure in the two chambers. In decoupled system, each of the chambers can vibrate independently of the other ones. The total number of eigenmodes of the system is greater, so the chances of an acoustic eigenmode interacting with flame dynamics are higher.

The pressure distribution was also calculated and plotted for the stable regime in figure 4-24. The profile shape is on the top pane and the phase is plotted in the lower pane. The overall behavior does not seem as consistent as two of the four measured stable regime profiles are somewhat similar to the unstable regime. This is the case of the points with the lower Reynolds number among the stable ones, which are the closest to the unstable conditions as well. Flame for particular parameters seem to have a mixed behavior, with all the characteristic of a unstable point but low amplitudes. As the inlet flow Reynolds number increases and the air flow is larger, the pressure profile evolves into the expected quarter wave mode, which was already seen in other LIMOUSINE configurations (version 2 and double liner). The phase jump in the burner is 0.4 radians for the purely stable points and 1.2 radians for the others.

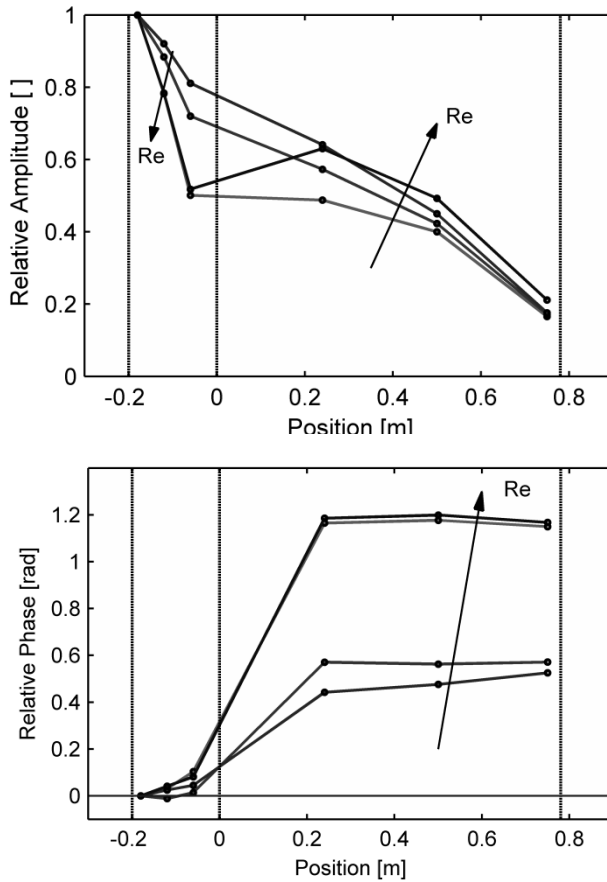


**Figure 4-24: LIMOUSINE version 3 single liner relative magnitude and relative phase of the pressure profile. Stable regime.**

The dimensionless numbers Helmholtz and Strouhal also provide information about the combustion dynamics in figure 4-25. Including all the measured points from both combustion regimes, the Strouhal number varies from 1.9 to 0.6 following a curve  $St = 5460.2 Re^{-0.95}$  and the Helmholtz number is constant at 0.4, pointing again to the acoustic origin of the instability.

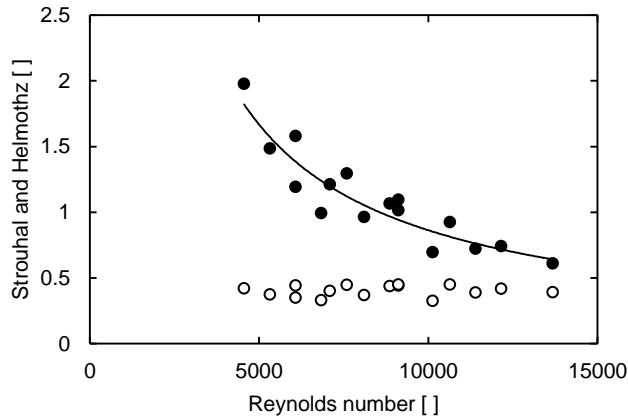


**Figure 4-25: LIMOUSINE version 3 single liner dimensionless numbers for all operating conditions. ○ Helmholtz number, ● Strouhal number.**

The associated relative wavelength of the oscillation is  $\lambda/L = 1/0.4 = 2.5$ . In the current configuration under study,  $L$  is 1.05 meter, which gives  $\lambda = 2.563$  m. Since the combustor is a closed-open cavity, and the fundamental mode is  $\lambda/4$  the associated wavelength is 0.656 m. This roughly corresponds to the length of the combustion chamber liner, leaving about 0.15 m for the source region of the flame. If the combustor flame is in the unstable regime, only this last fraction of the volume is resonating and responsible for the frequency of the combustion. The amplitudes of the perturbation produced by the flame are so high that they seem to prevent the formation of a standing wave in the full combustor length (plenum and combustion chamber). Subsequently, the burner and upstream duct behave like oscillators. Figure 4-26 shows the measured amplitude of the PMT and how the values bifurcate towards large perturbations or stable situations. The figure is less clear because there are points with an intermediate behavior at  $Re = 8866$  and  $Re = 12160$ .

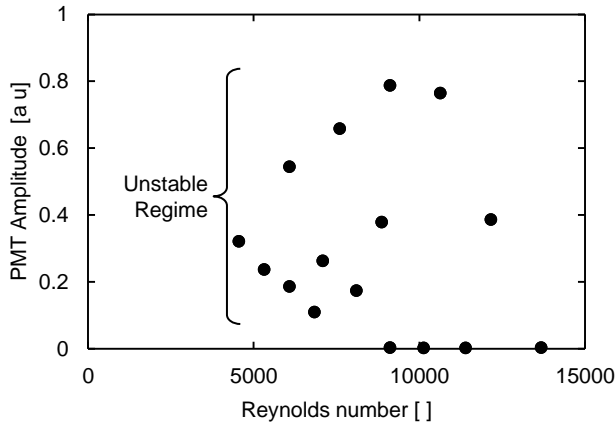


**Figure 4-26: LIMOUSINE version 3 single liner heat release rate.**

The change of regime is even clearer in the phase delay plot between the pressure oscillations and the heat release rate, in figure 4-27 below.

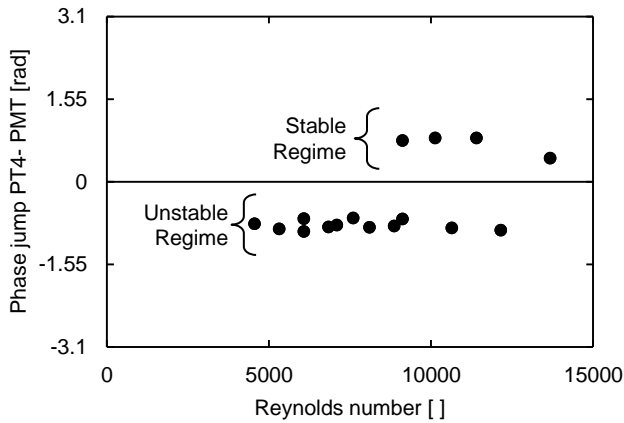


**Figure 4-27: LIMOUSINE version 3 single liner pressure – heat release phase jump.**

The unstable regime values show a constant phase delay around -0.9 radians and suddenly jumps 1.6 radians to reach 0.7 radians in the stable cases. This jump is enough to stop the feedback loop and the fulfillment of the Rayleigh criterion.

## LIMOUSINE Version 3 Double Liner

It was also possible to install an additional liner in LIMOUSINE version 3 combustor. The research in this configuration will lead to a better understanding of the time delays role in the limit cycle and will provide data to compare with the version 2 combustor and double liner.

The combustion dynamics with the extended combustion chamber length revealed a new flame regime that had never been observed before. In close to stoichiometric mixture conditions, the combustor operates in LCO regime, like in the single liner configuration. For lean mixtures, the stable regime is observed again. The new combustion regime appears between the two known regimes and features mixed characteristics from both regimes: It shares the pressure profile and the dimensionless numbers distribution with the stable case, but has oscillation amplitudes comparable to the unstable case. Once more, the transition between the regimes is not very repeatable and shows hysteresis effects. The distribution of the three regimes is in figure 4-28.

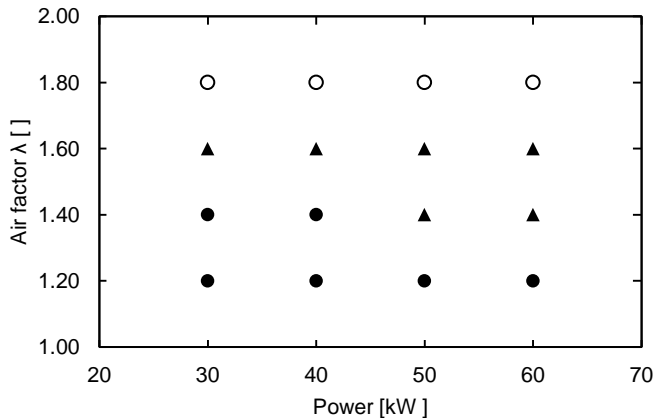


Figure 4-28: LIMOUSINE version 3 double liner stability map: ○ stable combustion, ▲ intermediate regime combustion, ● unstable combustion.

### *Stable Regime*

In the stable regime, the double liner configuration behavior is not different from the single liner configuration, in which the flame produces a similar combustion roar (with lower tone) to the single liner configuration. An example of this kind of combustion is the point 40 kW and air factor  $\lambda = 1.80$ . The spectrum in figure 4-29



shows pressure dynamics that reminds of the LIMOUSINE version 2 double liner during the stable regime. The main dynamics at 92 Hz and at 375 Hz are related to the first and third acoustic modes of the combustor (figure 4-10) but have low amplitudes. The structural modes are present in the usual range around 600 Hz.

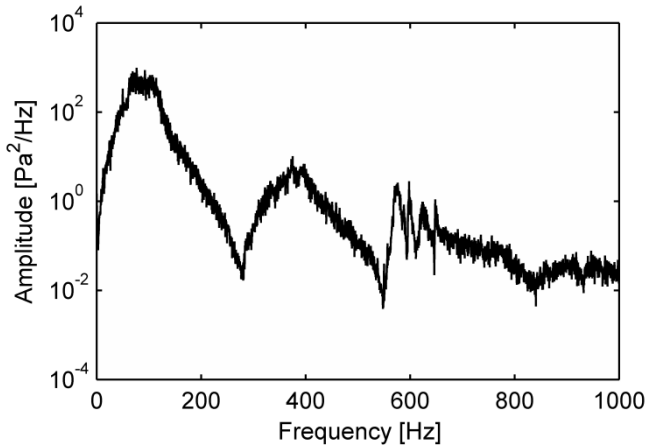


**Figure 4-29: LIMOUSINE version 3 double liner PT 4 pressure spectrum for 40 kW and  $\lambda = 1.80$ . Stable regime.**

### *Unstable Regimes*

The unstable regime develops for low air flows and near to stoichiometric mixtures, and produces a steady and large amplitude pressure oscillation. The point 40 kW and  $\lambda = 1.20$  is the chosen example of this regime. The spectrum at figure 4-30 shows the greatest dynamics at a frequency of 179 Hz. Similar to the version 3 single liner, the acoustic eigenmodes are not visible in the spectrum. As a consequence of the large combustion oscillations, there are some non-linear secondary dynamics. The most representative are located at 359 Hz ( $\sim 2 \times 179$ ) and 90 Hz ( $\sim 179/2$ ). The structural perturbation is present in the spectrum around 600 Hz and the spectrum decays until the end of the measured 1000 Hz range.

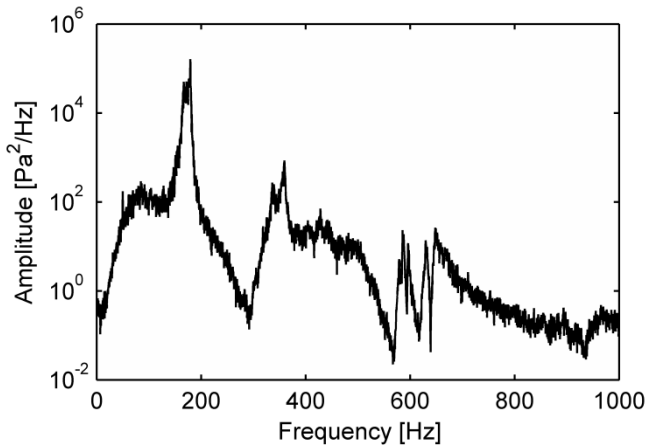


**Figure 4-30: LIMOUSINE version 3 double liner PT 4 pressure spectrum for 40 kW and  $\lambda = 1.20$ . Unstable regime.**

The example of the third *intermediate* regime is given by the pressure spectrum corresponding to the 50 kW power and air factor  $\lambda = 1.60$  case of figure 4-31. The flame emits a large amplitude humming sound that lacks of the nonlinear effects. The perceived sound is less rough and harsh than the usual unstable regime noise. The main peaks at 92 Hz and at 372 Hz are related to the first and third acoustic resonance in hot conditions for the double liner configuration (see figure 4-10) and identical to the pressure LIMOUSINE version 3 double liner (figure 4-29).

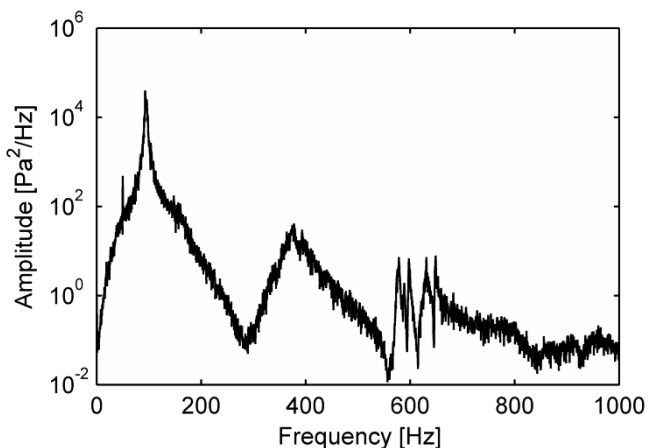


**Figure 4-31: LIMOUSINE version 3 double liner PT 4 pressure spectrum for 50 kW and  $\lambda = 1.60$ . Intermediate regime.**

Additionally, the pressure profile of the second acoustic mode is small in the vicinity of the pressure transducer PT 4 (figure 4-10) and this explains why it is not visible in the measured pressure spectrum.

An overview of all the experimental results is given in table 4-5. For each point, it shows the corresponding Reynolds number, amplitudes at two locations, frequency of the instability and temperature in the combustion chamber.

**Table 4-5: LIMOUSINE version 3 double liner results.**

Th. Power [kW]	Air factor $\lambda$ [-]	Re [-]	Peak Freq. [Hz]	PT 4 Amp. [Pa]	PT 1 Amp. [Pa]	Temp. in Comb. [°C]
30	1.20	4560	160.313	427.242	626.593	1197
30	1.40	5320	142.813	707.247	965.599	1145
30	1.60	6080	85.625	45.156	54.452	1135
30	1.80	6840	81.875	21.541	25.851	1105
40	1.20	6080	165.000	229.347	337.434	1264
40	1.40	7093	168.750	499.722	718.221	1213
40	1.60	8107	95.938	99.599	66.100	1195
40	1.80	9120	71.875	21.551	25.696	1140
50	1.20	7600	179.688	460.120	507.367	1313
50	1.40	8867	168.750	46.300	58.222	1276
50	1.60	10133	92.813	136.566	166.292	1224
50	1.80	11400	77.188	41.419	48.961	1168
60	1.20	9120	180.313	557.556	836.276	1352
60	1.40	10640	115.000	103.364	132.925	1318
60	1.60	12160	99.375	353.100	430.912	1258
60	1.80	13680	93.438	40.000	381.861	1226

### ***Heat Release***

In the version 3 double liner configuration, the flame spontaneous OH\* emission was recorded with the CCD camera aimed at the side window and the ensemble averaged movie frames picture is shown in figure 4-32. Similar to the previous cases, flames are symmetric. The right hand side of the figure presents the stable regime and in the left hand side, figure shows the unstable regime. The unstable case has longer reacting zone than the stable cycle, but smaller than the zone of

the single liner burner flame during the unstable regime. This agrees with the previous conclusion that the feedback loop only appears with significant amplification in the unstable regime.

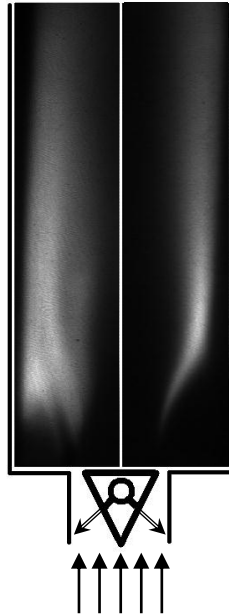


**Figure 4-32: LIMOUSINE version 3 double liner averaged OH\* emission. Unstable combustion (LHS), Stable and intermediate regime (RHS).**

### *Discussion Of Results*

The following section presents the analysis of the experimental results from the version 3 for the two liner construction. The analysis starts with the identification of the instability driving mechanism from the pressure profile of the combustor. The maximum complex pressure at PT 1 is used to normalize the rest of the data. The profile of the unstable cases is shown in figure 4-33. Each of the lines of the figure correspond to a specific Reynolds number and its plotted in a different gray color. The figure also shows the inlet, burner and exit plane with vertical lines. The behavior of the pressure mimics the LIMOUSINE version 3 single liner, including the observed decoupling between the combustion chamber and the plenum, but at lower magnitude.

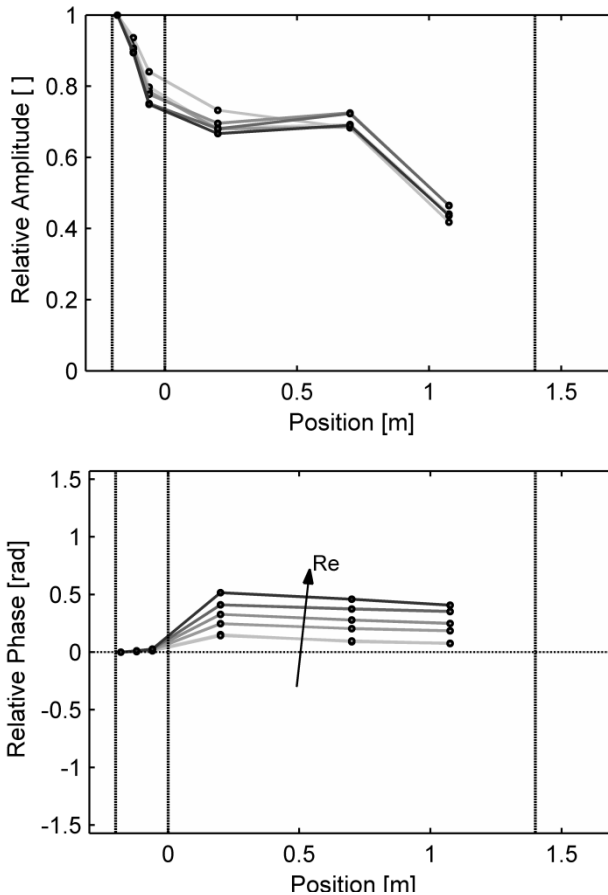


**Figure 4-33: LIMOUSINE version 3, double liner relative magnitude and relative phase of the pressure profile. Unstable regime.**

In the next figure 4-34, the stable and intermediate regime pressure profiles are plotted together. These regimes share the same quarter wave profile in magnitude and constant phase over the combustor. It is remarkable that despite the difference of almost one order of magnitude, both profiles match to a high extend in magnitude. The phase jump upstream and downstream of the burner increases with larger Reynolds number, but is less than 0.5 radian in the 60 kW and  $\lambda = 1.80$  case.

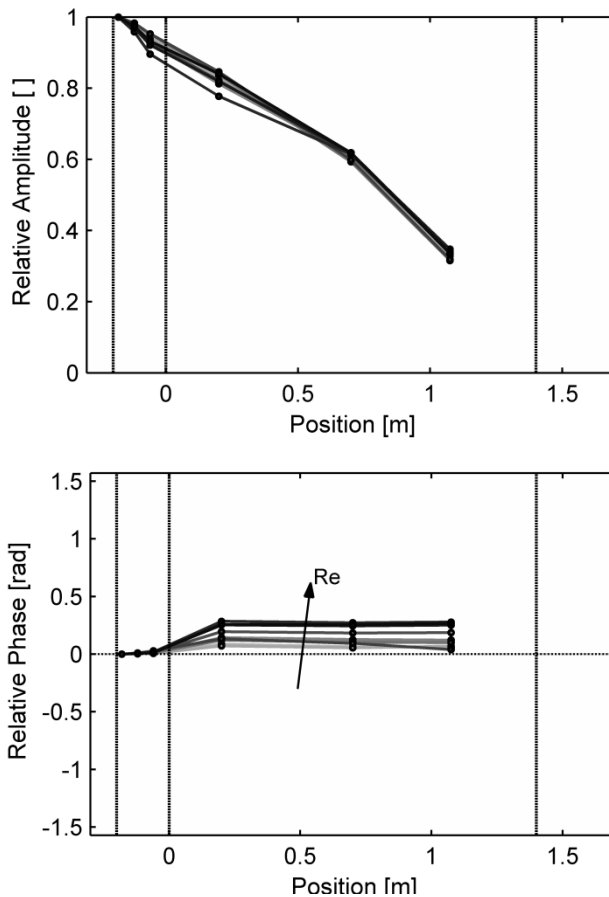


**Figure 4-34: LIMOUSINE version 3 double liner relative magnitude and relative phase of the pressure profile. Stable and intermediate regimes.**

The measured Strouhal and Helmholtz numbers corresponding to version 3 double liner tend to cluster in two different areas (figure 4-35), but they keep the same pattern within each group. The unstable cycle, associated with the lower Reynolds numbers and near stoichiometric mixture, presents relatively high Helmholtz number, around 0.4, and the Strouhal number follows the trend  $St = 977.07 Re^{-0.792}$ . The stable and intermediate regimes are clustered together, linked to higher Reynolds number and leaner mixture. They repeat the same distribution pattern of the unstable case, but in a different graph location. The Strouhal number points are now in the curve  $St = 989.85.07 Re^{-0.869}$ , and Helmholtz number reduces from the previous 0.4 to 0.22.

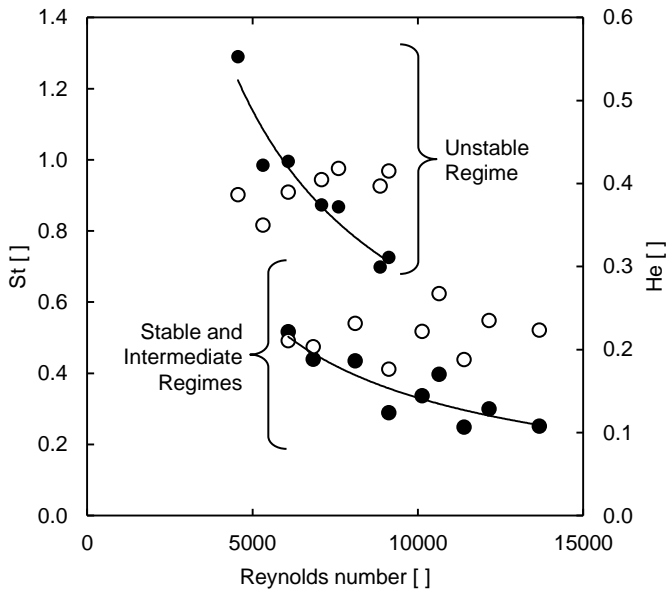


**Figure 4-35: LIMOUSINE version 3 double liner dimensionless numbers for all operating conditions: ○ Helmholtz number, ● Strouhal number.**

Helmholtz numbers of 0.22 are related to a fundamental quarter wave mode in all combustor, as seen in LIMOUSINE burner version 2 double liner configuration. The wavelength associated with unstable mode ( $He = 0.4$ ) is calculated with the previously used equation (4.6), resulting in 4.175 m wavelength. Thus, a length cavity of 1.04 m can resonate with a quarter wave mode. This is the very same mechanism of the version 3 single liner, although flame region is longer ( $1.37 - 1.04 = 0.33$  m versus 0.15 m). This not so compact flame is less efficient in the decoupling of the combustor. The analysis for the double liner combustor finishes with the heat release amplitude graph (figure 4-36) and the plot of the phase difference between heat release rate and pressure (figure 4-37). In the heat release rate graph, the unstable regime has higher heat release values than the other two regimes. In the phase jump plot, the relative jump between unstable and the other two regimes is almost  $\pi$  radians. If the energy transfer between flame and acoustics is enough to sustain the feedback loop, the  $\pi$  radians then should stop it, according to the Rayleigh criterion. This indicates that the intermediate cycle may achieve large perturbation amplitudes, but without powerful amplification by the thermoacoustic phenomenon.

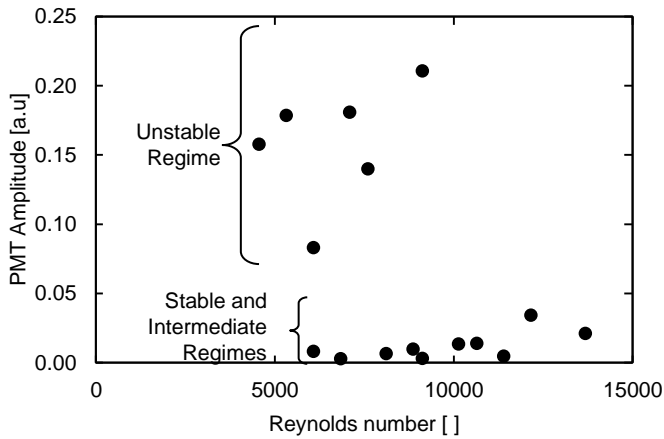


Figure 4-36: LIMOUSINE version 3 double liner heat release rate.

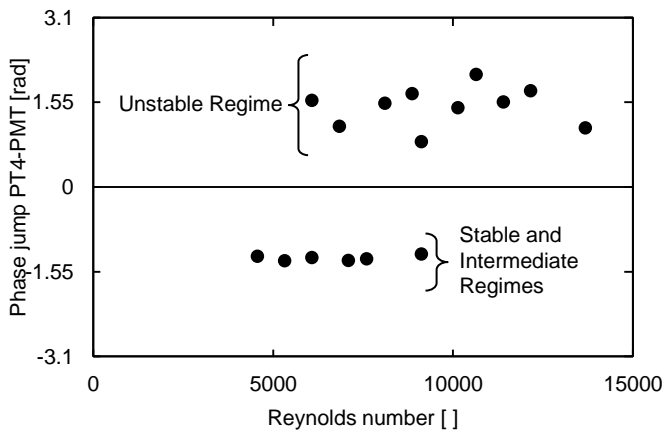


Figure 4-37: LIMOUSINE version 3 double liner pressure – heat release phase jump.

### Stability Analysis of LIMOUSINE Version 3

The previously presented analysis of the dimensionless numbers  $St$  and  $He$  pointed to the acoustic field as the driving mechanism. This mechanism is responsible for the frequency of oscillation, based on partial or full combustor resonance. While the mechanism, acoustic driven oscillation, is the same in versions 2 and 3, their stability maps are different. In version 2, the unstable regime is characteristic of lean flames with high Reynolds numbers while the



version 3 has the opposite behavior, independently of the combustion chamber length. In version 3, the instability appears for near stoichiometric mixtures at low Reynolds numbers.

It was already established that the stability of version 2 combustor depends on the time delays between the flame and the acoustic field. If the flame dynamics and the acoustic period match within certain limits, the feedback loop enhances the energy exchange from the flame to the pressure field, leading to the limit cycle. However, the time delay model from the version 2 does not fit into version 3 behavior. For example, the thermoacoustic instability of the version 3 single liner for 50 kW power and air factor  $\lambda = 1.40$  has a frequency of 257 Hz and a first predicted acoustic eigenfrequency of 175 Hz (independent of burner version).

$$\frac{\tau_{conv}}{T} = \frac{1}{\frac{257 \text{ s}^{-1}}{175 \text{ s}^{-1}}} = \frac{3.89 \cdot 10^{-3}}{5.71 \cdot 10^{-3}} = 0.68 \quad (4.7)$$

The delay ratio is 0.68, and the criterion of the instability (4.2) is thus not satisfied. The same happens as well in the double liner configuration. Version 2 and 3 have identical length and almost identical speed of sound. The instability frequency shifts from around 100 Hz for version 2 to the order of 180 Hz for version 3, almost halving the ratio. The version 3 burner adds two additional recirculation zones and greater jet velocity in the inlet slits, compared to version 2. This evidence indicates that version 3 must have a smaller convective time and hence a more compact flame. The sketch in figure 4-38 shows the convective time delay for both LIMOUSINE burners as function of the Reynolds number. For constant

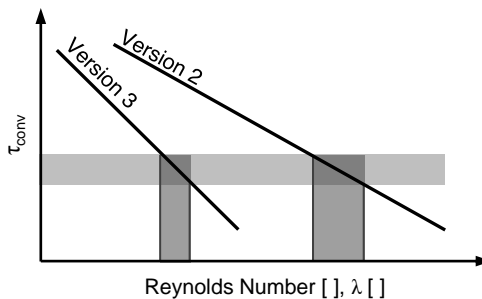


**Figure 4-38: LIMOUSINE instability regions for constant thermal power.**

thermal power, the air factor is proportional to the inlet Reynolds number, so the horizontal axis can represent  $\lambda$  as well. The horizontal light gray band represents the values at which the ratio  $\tau_{conv}/T$  fulfills the criterion. The shorter delays associated with version 3 burner explain why the unstable regime is observed for near stoichiometric mixtures and why the LCO in version 2 requires leaner conditions. In version 3, it is reasonable to assume that the aerodynamics of the fluid have much larger influence.

The temporal evolution of the flow can be studied using the video recording of the CCD cameras. Phase locked pictures help to understand the dynamics of the flame, condensing the information of the movie into a few representative images distributed over one period of oscillation. The technique is commonly used in externally forced systems or self-excited systems with a high repeatability. Neither of those is the case of the LIMOUSINE combustor. Only in a few cases it was possible to obtain a series of meaningful phase locked pictures using off line technique [106]. The presence of the instability introduces a continuous shift in the phase of the flame (figure 6-3) that makes the flame evolution between two consecutive movie frames not constant. Nevertheless the instantaneous frames still reveal much information.

Figure 4-39 shows the main mechanism of the oscillation of the flame. The cycle starts with the first and second frames as the fresh gases enter the combustion chamber through the burner slits. Next, the mixture is trapped in the central recirculation zone, where the combustion reaction starts. The main reaction is observed in the center of the recirculation zone (third frame). This reaction is fast, and after it is finished, flue gases leave the recirculation zone and the cycle ends (fourth frame). The frames are not consecutive in the recorded clip and were chosen for clarity purposes, but the cycle is consistently recorded in the movie. More information for this picture is in figure 6-4 and the chapter 6. The role of the acoustic field and specially, the acoustic velocity is crucial. During the first part of the cycle, which includes mixing and delivery of the gases from the injection holes to the combustion chamber, the acoustic velocity is in the direction of the upstream end. The negative velocity forces the mixture inside the central vortex, and creates the compact flame region. In the second part of the cycle, the acoustic velocity has changed direction to the downstream end, which helps to clear the flue gases out of the burner. The acoustic velocity has another effect in the upstream end of the burner. Due to the large velocity magnitude, there is flow

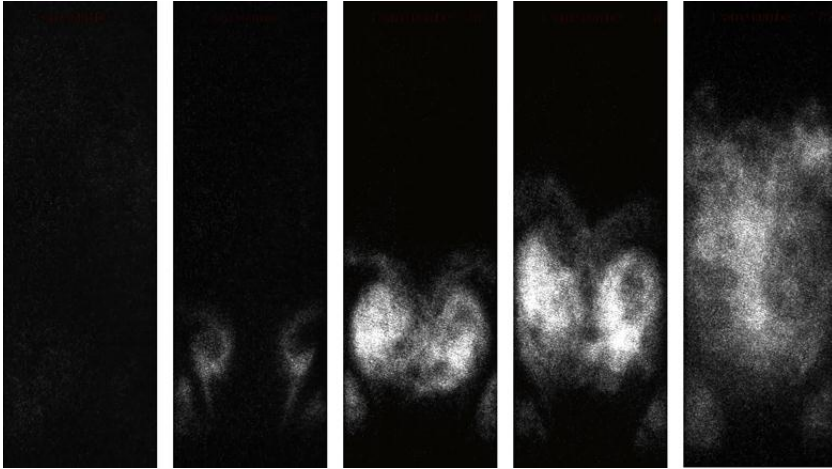


**Figure 4-39: LIMOUSINE version 3 single liner instantaneous OH\* emission for 50 kW and  $\lambda = 1.40$ . Unstable regime.**

reversal in the slits at both sides of the bluff body. This gas parcel behaves as a plug that stops the flow through the burner for a small instant. The injection of the fuel is continuous and, due to the blockage, fuel accumulates at the upstream side of the wedge. At that moment, the mixture is close to stoichiometric stores a high amount of chemical energy. After half a period, the acoustic velocity is reversed and the combined effect of the mean and acoustic velocities pushes the accumulated gas into the burner. During this interval the formed mixture is leaner and has lower energy content.

The same behavior is also seen in the LIMOUSINE version 3 with two liners, but in this case, the vortices of the two jets are not strong enough to converge in the central recirculation zone (2<sup>nd</sup> frame of figure 4-40). The flame is distributed in a larger area between the central and the lateral recirculation zones and burns less violently. The most interesting frames correspond to figure 4-41. These pictures were recorded during the so-called intermediate regime (case 50 kW power and air factor  $\lambda = 1.60$ ) in the LIMOUSINE version 3 double liner. Due to the acoustic velocity, the flame tends to bend to the center of the combustor. However, most of the mixture has either already burned or traveled further downstream of the central recirculation zone, and the flame cannot create a strong vortex. The OH\* movies corresponding to the stable regime in either version 2 or version 3 are not shown here, as the frames do not show any significant repetitive temporal perturbation.

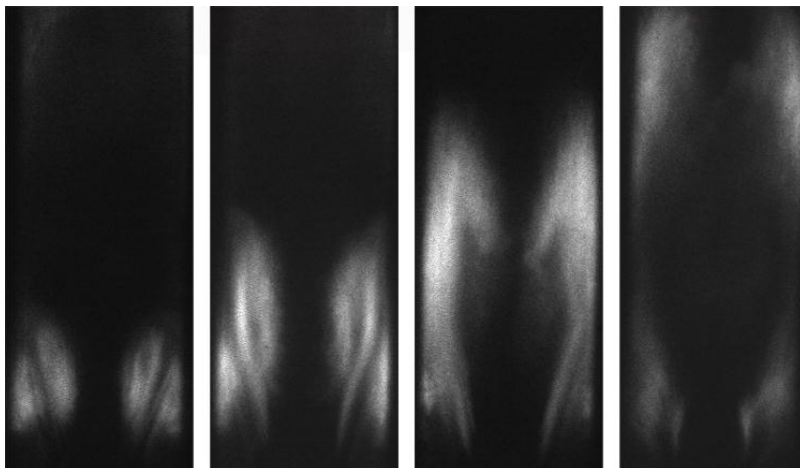


**Figure 4-40: LIMOUSINE version 3 double liner instantaneous OH\* emission for 50 kW and  $\lambda = 1.20$ . Unstable regime.**

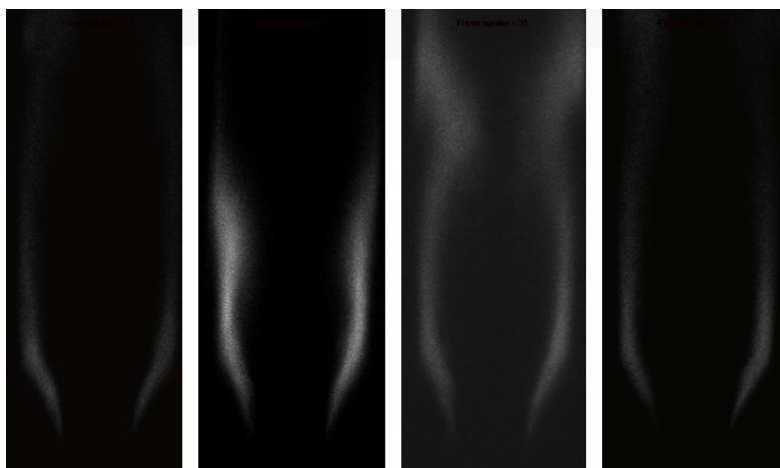


**Figure 4-41: LIMOUSINE version 3 double liner instantaneous OH\* emission for 50 kW and  $\lambda = 1.60$ . Intermediate regime.**

### ***AA Ratio***

It can be summed up that flame stability is a matter of the ratio of convective and acoustic time delays. There is, nevertheless, more to it. The strength of amplification of the instability depends on the acoustic transport in the flame and not in the convective time. It is possible to reach an unstable regime as long as the acoustic velocity can force enough fuel into the upstream of the wedge to accumulate chemical energy and release it at the right time delay in the central recirculation zone. If it fails to store the energy or burn the mixture it in the central reticulation zone, e.g. the intermediate regime, the feedback loop is stopped.

Time delays can be measured using the velocity contours from the PIV pictures (figure 4-22). PIV pictures were recorded at different operating parameters, but the values can be scaled to match with the presented cases here and calculate the mean values of the velocity  $U_{jet}$  of the jets from the burner slits. The length of the recirculation zone  $L_{CRZ}$  is 70 mm and the variations of the length with the Reynolds number are small [107, 108]. The experimental measurements confirm that flue gas temperatures stay about 1100 °C, and a density correction is not necessary. The *aerodynamic-acoustic* (AA) ratio between the two vales is defined in equation (4.8):

$$Aerodynamic/Acoustic\ ratio = \frac{\frac{L_{CRZ}}{U_{jet}}}{\frac{1}{f_{instability}}} = \frac{L_{CRZ}}{U_{jet}} f_{instability} [-] \quad (4.8)$$

The AA number appears as a modification of the Helmholtz or Strouhal number. The characteristic dimension is the recirculation zone length and the characteristic speed is the mean velocity of the inlet jets. The calculated values are plotted in figure 4-42 for the single liner and double liner of the LIMOUSINE combustor version 3. The ratios take values between 0.15 and 1.25, and tend to zero for increasingly higher Reynolds number.

The distribution trend seems to be independent of the length of the combustion chamber. For ratios lower than 0.5, which means that the acoustic period is more than two times the aerodynamic period (or that the frequency of the aerodynamics is twice the acoustic frequency), the combustor is in the stable regime. As the two time periods of the acoustic and flame start to get closer to

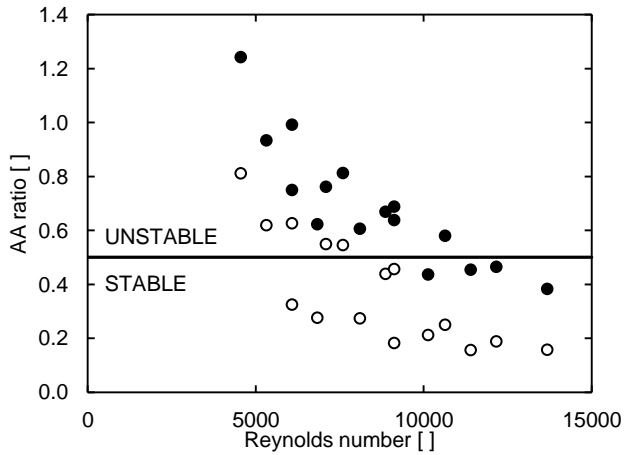


**Figure 4-42: LIMOUSINE version 3 AA ratio as function of the Reynolds number, ● single liner, ○ double liner.**

each other, the combustor enters the LCO. The AA ratio is important in the amplitude of the oscillation, if any. To compare between the two cases, the measured amplitudes were normalized with the largest measured pressure of all the studied flame conditions.

The results, in figure 4-43, show a cluster of the points pointing to the optimal value of the AA for a LCO of 0.70. The central vortex length seems the most indicated characteristic length to be considered in these cases.

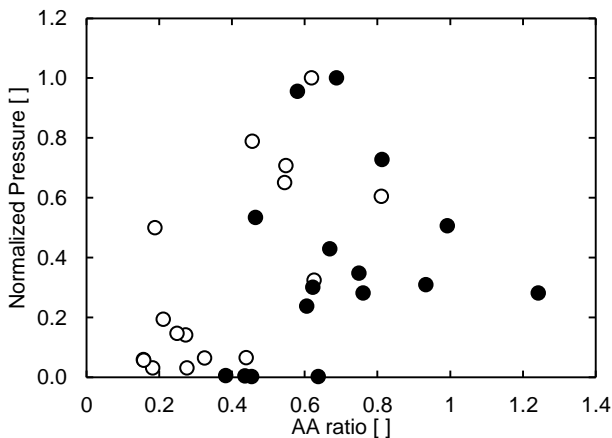


**Figure 4-43: LIMOUSINE version 3 normalized pressure amplitude versus the AA ratio for ● single liner, ○ double liner.**

## Structural Behavior

There is one common feature in all the measured pressure spectra shown in the previous sections, which is the presence of a few discrete peaks in the range of 550 to 600 Hz. These dynamics are independent of the inlet fuel or air flows or the flame regime. They are recorded by both the Laser Doppler Vibrometer and the pressure transducers. Pressure transducers cannot directly record the motion of the liner, but they can capture the effects of the breathing modes of the liner walls (the only ones that effectively change the volume of the combustor). Under certain circumstances, the effect of the modes can be crucial for the flame dynamics, like in LIMOUSINE version 1, but very limited in others. Structural modes depend on the material properties, which are function of the temperature. Despite the fact that it is technically possible to measure the combustor modes during combustion at high temperatures, it is not possible to perform such experiment in the laboratory of the University of Twente. Instead, the modes are measured at room temperature and later corrected for the firing temperatures with empirical models.

The structural vibration modes are measured with piezoelectric accelerometers and an instrumented hammer. The hammer's point of impact is in the vertical symmetry axis of the combustor and at 15.4 cm of the distance from the downstream flange, which corresponds to  $\frac{1}{4}$  of the top section liner length. The accelerometer is located at the same height as the hammer, but moved  $\frac{1}{4}$  of the

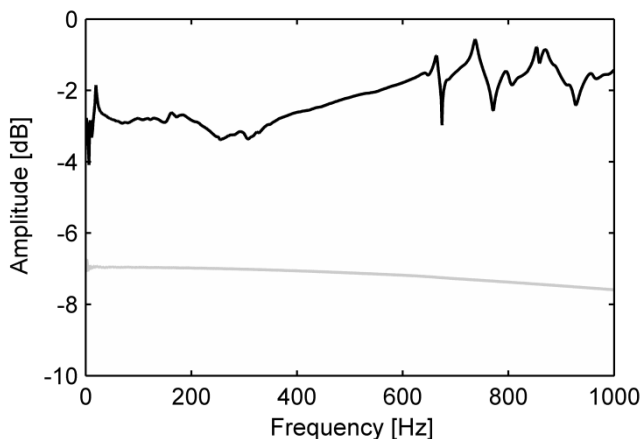


**Figure 4-44: Measured Spectrum of the wall liner vibration (black liner) and autospectrum of the stimulus signal (gray).**

liner width (3.75 cm) to its right. These points were specially chosen because high frequency modes can be recorded on them. Figure 4-44 shows the magnitude spectrum of the frequency response function to the hammer shock (black line) and is the autospectrum of the stimulus signal (gray line). The peaks of the response function are located at 664, 737 and 870 Hz and correspond to structural eigenmodes. The hammer impulse autospectrum is very flat, indicating that adequate level of excitation is provided for the range under study.

In the reference [109] the expression (7.1) is an empirical relationship for the structural frequencies of a plate with particular boundary conditions. The frequency is proportional to the square root of the Young's modulus of the material, which depends on temperature (figure 4-45). During the experiment, due the heat transferred by the burned gases, the steel walls of the liner spontaneously glow with an orange color, which corresponds to a temperature of the material of 600 to 650 degrees °C. The measurements of the optical pyrometer confirm these values. The Young modulus reduces from 198 GPa at room temperature to 150 GPa at 600 degrees °C, a 32.0 % a reduction. Therefore, a reduction of 13.5 % in the frequency of the structural modes is expected. The predicted frequencies in hot conditions are 570 Hz, 634 Hz and 749 Hz, which agree well with the measured data. In the next section, the LDV measurements are presented to the reader for the version 3 single liner. Neither the change of the operating parameters nor the addition of the extra liner does bring changes to the flame dynamics. The extra liner indeed lowers the frequency of the bending and torsional modes due to the added mass, but because of the reinforcement of the edges due to the connecting flanges, the breathing modes remain at the same frequency.

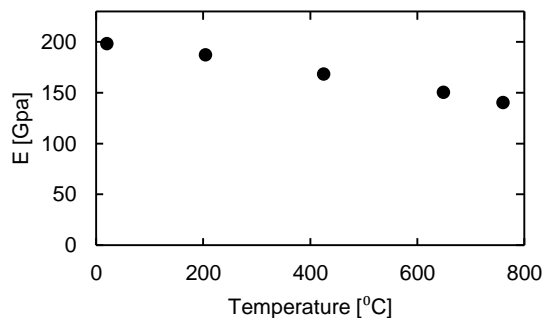


**Figure 4-45: Evolution of the Young's modulus of the SS310 with temperature.**



The results in stable combustion show the first two peaks to be located at 587 Hz and 652 Hz, but the third peak is absent from the spectrum (figure 4-46). This can be explained if measurements were done in one of the displacement nodes. Meanwhile, in the unstable situation, the flame dynamics are responsible for the two perturbations at 257 Hz and 514 Hz (the main perturbation and frequency doubling). The structural peaks are at 582 and 635 Hz, coincident with the previous stable case but their amplitude is three order of magnitude higher. The large magnitude also promotes the occurrence of more structural dynamics at 766, 833 and 911 Hz from the background vibration.

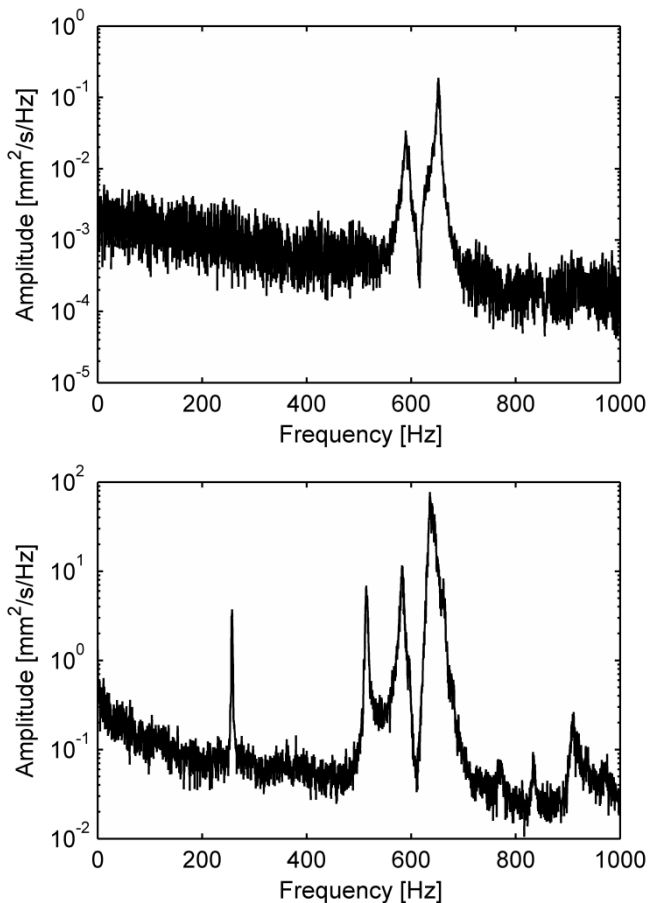


**Figure 4-46: LIMOUSINE version 3, single liner wall velocity spectrum for 40 kW and  $\lambda = 1.80$  (top) and 50 kW and  $\lambda = 1.60$  (bottom).**

## Emissions

The emission of pollutants (NOX) was measured with the portable gas analyzer in the flue gases. The emissions were found to be very dependent on the air factor of the burned mixture and independent of the thermal power, leading to a strong correlation between the combustion regime and the emissions. The values in figure 4-47 (top pane) are the averaged values for a given air factor but different thermal power. The emission trend appears independent of the length of the liner.

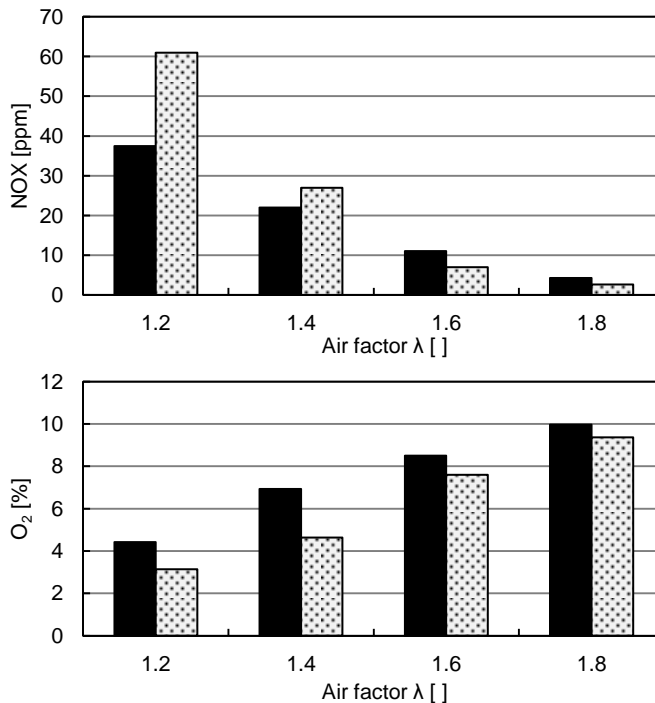


**Figure 4-47: LIMOUSINE version 3 single liner NOX emission (top) and O<sub>2</sub>% level (bottom). Bar fill: single liner (black), double liner (gray).**

The more violent combustions associated with the limit cycle oscillations appear to produce higher values of the NOX, related to the combustion of locally rich gas mixture spots. On the contrary, the stable regime has a much cooler flame that reduced the production of NOX to levels below 10 ppm. Figure 4-47 (bottom) also displays the oxygen content in the flue gases.



# Chapter 5 **Non-linear effects and Chaos Analysis**

## **Introduction to Bifurcation Analysis**

In chapter 4, the combustion dynamics were analyzed with classic tools like the description of the acoustic field in the combustor and evolution of the characteristic dimensionless  $He$  and  $St$  numbers. This present chapter focuses on the non-linear characteristics of the combustion process instead, with special attention to the chaotic nature of the dynamic and its possible applications to control systems.

From the combustion control point of view, the most important parameter of the stability of the combustor is the air factor. Overall, limit cycle oscillations are always present for flames with air factor  $\lambda = 1.60$  or richer. However, the change of regime does not always takes place every time at the same conditions, because the bifurcation is related to the thermal inertia of the combustor. For a fixed thermal power, the transition from unstable to stable combustion will happen at leaner values than the transition from stable to unstable flames.

The two paths can be clearly seen in figure 5-1, recorded at 40 kW thermal power. In this figure, the horizontal axis represents the air factor of the mixture of fuel and air and the vertical axis is the normalized oscillation amplitude with the mean atmospheric pressure. To increase the precision and accuracy of the data, extra measuring points at air factor  $\lambda = 1.50$  and  $\lambda = 1.70$  were used. The hysteresis of the combustion bifurcation can be clearly observed. The extreme points at  $\lambda = 1.40$  and  $\lambda = 1.70$  always have the same behavior, but the regime of the intermediate points depends on the mixture air factor evolution.

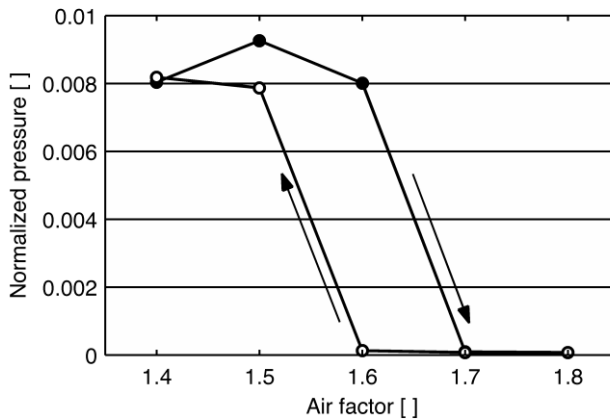


Figure 5-1: Bifurcation diagram ● increasing air factor, ○ decreasing air factor.

## Experimental Results

For the following analysis, only three representative conditions from the LIMOUSINE combustor version 3 single liner are shown. These results were already explained in the preceding chapter 4, but are presented again here to create a compact unit and allow the reader to compare the dynamics more easily. The first point is measured at 50 kW power and air factor  $\lambda = 1.20$  and corresponds to a fully developed limit cycle. The second point also represents an unstable situation, but in this case the conditions are closer to the bifurcation (50 kW and air factor  $\lambda = 1.40$ ). The last condition, 50 kW power and mixture  $\lambda = 1.60$ , is an example of stable combustion. The following figures show 0.15 seconds of the time trace and its associated Power Spectral Density (PSD) for four sensors: the pressure transducer PT 1 located in the plenum of the combustor, the pressure transducer PT 4 located in the combustion chamber, the spontaneous CH\* emission of the flame measured with the PMT tube and the wall displacement recorded with the Laser Doppler Vibrometer (LDV). Upstream and downstream are used to describe the relative position with respect to the triangular body of the burner assembly.

## Pressure Measurements in the Combustion Chamber

The measured pressure time series and spectrum in the combustion chamber for the three mentioned flame conditions are in figure 5-2. The most important characteristics of the unstable regime are the large dynamic at 255 Hz, the secondary nonlinear dynamics at multiple times the fundamental frequency and the structural peaks at around 600 Hz.

The time trace of the stable case is different from the unstable case, as it shows an irregular evolution. The spectrum for this stable case shows the broadband noise in the 50 to 250 Hertz range and structural modes around 600 Hz to 700 Hz.

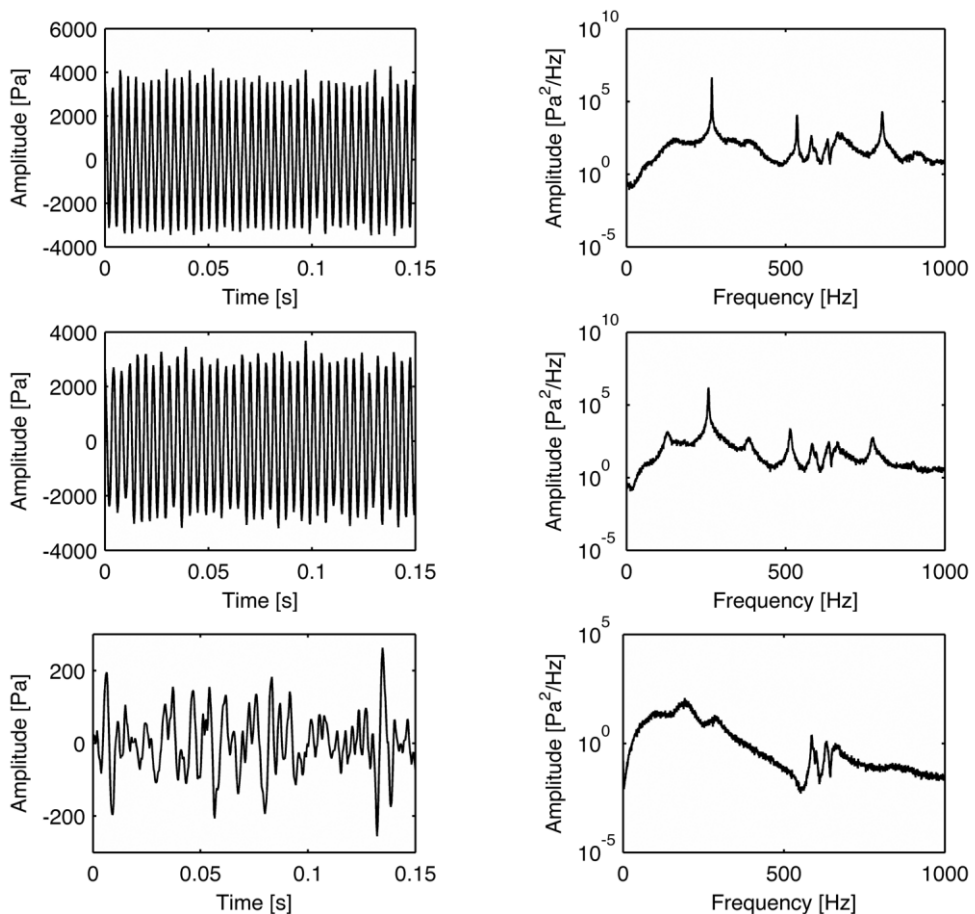


**Figure 5-2: PT 4 time trace and PSD for 50 kW and  $\lambda = 1.20$  (top), 1.40 (middle), 1.60 (bottom).**

## Heat Release Measurements

The study of the measured time series of the heat release rate in figure 5-3, highlights many interesting features of the combustion process. The unstable cases show a periodic signal whose amplitudes are higher for richer mixtures. After the regime swap to stable combustion, the time trace decreases in amplitude and becomes irregular, with a smoothly amplitude decay in the PSD. Additional information can now be retrieved from the frequency domain. Similarly to the pressure signal, there is a main dynamic and secondary nonlinear effects in the spectrum, but the relative amplitude of these oscillations are higher than the relative amplitudes of the secondary peak at the pressure spectrum.

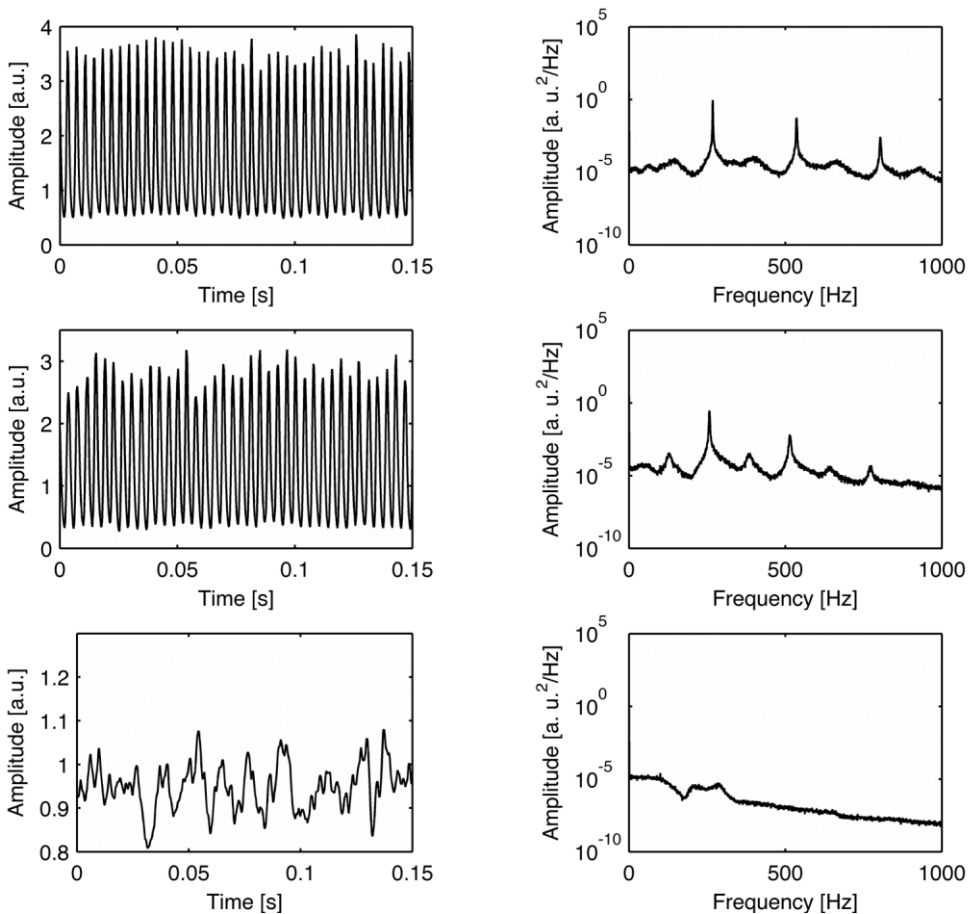


**Figure 5-3: PMT: time trace and PSD for 50 kW and  $\lambda = 1.20$  (top), 1.40 (middle), 1.60 (bottom).**

## Pressure Measurements in the Upstream Plenum

The measured pressure fluctuations in the upstream plenum of the combustor show very similar behavior to the pressure downstream of the burner in the combustion chamber. However, due to the smaller cross-section of the plenum duct, the measured amplitude of the pressure oscillations are much higher than in the combustion chamber. In fact, the measured values can easily reach values of thousands of Pascal. The figure 5-4 also presents the calculated PSD at the right hand side. The stable combustion regimes is almost identical to the downstream behavior.

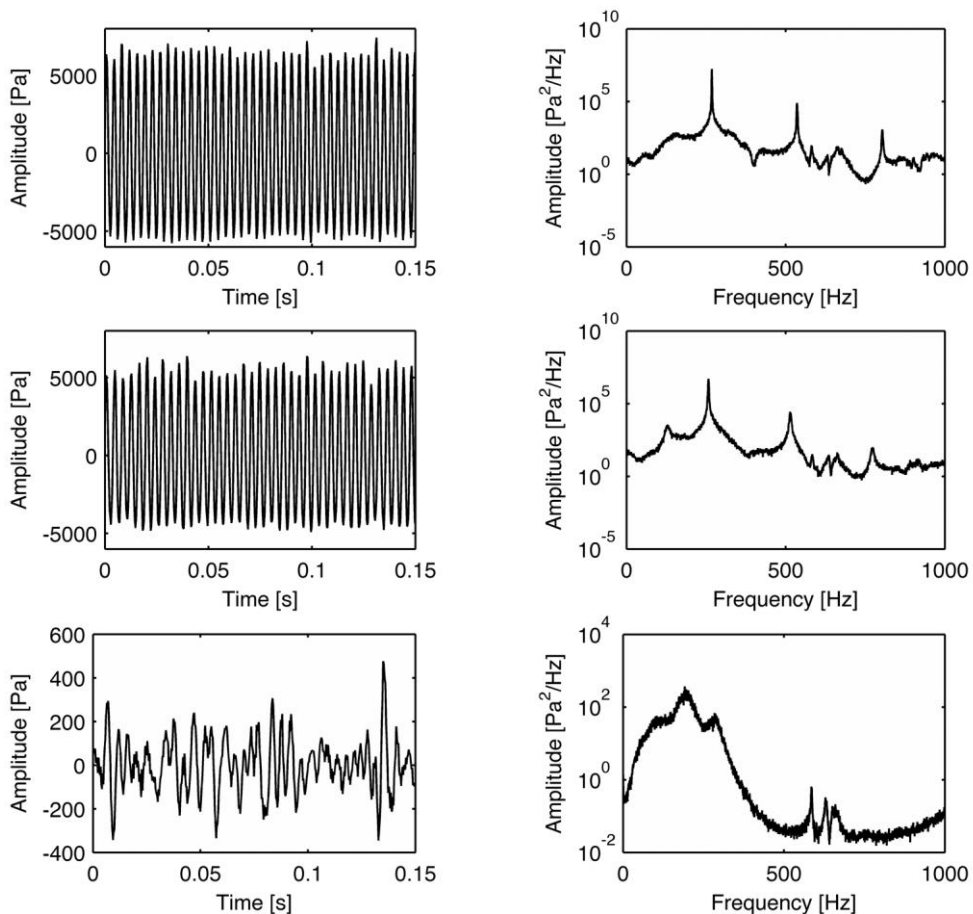


**Figure 5-4:** PT 1 time trace and PSD for 50 kW and  $\lambda = 1.20$  (top), 1.40 (middle), 1.60 (bottom).



## Wall Vibration Measurements

Figure 5-5 shows the measured wall velocity normal to the liner surface in the three operational conditions. The time traces of the three cases are, at first sight, similar to each other and the main effect of the combustion bifurcation is the change in signal magnitude. Velocity oscillations of the wall decrease from the 50 - 80 mm/s range to the 3 - 4 mm/s range. The most prominent characteristic of the spectrum are the three peaks located in the middle frequency range (514, 582, and 635 Hz), that correspond to plate modes of the combustor liner wall. It is also observed that, a high and narrow peak close to 235 Hz (frequency of the thermoacoustic instability) rises from the background noise in the unstable combustion regimes at  $\lambda = 1.20$  and  $\lambda = 1.40$  air factor. This particular vibration

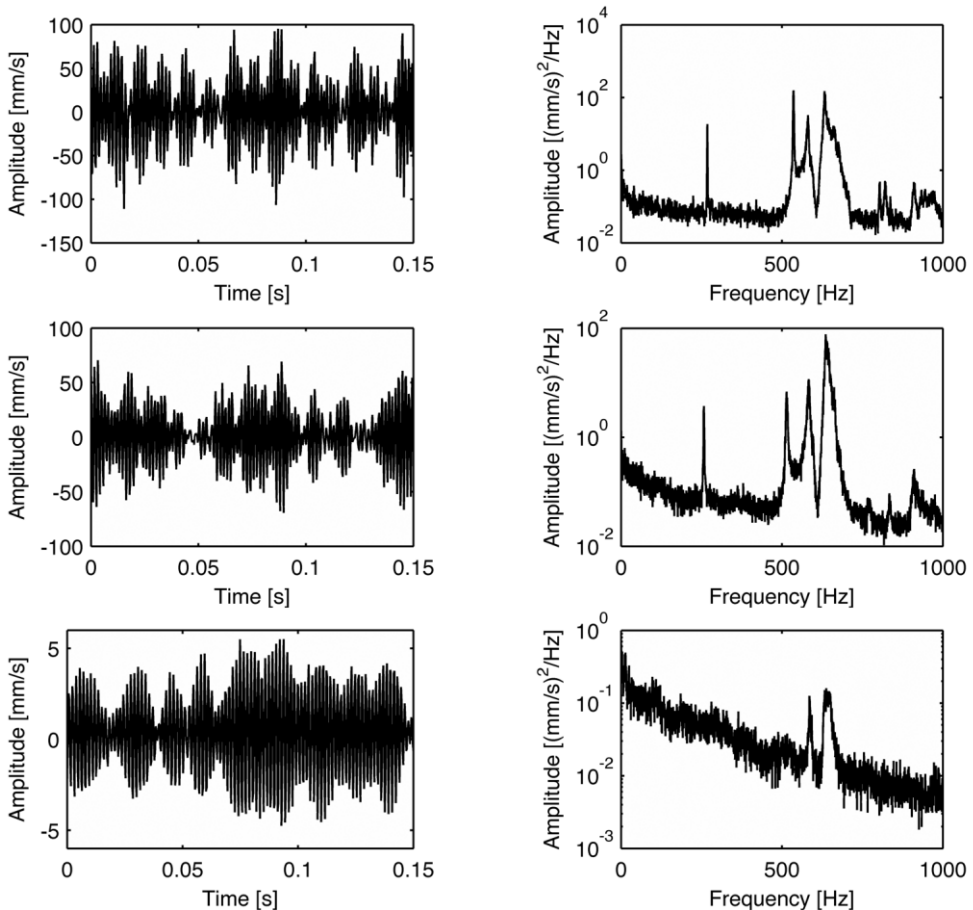


**Figure 5-5: LDV time trace and PSD for 50 kW and  $\lambda = 1.20$  (top), 1.40 (middle), 1.60 (bottom).**

dynamic is driven by the acoustic oscillations of the LCO. It is remarkable that the vibration levels of the plate modes in the 500-700 Hz range are much higher in the stable regime. This can be explained by the large overall broadband noise amplitudes in the LCO and the consumption of energy by the plate at LCO frequency and release at plate eigenmodes.

## Non-linear Dynamics

The response of complex systems, like combustion test rigs in general and the LIMOUSINE combustor in particular, is usually intricate and irregular in time. The measured signals from the setup may be similar to harmonic signals or appear as a random succession of values. Hence, it is very difficult or even impossible to predict the temporal evolution of the output signal in these systems. For this reason, the development of robust control systems that are effective for a large range of operational parameters is not a trivial task. Moreover, the control system must be able to deal efficiently with bifurcations of the combustion regime or changes in the inlet conditions. To achieve this goal, the knowledge of the driving mechanism of the Limit Cycle Oscillations is essential and requires a wider non-linear approach based on chaos theory.

Chaos theory is the field of mathematics that studies the behavior of systems that are highly sensitive to initial conditions. Small differences in the initial conditions yield widely diverging outcomes for such dynamical systems [110]. Popular culture sums up chaotic systems with the butterfly effect: the flap of a butterfly's wings in Brazil can start a tornado in Texas.

An invariant is a parameter that characterizes a system and is independent of the initial conditions, the measuring technique or the data acquisition system. Therefore, they can be used to compare different systems with analytical solutions or empirical results from other physical systems. Sufficient knowledge of certain invariants of the system can be enough to implement advanced control systems, e.g. neural networks [31, 32, 111-113]. For linear signal processing techniques, such as the transformation of the signal to the frequency domain with a FFT algorithm, the invariants are amplitude and frequency. Resonance modes and eigenfrequencies are also invariants. Non-linear invariants can be obtained from the analysis of the time trace of the signal: the attractor shape in the phase space and fractal dimension.

## Reconstruction Theorem

The phase (or sometimes state) space is a Euclidean space of dimension  $N$ , where  $N$  is the number of degrees of freedom that fully determine the dynamics of a system. Therefore, every possible phase of the system is represented as a point in this space. Systems with 3 or fewer degrees of freedom can be easily visualized in phase space, but for systems with more degrees of freedom, it is only possible to see some projections of it. An attractor is the set of points in the phase space that the system under study has visited during its evolution in time, once the initial transients have died out.

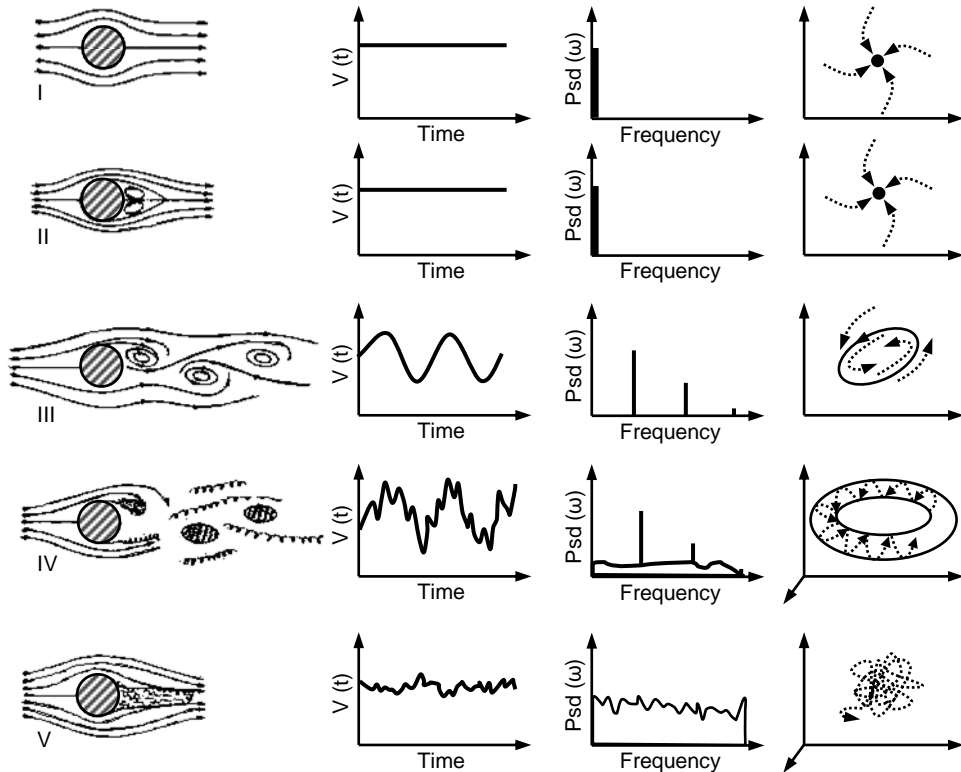


**Figure 5-6: Patterns of hydronamic flow after a cylinder for increasing Re numbers, from laminar (I) to turbulent (V) flow. The second column plots the time variation of the velocity  $v(t)$  in the wake, the third column plots the corresponding power spectrum PSD ( $\omega$ ) and the fourth column is the associated attractor for each case. Adapted from [110, 114].**

Figure 5-6 in the previous page shows the relationship between the time trace, the spectrum and the attractor for the velocity on the wake of a cylindrical body. For laminar regimes, the velocity is constant in time and the attractor is a fixed point (I and II). As the  $Re$  number increases, the flow starts to oscillate periodically (III), which is clearly seen in the power spectrum plot of the second column. The attractor is a limit cycle, a 2D closed loop. As the speed of the coming flow increases, the swirls begin to induce irregular internal vortices in the flow pattern (IV). In this case, there is a partially periodic and partially irregular velocity history, which creates a torus-shaped attractor. A further rise of the flow  $Re$  number produces a very complex turbulent velocity field in the wake (V). The attractor is said to be chaotic and does not show a recognizable shape in a 3 D space.

One key property is that trajectories of the system in the phase space that get slightly deviated from the attractor will remain close to it. The dimension of the attractor can be an integer or a fractional number, depending on its geometry. Attractors can be constructed from the solution of the differential equations that define the dynamic system, if known, or from experimental observations. In this case the Taken's Theorem [115] allows to define the vectors  $B_j$  that form the basis of the space phase in terms of the measured time series  $s(t)$ :

$$B_j = s(t + (j - 1)\tau) \quad (5.1)$$

Where  $j = 1, 2, \dots, dE$ . The embedding dimension of the phase space is  $dE$  and  $\tau$  is the system delay time. From now on, the dynamic system is assumed to be in a cyclic process.

The delay time  $\tau$  is the first value needed to re-construct the phase space. A optimal displacement in the time dimension is long enough to allow the system to produce new information, but sufficiently short to ensure that the new points under consideration have not become completely independent. In most of the cases the data is only available at discrete (fixed) time instants and then, the best choice would be a time shift that is a multiple of the time constant. There are many approaches to determine the optimal time shift, for example, use the first time delay at which the autocorrelation function crosses zero. In the present study the first minimum of the average mutual information for different lags is used. Mathematically, the average mutual information function evaluates the amount of information learned by measurements of  $s(t)$  through measurement

of  $s(t + T)$ . The function  $P_{AB}(a, b)$  is the joint probability density for measurements  $A$  and  $B$  resulting in values  $a$  and  $b$ . The individual probability density of the measurements  $A$  is  $P_A(a)$ . In expression (5.5), the target values are below the summation operator.

$$I(t) = \sum_{s(t),s(t+T)} P(s(t),s(t+T)) \log_2 \left[ \frac{P(s(t),s(t+T))}{P(s(t))P(s(t+T))} \right] \tag{5.2}$$

There are many methods to determine the embedding dimension  $dE$  of a system. The chosen method evaluates the number of *false neighbors* points for an increasing number of dimensions. False neighbors are points of the attractor that are close to each other, not because they are along the path of attractor, but because they are originating from projections of unfolded higher dimensions. As more dimensions are added, the attractor points move to their true location in the phase space and the number of “false neighbors” tends to zero. Once the space has enough dimensions to be fully unfolded, the addition of extra dimensions does not change the false neighbors percentage. Hence, the dimension size for this occurs at  $dE$ . To evaluate if two values are false neighbors, with embedding dimension  $dE$ , they should satisfy the following criterion [116]:

$$\frac{|s(t + \tau) - s(t_{ref} + \tau)|}{R_{dE}(t, r)} > R_{tol} \tag{5.3}$$

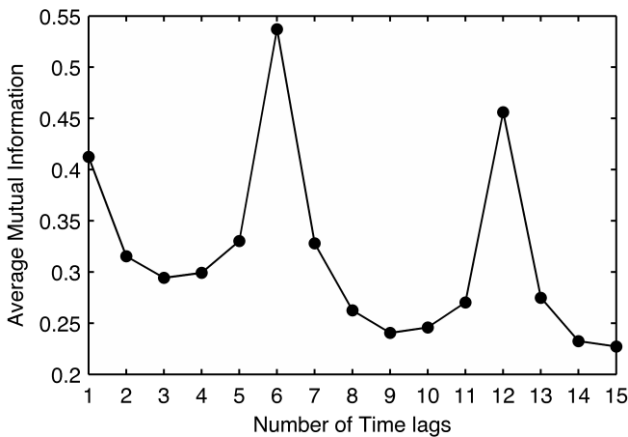


**Figure 5-7: PT 4 Average mutual information for 50 kW and  $\lambda = 1.40$  The first minimum is  $\tau = 3$ .**

The time  $t$  and  $t_r$  correspond to the neighbor and the reference point, respectively.  $R_{dE}(t, r)$  denotes the distance in phase space, and  $R_{tol}$  is the tolerance threshold [117]. In figure 5-8, for the 50 kW power and air factor  $\lambda = 1.40$  case, the number of false neighbors for the pressure signal decreases to 0 at dimension  $dE = 4$ .

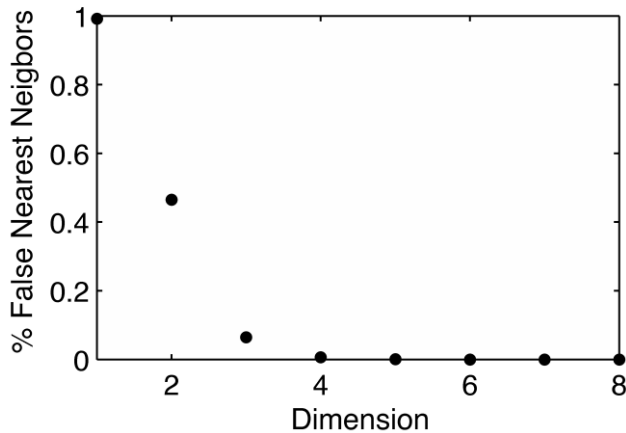


Figure 5-8: PT 4 False nearest neighbors for 50 kW and  $\lambda = 1.40$ .

A constant signal in time has a 0 dimensional attractor. A dimension of 1 is related to pure harmonic motion and dimension 2 corresponds to systems that show two incommensurate harmonic frequencies [118]. Chaotic behavior is characterized by dimensions higher than 2 and noise is related to an infinite number of dimensions. The Embedded Theorem also establishes, that for a given system with dimension  $dA$ , which could be integer or fractional dimension, then the sufficient dimension  $dE$  to fully unfold all overlaps and avoid any ambiguity is  $dE > 2dA$ . Nonetheless, for particular cases, the necessary dimension could be less.

### Pressure Attractors in the Combustion Chamber

The left hand side panels of the plot in figure 5-9 show the reconstructed attractor represented in a 3 dimensional phase space for the pressure signal in the combustion chamber at 50 kW and air factor  $\lambda = 1.20, 1.40$  and  $1.60$ . Unstable cases (top and middle panes) show that all the time series points create trajectories confined to a tightly packed torus subspace in the phase space. The size of the attractor and sharpness of the bends diminishes for leaner fuel-air

mixtures. Although the predicted sufficient dimension was 4, only a 3 dimensional space seems necessary to fully unfold the attractor. The torus shape in two top left figures have been previously observed in other bluff body combustion systems [119] and is known to be related to systems that present limit cycles with two or more incommensurate frequencies. The bottom left pane of figure 5-9 shows the stable regime attractor for 50 kW and  $\lambda = 1.60$  clustering around the origin of the phase space. Some of the attractor trajectories revolved around the attractor while most of them concentrate in the origin. The embedded dimension of the attractor is 4, according to the number of nearest neighbors. A 3 dimensional phase space is not sufficient to unfold the attractor in this case.

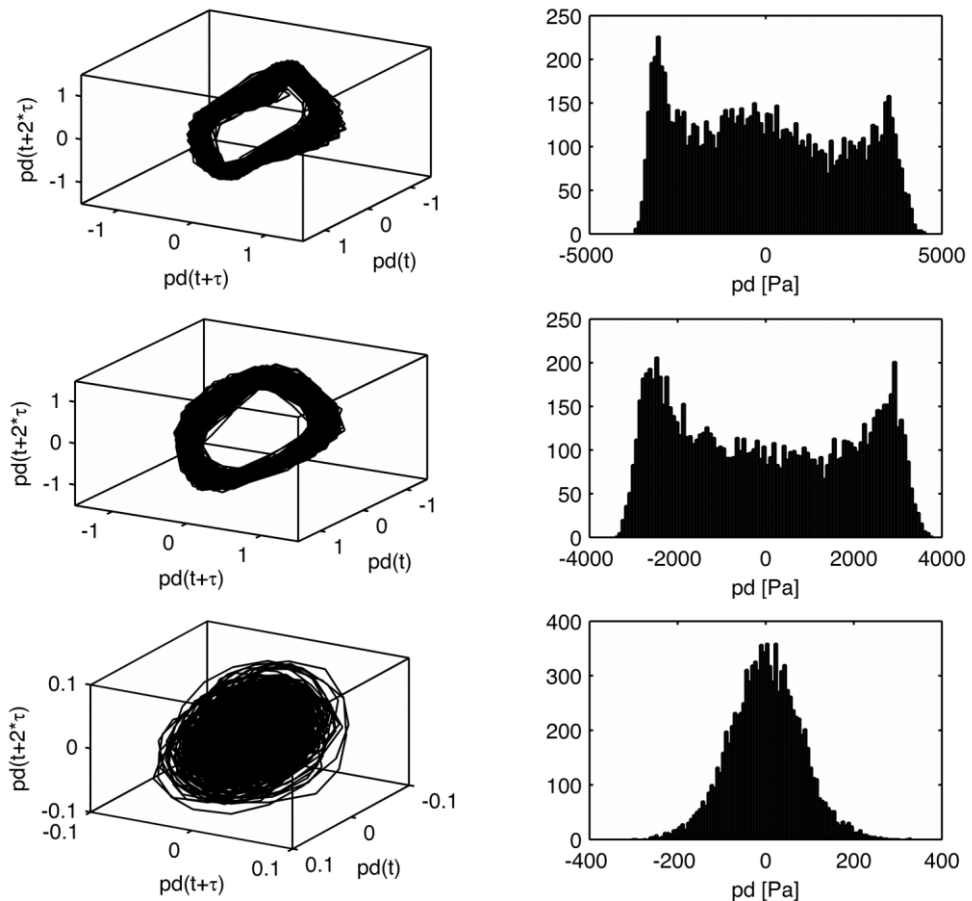


**Figure 5-9: PT 4 attractor in a 3D phase space and histogram for 50 kW and  $\lambda = 1.20$  (top), 1.40 (middle), 1.60 (bottom).**

Additional information can be retrieved from the time series by looking at the probability density functions, in the right hand side of figure 5-9. Figures that correspond to the unstable regime resemble the superposition of a sinusoidal signal histogram and random noise. The distribution is almost symmetric, with a slightly taller left hand side peak (negative pressure). The spectrum for the stable regime has a Gaussian bell shape, with some noise superimposed, centered on  $p' = 0$ . This histogram shape is characteristic of random walk time series.

### Pressure Attractors in the Plenum

The data in this section is measured from the pressure transducer located in the plenum (PT 1) of the combustor and shown in figure 5-10. The results are almost

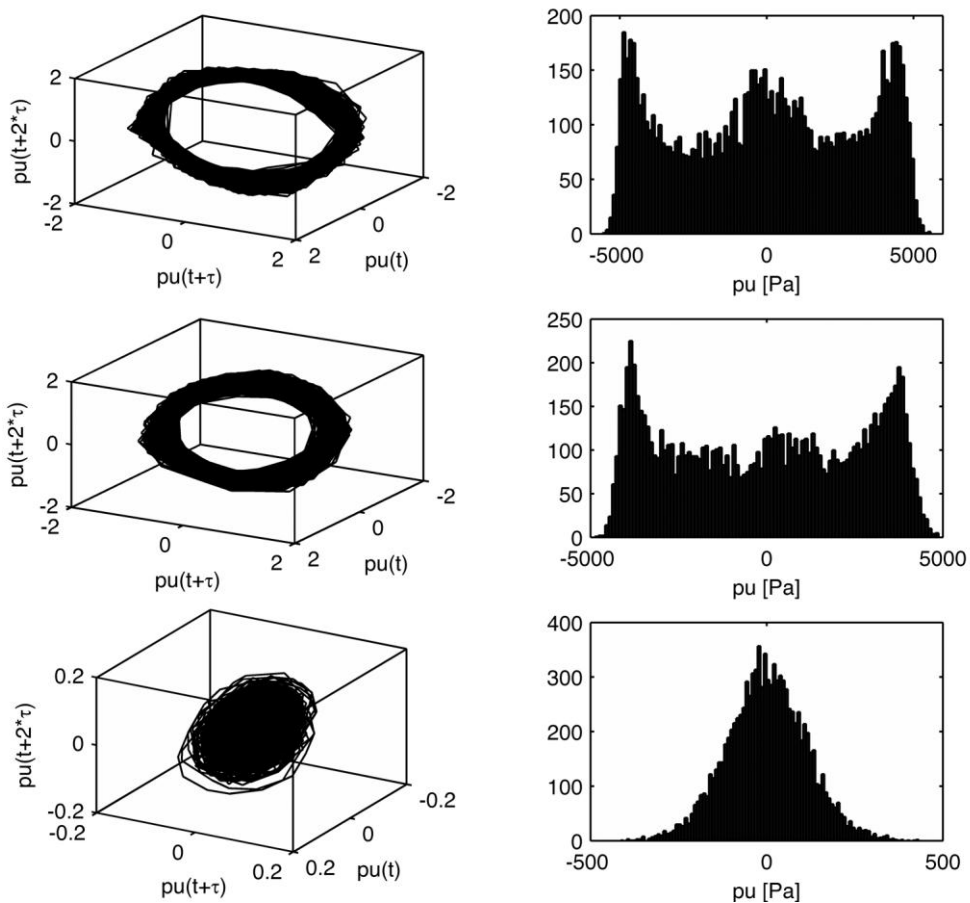


**Figure 5-10: PT 1 Attractor in a 3D phase space and histogram for 50 kW and  $\lambda = 1.20$  (top), 1.40 (middle), 1.60 (bottom).**



identical to the presented in previous sections, especially in the situations of the developed unstable regime and the stable combustion regime. The difference lies in the case with the richest mixture,  $\lambda = 1.20$ . This attractor's shape is still a closed loop, but is not contained in a 2 dimensional plane anymore. Two of the corners of the attractor have been bent in opposite directions, so the figure has an anti-symmetry axis through the origin. This effect is also seen in the histogram, that now shows a bump in  $p' = 0$ . This can be explained due to the presence of large amplitude LCO and number of low amplitude nonlinear oscillations.

### Heat Release Attractors

Heat release attractors are the most interesting of the group. Once again, the attractor shapes are different depending on the regime under study. For unstable cases, the trajectories form a 3 dimensional closed loop, in the manner of a square rim bent by one of its diagonals circa  $90^\circ$ . The bends of the attractor become sharper as the flame air factor is decreased. The size (radius) of the attractor is sensitive to both the mixture air factor and thermal power: attractors measured in higher power or richer mixtures conditions tend to have larger radius. These features appear as asymmetry in the histogram of the time series. There is a narrow and tall peak in the left hand side, close to values of -1 and a small protuberance between 1 and 2 intensity arbitrary units. Despite the heat release rate signal is always positive; the mean value of the trace was subtracted before the processing algorithm. This is the explanation of the negative values of the histogram.

The attractor of the stable case is different in shape and smoothness from the two other cases. It is hard to find any coherent structure in the trajectories in the phase space, indicating that the attractor has not been fully unfolded yet. Hence, the necessary dimension of phase space has to be higher. This attractor shows similarity to the one reported by Fichera et al [120]. The histogram of the time trace shows only the typical Gaussian bell of the stable combustion regimes.

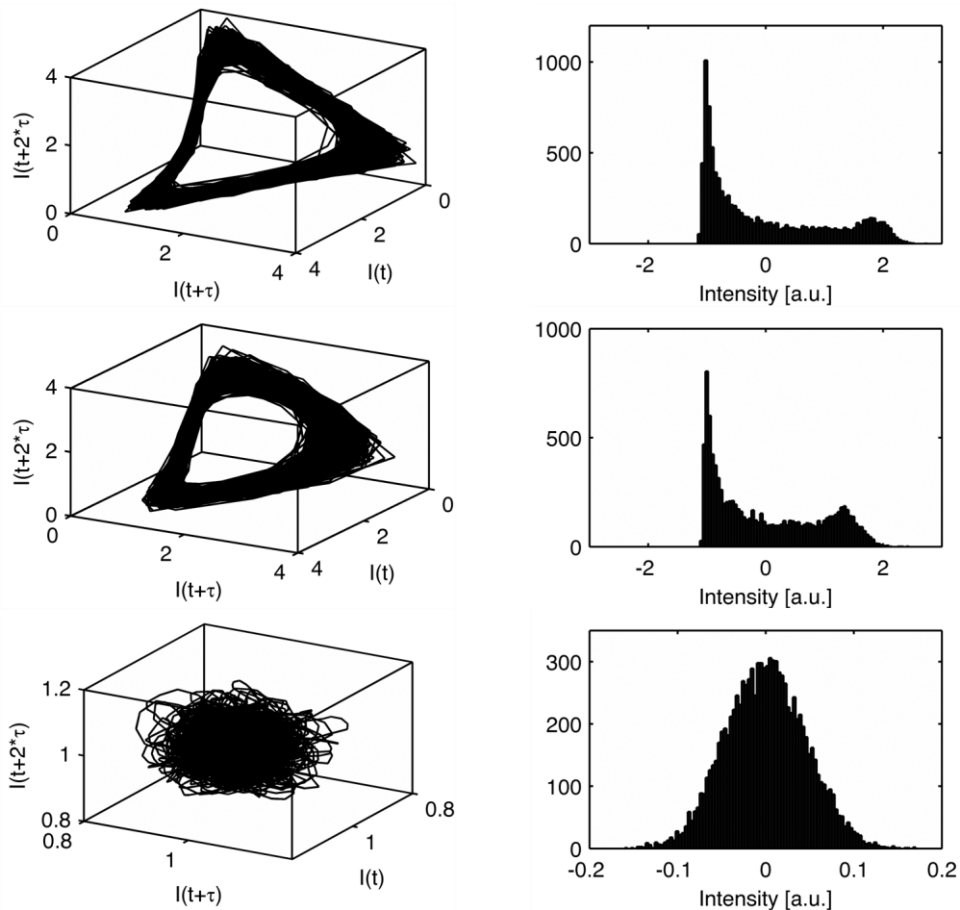


**Figure 5-11: PMT attractor in a 3D phase space and histogram for 50 kW and  $\lambda = 1.20$  (top), 1.40 (middle), 1.60 (bottom).**

## Wall Vibration Attractors

The LIMOUSINE combustor was specifically designed to study Fluid Structure Interaction (FSI). The unsteady pressure fluctuations inside the combustion chamber are an excitation source for the vibrations of the structural domain composed of the liner walls. From this point of view, the flame can be considered as an impact hammer that shakes the structure and can start the resonance of the structural eigenmodes. In gas turbine engine liners, the excited modes are indeed dangerous for the integrity of the combustor, increasing the negative effect of fatigue and creep in the material. The effect of the wall vibration can also have some influence in the pressure field, creating two way interaction. This interaction

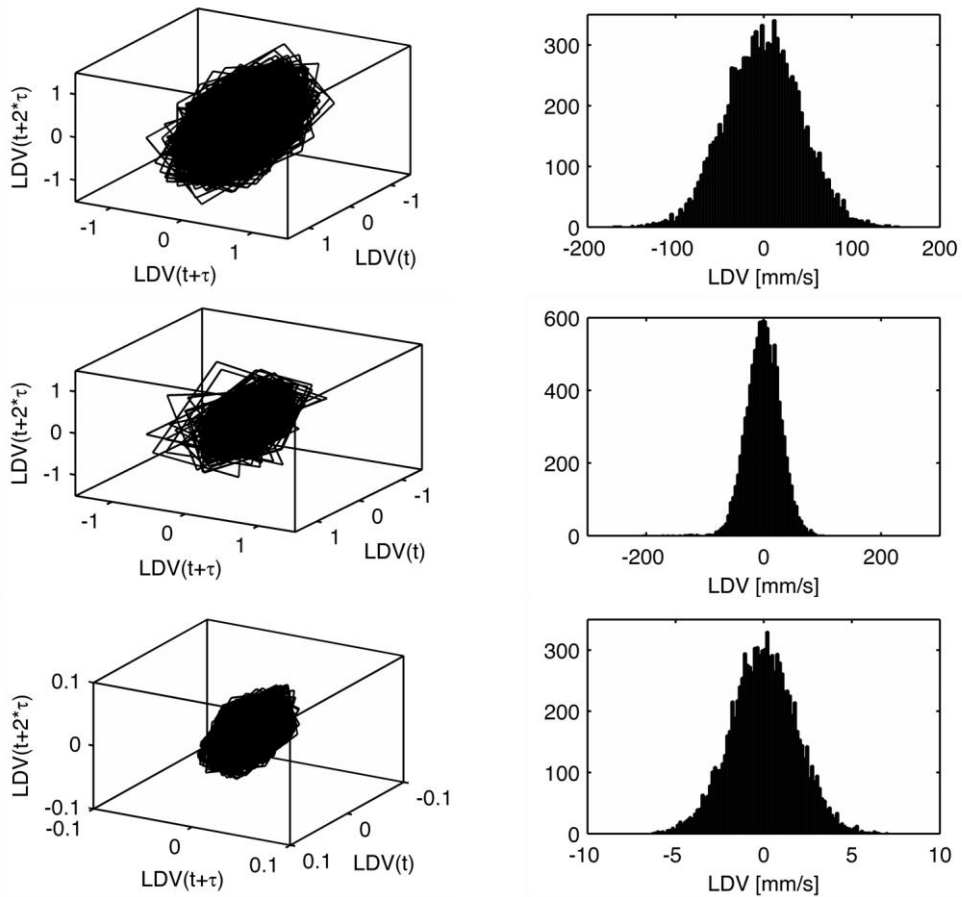


**Figure 5-12: LDV attractor in a 3D phase space and histogram for 50 kW and  $\lambda = 1.20$  (top), 1.40 (middle), 1.60 (bottom).**

can be sufficiently strong to induce a limit cycle where the frequency is not related to acoustic or fluid phenomena, but has its origin in the structure [79]. Unlike other signals, the first local minimum of the average mutual information for the LDV time series is at one time delay for all studied inlet conditions except in the case 50 kW power and  $\lambda = 1.80$ , which is at three time delays. The dimension  $dE$  obtained with the embedding theorem is 4 (or 5 for the 50 kW power and air factor  $\lambda = 1.80$  case). The attractor is plotted in a 3 dimensional phase space with the vector basis  $[ldv(t), ldv(t + \tau), ldv(t + 2 * \tau)]$ . The attractor trajectory evolves as a flat 2 dimensional hypotrochoid figure centered in the origin of the phase space. The sufficient dimension  $dE$  for this case is 2, and therefore, according to the embedding theorem,  $dA$  has a value below one.

The histogram and shape of the attractor are independent of the combustion regime. Similarly to the previous cases, the attractor's size is maximum for near to stoichiometric mixtures, high power and unstable regime and its radius decreases with leaner mixture, less thermal power or stable combustion. Nevertheless, the size of the stable regime attractor is one order of magnitude smaller than the attractor for unstable conditions.

## Fractal Dimensions

The most important characteristic of chaotic dynamic systems is the sensitivity to small perturbations in the initial conditions. In fact, minimal changes in the initial conditions lead to completely different temporal evolutions. These systems are difficult to characterize with linear analysis tools, such as the Fourier transform, because many of the chaotic dynamics will appear as additional peaks or noise in the frequency spectrum. Especially during the 20<sup>th</sup> century, many new tools for the study of the chaotic were developed. The aim of these tools is the characterization of the system with certain values that are independent of the initial conditions and truly related to the inner nature of the system.

The fractal dimension measures the change in the attractor point density of a phase space region as it is measured in smaller and smaller scales. A typical use of the fractal dimensions is to characterize the apparent coast length growth when it is measured with shorter and shorter rulers. The name fractal refers to fractional, because this behavior can be described with non-integer dimensions. Fractal dimensions are an invariant of the system, so they are intimately related to the attractor shape and do not depend on other details. The fractal dimension size is a good indicator about the chaotic nature of the system; a dimension higher than two is necessary to have observe some chaotic behavior [115].

Fractal dimension can be calculated with different algorithms. The algorithm used in this study uses the correlation function  $C$  develop by Grasberger and Procaccia [121]. This equation (5.4) has been already used in the past for the study of combustion thermoacoustic instabilities.

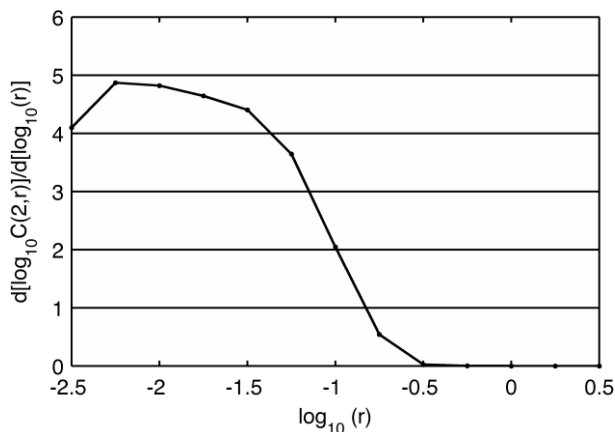
$$C(q, r) = \int d^d x \rho(x) n(x, r)^{q-1} \quad (5.4)$$

The function  $n(x, r)$  counts the number of observed points  $s(k)$  within a ball of radius  $r$  around some location in the space  $x$ , where  $\theta(x)$  is the Heaviside function (0 if  $x$  is negative and 1 if is zero or  $x$  positive).

$$n(x, r) = \frac{1}{N} \sum_{k=1}^N \theta(r - |s(k) - x|) \quad (5.5)$$

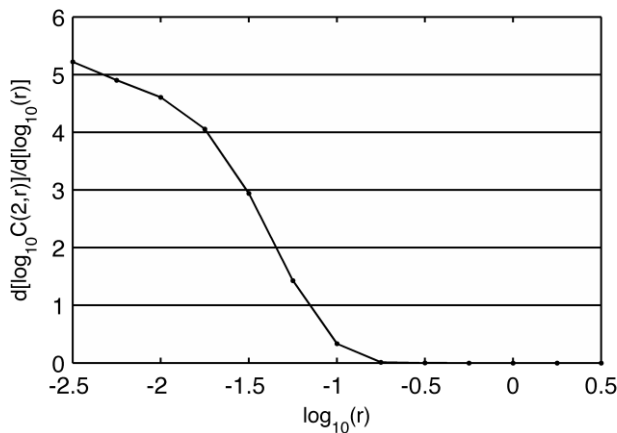
Strange attractors do not have uniform density, so it is very interesting to look at the momentum of the function  $n(x, r)$  to the power  $(q - 1)$ . The mean of this function will reveal interesting features about the distribution of points in the space. Most of the literature agrees to  $q = 2$ . The dimension can be found by examining this function  $C$  for a range of values. If the time series under study is known to have chaotic behavior and the number of points is sufficient high, the correlation function will provide the dimension  $dA$  of the system as the slope of the linear range (if it is present) of  $\log_{10} C(2, r)$  with the variable  $\log_{10} (r)$ .

Figure 5-13 shows the slope of  $\log_{10} C(2, r)$  against  $\log_{10} (r)$  for the measured heat release time series in the combustion chamber at 50 kW and air factor  $\lambda = 1.60$  (stable regime). On basis of the measured PMT signal, it shows a possible flat segment between  $r = -2.2$  and  $r = -1.5$ . The presence of this mentioned flat segment indicates the existence of a chaotic attractor that results in a dimension  $dA$  between 4 and 5. Hence, the heat release signal during stable combustion regime has without doubts, a chaotic behavior.



**Figure 5-13: PMT correlation function  $\log_{10} C(2,r)$  with respect to  $\log_{10} (r)$  for 50 kW and  $\lambda = 1.60$ . Stable combustion.**

In figure 5-14, the slope of  $\log_{10} C(2, r)$  is plotted for the pressure time series in the combustion chamber. It does not show any flat segment and in this case, the fractal dimension  $dA$  cannot be retrieved from the data. However, it was already known that 3 dimensions were not enough to fully unfold the attractor and, even if it is not possible to determine the dimension, it is possible to categorize the motion as chaotic. Apparently, the fractal dimensions of the pressure signal is higher than fractal dimension of the PMT signal, but still pointing to values in the 4 or 5 range.



**Figure 5-14: PT 4 correlation function derivative  $\log_{10} C(2,r)$  with respect to  $\log_{10}(r)$  for 50 kW and  $\lambda = 1.60$ . Stable combustion.**

## Discussion

This chapter has looked at the bifurcation dynamics of a turbulent and stable flame to and from limit cycle oscillations regime. The recorded data from the different sensors was studied in the frequency domain, with the Fourier transform method, and in the time domain, by looking at the dimension and shape of the attractors.

On the stable combustion cases, the heat release rate and pressure time trace of the combustor showed a fractal behavior. With the limitations of the available data in terms of sampling rate and signal length, the flame in the LIMOUSINE version 3 single liner combustor can be characterized by a correlation dimension between 4 and 5. The corresponding attractor from the time series cannot be fully unfolded in a 3 dimensional phase space and has a chaotic nature. The histograms

of pressure oscillation and PMT signals present a Gaussian Probability Density Function (PDF) distribution.

The unsteady combustion regime is characterized by the high amplitude periodic oscillations of the flame. The pressure and heat release spectra show the fundamental frequency and nonlinear effects leading to the frequency doubling dynamics. The histogram of the heat release amplitude is very characteristic, with high values for low heat release (LHS of the figure), as a result of the condition that heat release must always be positive. However, the pressure histogram has symmetric shape since pressure oscillations are still small compared to the mean pressure. The attractors can be generally described with shapes of torus and the motion can be classified as deterministic.

The motion of the structural elements of the combustor was measured as well. The vibration of the liner is independent of the combustion regime and the structural modes are present in the spectrum above the background noise. An independent extra dynamics with the frequency of the flame is also registered in the unstable combustion case. The motion fractal dimension is two and deterministic, because the attractor can be represented as a hypotrochoid curve in a two dimensional plane. The PDF of this time series follows a normal distribution.

The final results are gathered and presented in table 5-1, that shows several important aspects of the two combustion regimes. The unstable regime shows a relatively simple motion, with small dimensions  $dE$  and  $dA$  associated to the attractor. On the other hand, the stable regime has significant higher dimensions  $dE$  and  $dA$  and much more complex behavior, sometimes with chaotic characteristics. There is no need for a control system in a stable regime but if installed, it can be used to prevent the rise of instability once the system reaches a bifurcation point.

**Table 5-1: Non Linear results summary.**

Magnitude	Flame Regime	Attractor	Dimension $dE$	Dimension $dA$
Pressure	Stable	High dimensional motion (chaos)	4	$>2$
	Unstable	Low dimensional motion (straight torus)	3	2
Heat release	Stable	High dimensional motion (chaos)	5	4 to 5
	Unstable	Low dimensional motion (bent torus)	3	2
Wall Displacement	Stable & Unstable	Hypotrochoid	2	1





# Chapter 6 Frequency Doubling

## Introduction

Frequency doubling is the phenomenon in which high amplitude secondary narrow bands dynamics appear in the pressure and heat release spectra of unstable combustion systems. These dynamics have their origin in the large amplitudes found on thermoacoustic oscillations and the flame dynamics. The effect is called frequency doubling because these peaks have oscillation frequencies that are an integer number of times the fundamental frequency. The frequency doubling effect may be mistaken for higher acoustic harmonics, but there is an essential difference between them. While frequency doubling dynamics are always equally distributed in the frequency domain, the acoustic eigenmodes are unevenly spread due to the temperature gradients and the geometry discontinuities. With respect to the amplitudes, the dynamics become weaker for higher frequencies. Many articles and studies do not present the pressure or heat release spectra, so it is not possible to verify the presence of the effect.

Chatterjee et al [122] presented in their research the pressure spectrum of the limit cycle regime in their closed-open Rijke tube. Only odd acoustic modes should be present, but their experimental spectrum shows peaks at every frequency equal the limit cycle frequency multiplied by an integer number. This is similar to the results by Tran et al [123]. The frequency doubling is also present in the unstable combustion regime of Sato [35] before the control strategies were applied. The experiments of Bothien [124, 125] shows the equidistant pressure peaks in the spectrum for the different artificial boundary conditions. Moeck et al [126] observed many peaks in his experiments in a lean flame supported by a perforated plate. However, they did not identify the frequency doubling and linked each of the dynamics to either acoustic modes, subharmonics of the fundamental peak or a combination of the two.

## Measured Results

All the results in this chapter are based on data from LIMOUSINE version 3 and single liner combustor. In the first place the temporal series data measured by the sensors are reported followed by the pictures from high speed cameras.

### Pressure and Heat Release Rate Temporal Series

The investigation focuses on the behavior at a unstable combustion conditions. This is the case for 40 kW power and mixture air factor  $\lambda = 1.40$ , which main peak has as a frequency of 234 Hz and amplitudes in excess of 4000 Pascal. The pressure spectrum of the combustion chamber (pressure sensor PT 4) and the heat release rate are in top and bottom plane of figure 6-1 respectively.

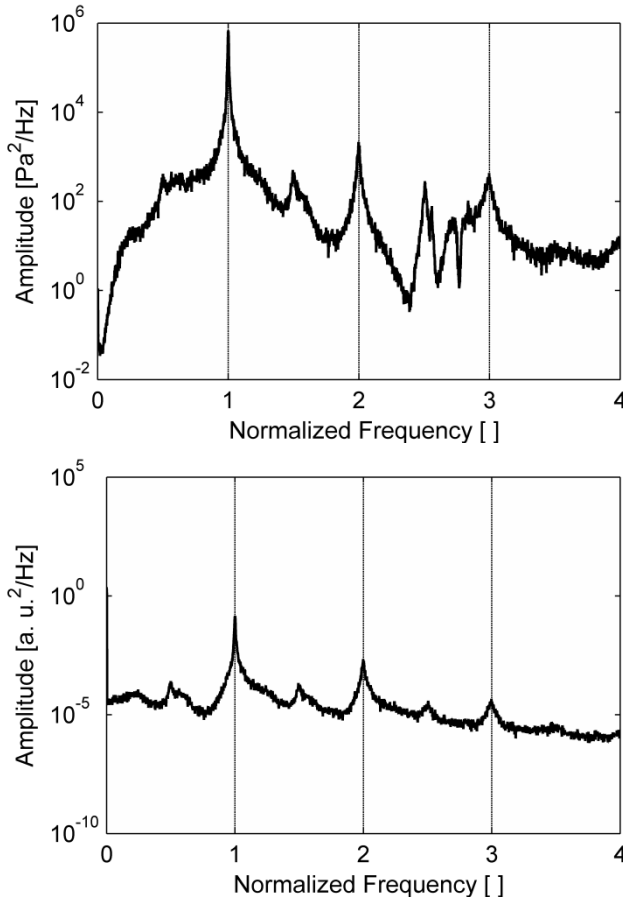


**Figure 6-1: PT 4 Pressure spectrum (top) and OH\* emission spectrum (bottom) for 40 kW and  $\lambda = 1.40$ .**

The frequency axis of the figure was normalized with the frequency of the maximum amplitude peak for both signals. It clearly reveals the precise location of the secondary peaks at integer multiples of the based frequency. The relative magnitude of the secondary peaks is higher in the heat release rate than the pressure spectrum. In the interval between the second and third peak of the pressure spectrum, there are some dynamics rising from the background. These dynamics are related to the vibrational motion of the liner walls and other structural elements and they are not present in the heat release plot.

As the pressure and heat release signals are closely examined one cycle a time, it becomes clear that their wave shape is not sinusoidal and it mimics a saw tooth waveform instead. In saw tooth waveforms, the signal changes between the minimum and the maximum values linearly. The slopes of the two segments do not need to be equal; a triangular waveform is a special case of a saw tooth in which both segments have the same slope. Figure 6-2 shows a single cycle of the heat release rate time trace from the Photo Multiplier Tube time signal. The magnitude of the signal has been normalized and centered on zero value for better visualization. The cycle rising time is much shorter (40% of the period) than decaying time (60% of the cycle time). In addition to the different slopes of the segments, the transition from rising to decreasing is very sharp, while the change from decaying to rising is more gradual. This signal cannot be considered as a harmonic sinusoidal function.

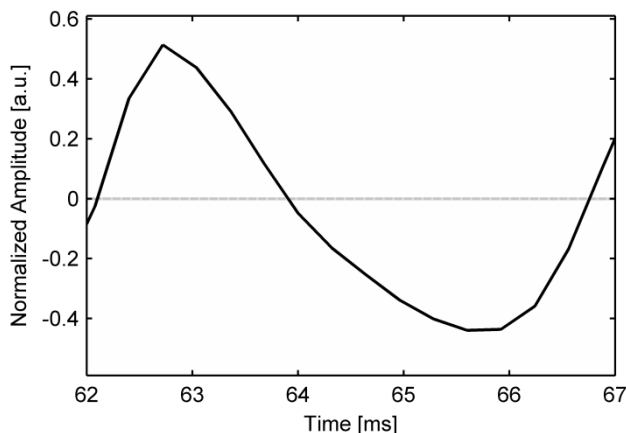


**Figure 6-2: Normalized heat release time trace for 40 kW and  $\lambda = 1.40$ .**

Then the non-linear behavior of the combustion manifest in different ways: Nonlinearities are the origin of the secondary peaks of the spectrum plot, the skewedness of the histograms in chapter 5 and the saw tooth waveform in the time domain. The only different between them is the point of view of the observer. The influence of the non-linear effects in each field can be evaluated as well. The non-linear effects for the pressure are small, which results in relatively low amplitude peaks in the spectrum and in a symmetric histogram. As shown above, the non-linearity of the heat release signal is larger. Other manifestation of the nonlinearity are more prominent secondary peaks, more skewedness in the histogram graph and more pronounced saw tooth waveform of the temporal signal.

### Optical Measurements

In this section, the non-linearity is studied with the spontaneous radical emission captured with the cameras. It is not possible to reveal very fine flame details, because the images are integrated line of sight pictures. However, the main motion and dynamics of the flame can still be described. In combustion experiments, the shutter signal of the high speed camera was recorded in the DAQ to perform an offline phase lock [127] of the images and pressure traces afterwards. This procedure was not successful because continuous shift of the oscillation frequency. Figure 6-3 shows this issue by fitting a harmonic signal to the measured data. For some time instants in the beginning of the signal, there is a good agreement between predicted and measured signal, but after a certain

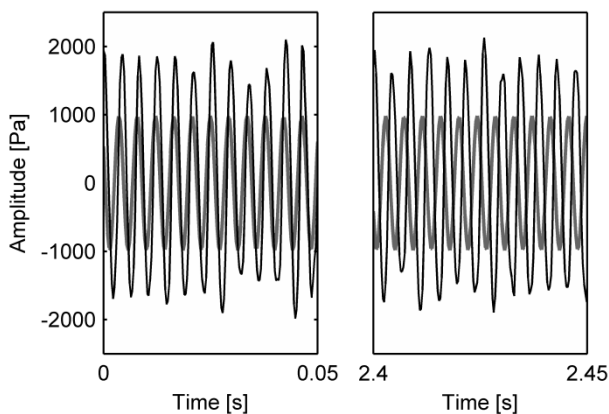


**Figure 6-3: Pressure time trace (thin line) and fitted signal function (thick line).**

number of cycles the signal and fitted function do not agree with each other anymore. The consequence is that the phased-locked pictures only show blurred imaged images. But this does not mean that it is not possible to recover any information from the recorded movies. Figure 6-4, based on the figure 4-39 of chapter 4, shows the flame evolution by plotting the flame contours in a sketch fashion. In the unstable regime, the cycle starts with the combustion of the jets of fresh gases from the burner slits. The reaction zones quickly grows and splits into two areas characterized by high light emission levels. At this point, the two flames still are independent from each other. In the next step, the rest of the gases are violently burnt in the central recirculation zone. The flame length corresponding to this time instant is around two to three times the characteristic dimension of the burner. The flame intensity decreases slowly until it is so weak that it cannot be detected by the camera. The cycle re-starts again as the jets with fresh gases enter the combustion chamber in the next cycle.

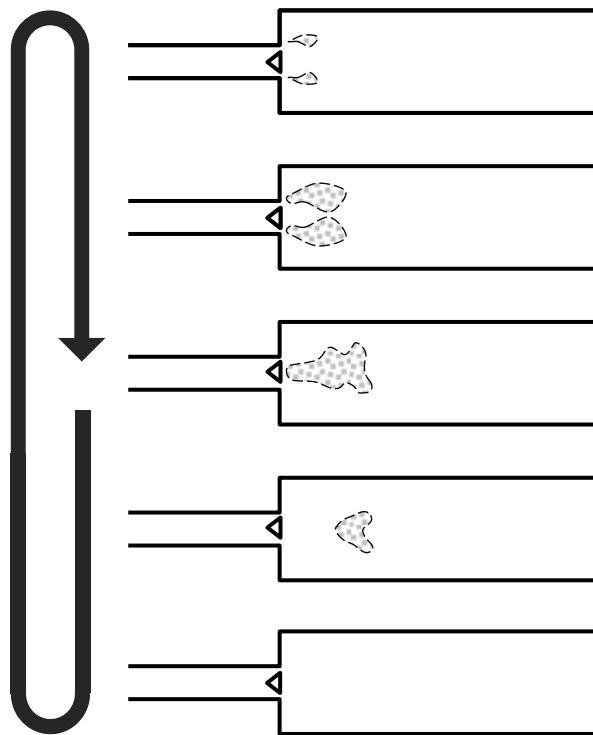


**Figure 6-4:** Flame evolution sketch from the high speed CCD camera movie clip.

The Flame Transfer Function relates the velocity in the burner entrance to the heat release. One of the most common parametric models for transfer function is the  $n - \tau$  model given by equation (6.1) [34, 48, 128]. The heat release perturbations are proportional to the amplitude of the velocity perturbations with a constant time delay. Like all transfer function for flames, the frequency of the response signal is equal to the frequency of the input signal as it is based on linear theory. These functions are therefore, unable to capture the frequency doubling effects.

$$\frac{Q'(t)}{\bar{Q}} = n \frac{u'(t - \tau)}{\bar{u}} \quad (6.1)$$

The natural way to account for these effects is to add nonlinear terms to the function. In general, the series can be expanded in a Taylor (6.3) series manner.

$$\frac{Q'(t)}{\bar{Q}} = \sum_i \left( n_i \frac{u'(t - \tau_i)}{\bar{u}} \right)^i \quad (6.2)$$

As many terms as desired may be used in (6.2), the maximum degree used in this dissertation is two. The first two terms also carry most of the energy of the signal. In equation (6.3), the second term is assumed to have a negative sign, so it can produce meaningful physical results.

$$\frac{Q'(t)}{\bar{Q}} = n_1 \frac{u'(t - \tau_1)}{\bar{u}} - \left( n_2 \frac{u'(t - \tau_2)}{\bar{u}} \right)^2 \quad (6.3)$$

## Fitting Code Results

The LIMOUSINE setup does not have any sensor to directly measure the velocity perturbations at the upstream of the burner (5 mm upstream of the tip of the burner) during combustion experiment, but there are at least two alternative ways of measuring the velocity with the installed pressure transducers. The first way uses the Multi Microphone Method to estimate the acoustic velocity in the burner inlet. The second approach uses an empirical transfer function between the measured pressure signal at one transducer and the recorded velocity with a hot wire probe inside the burner inlet. These measurements were done in a measurement campaign prior to the start of the ignition tests. The correlation is measured for different operational parameters and perturbation levels. Results

suggest that both methods give the same result, and the transfer function approach is used in the final calculations. Later, the measured velocity trace is modeled as the combination of harmonic signals. Only the amplitudes are fitted, as the frequency is already known from the pressure spectrum.

$$\Omega = 2\pi f_{peak} [Hz] \quad (6.4)$$

$$u(t) = \alpha \cos(\Omega t) + \beta \sin(\Omega t) \quad (6.5)$$

The velocity can be also expressed using the exponential function and complex numbers ( $i = \sqrt{-1}$ ) instead of the combination of harmonic functions.

$$u(t) = Re[\Gamma e^{-i\Omega t}] = \frac{1}{2} [\Gamma e^{-i\Omega t} + \Gamma^* e^{i\Omega t}] \quad (6.6)$$

$$\Gamma = \alpha + i\beta \quad (6.7)$$

A script was written in MATLAB to obtain the unknown parameters  $n_1$ ,  $n_2$ ,  $\tau_1$  and  $\tau_2$  of equation (6.3). The fitted velocity trace in equation (6.6) is the input values and with the target are the heat release data. Both signals were fitted to harmonic functions based on local values. This is a constrained nonlinear optimization problem, that can be simplified using boundary condition for the parameters under study.

Values of  $n_i$ ,  $i = 1, 2$  may only take strictly positive values, since zero or negative numbers will not have any physical meaning. To ensure causality, the time delays have to be zero or positive values. A negative delay will place the effect of the flame (heat release) before its cause (velocity perturbation), which is not physically possible. On the other hand, the measured signals are not continuous, as they are sampled at a fixed rate. That means that the data is only available at certain time instants  $T_{sampling}$ .

$$\tau_i = m_i * T_{sampling} \quad (6.8)$$

It is possible to define an upper boundary for the values  $m_i$  if we assume the delay is shorter than the perturbation period. The  $T_{sampling}$  in the experiments is  $3.2 \cdot 10^{-4}$  second (3125 samples per second) and the measured frequency of the pressure oscillations is 240 Hz. This gives that the order of the period of the oscillation is  $T = 4.0 \cdot 10^{-3}$  s. Then, if  $m_i > 13$  the function correlates the current heat release rate with the previous cycle velocity perturbation, and should be



avoided. Table 6-1 shows all the boundary conditions for the optimization problem.

**Table 6-1: Boundary conditions to the optimization problem.**

variable	Type of number	Minimum value	Maximum value
$n_i, i = 1, 2$	Irrational	0	$\infty$
$\tau_i, i = 1, 2$	natural	0	13

The optimization strategy was designed to take advantage of the boundary conditions of the problem, in this case, the finite number of combinations of  $\tau_i$ . For each possible combination of  $\tau_1$  and  $\tau_2$ , the system in (6.9) is solved for two time instants  $t_i$ :

$$\begin{pmatrix} \frac{Q(t_1)}{\bar{Q}} \\ \frac{Q(t_2)}{\bar{Q}} \end{pmatrix} = \begin{pmatrix} \frac{1}{2\bar{u}} [\Gamma e^{-i\Omega(t_1-\tau_1)} + \Gamma^* e^{i\Omega(t_1-\tau_1)}] & \frac{-1}{(2\bar{u})^2} [\Gamma^2 e^{-2i\Omega(t_1-\tau_2)} + \Gamma^{*2} e^{2i\Omega(t_1-\tau_2)} + 2\Gamma\Gamma^*] \\ \frac{1}{2\bar{u}} [\Gamma e^{-i\Omega(t_2-\tau_1)} + \Gamma^* e^{i\Omega(t_2-\tau_1)}] & \frac{-1}{(2\bar{u})^2} [\Gamma^2 e^{-2i\Omega(t_2-\tau_2)} + \Gamma^{*2} e^{2i\Omega(t_2-\tau_2)} + 2\Gamma\Gamma^*] \end{pmatrix} * \begin{pmatrix} n_1 \\ n_2 \end{pmatrix} \tag{6.9}$$

The term  $2\Gamma\Gamma^*$  is subtracted from the second column of the matrix. By doing this, the magnitude FTF is forced to start from zero for zero velocity perturbation in (6.10)

$$\begin{pmatrix} \frac{Q(t_1)}{\bar{Q}} \\ \frac{Q(t_2)}{\bar{Q}} \end{pmatrix} = \begin{pmatrix} \frac{1}{2\bar{u}} [\Gamma e^{-i\Omega(t_1-\tau_1)} + \Gamma^* e^{i\Omega(t_1-\tau_1)}] & \frac{-1}{(2\bar{u})^2} [\Gamma^2 e^{-2i\Omega(t_1-\tau_2)} + \Gamma^{*2} e^{2i\Omega(t_1-\tau_2)}] \\ \frac{1}{2\bar{u}} [\Gamma e^{-i\Omega(t_2-\tau_1)} + \Gamma^* e^{i\Omega(t_2-\tau_1)}] & \frac{-1}{(2\bar{u})^2} [\Gamma^2 e^{-2i\Omega(t_2-\tau_2)} + \Gamma^{*2} e^{2i\Omega(t_2-\tau_2)}] \end{pmatrix} * \begin{pmatrix} n_1 \\ n_2 \end{pmatrix} \tag{6.10}$$

For the calculated values  $n_i$ , it is now possible to evaluate the error between the predicted and measured heat release (6.11).

$$error = \left| \int_{t_1}^{t_2} \frac{Q(t_1)}{\bar{Q}} dt - \int_{t_1}^{t_2} \left[ n_1 \frac{u'(t - \tau_1)}{\bar{u}} - \left( n_2 \frac{u'(t - \tau_2)}{\bar{u}} \right)^2 \right] dt \right| \quad (6.11)$$

Once all the possible combinations of  $\tau_i$  are tested, the best combination of parameters is the one with minimal error and  $n_i > 0$ .

## Discussion

The MATLAB code is tested with the data from the flame at 40 kW power and air factor  $\lambda = 1.40$ . The best fit found by the code has the parameters  $n_i$  and  $\tau_i$  given by table 6-2, as well as the period of the oscillation.

**Table 6-2: Parameters for the two terms case.**

$i$	$n_i$	$\tau_i$ [ms]	$T$ [ms]
1	0,331816	3,088696	4,26116129
2	0,05779	1,795556	

The results are tested using the equation (6.3) and the measured velocity trace. The agreement between the predicted and measured heat transfer signal is very good (figure 6-5).

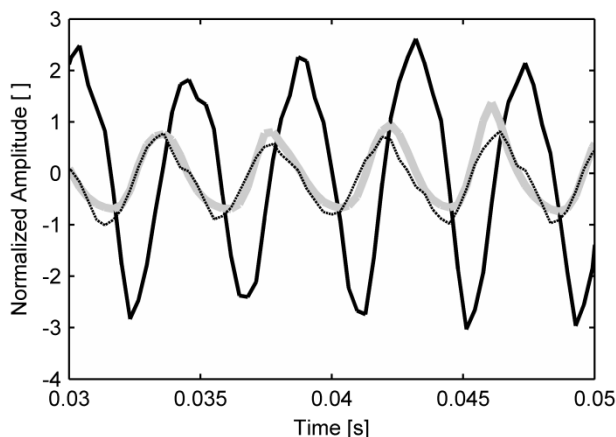


**Figure 6-5: Best fit using two terms for 40 kW and  $\lambda = 1.40$ . Velocity (black), measured heat release (gray), predicted heat release (dotted).**

To do a results comparison, the same model is used but with the term  $n_2$  equal to zero. This situation, shown in (6.3), the transfer function is effectively a standard linear  $n - \tau$  model ( $n = 0.537$  and  $\tau = 2.72$ ). Agreement between the measured and predicted signals is much poorer, figure 6-6. This was the expected outcome, because the process under study is known to be nonlinear.

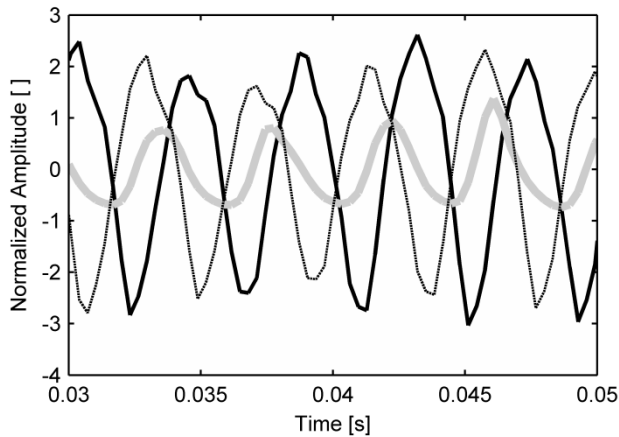


**Figure 6-6: Best fit using one term for 40 kW and  $\lambda = 1.40$ . Velocity (black), measured heat release (gray), predicted heat release (dotted).**

The required parameters to build the nonlinear transfer function curve of equation (6.3) are specified in the table 6-2 and plotted in a normalized heat release versus normalized velocity graph (figure 6-7). The values were determined using only one point in unstable combustion regime, and therefore, they are only valid for this particular situation. The curve starts from the origin, as a consequence of the third term  $2\Gamma^*$  of the equation (6.9) assumed to be zero. The curve rises to a maximum value at  $u'/\bar{u} = 4.3$  and then decreases. It can be observed the transfer function reaches a maximum and therefore, the oscillations have saturated amplitude amplification. The amplitude is defined by a balance between gain and losses [51]. This curve differs from the linear FTF because the system is in a limit cycle oscillation. However, it contains information about the relation between pressure and heat release when subjected to high amplitudes perturbation.

This curve can also be used to predict the magnitude and frequency of both primary and secondary oscillations, which can be useful for the design of systems that need to stay clear of operation in limit cycle.

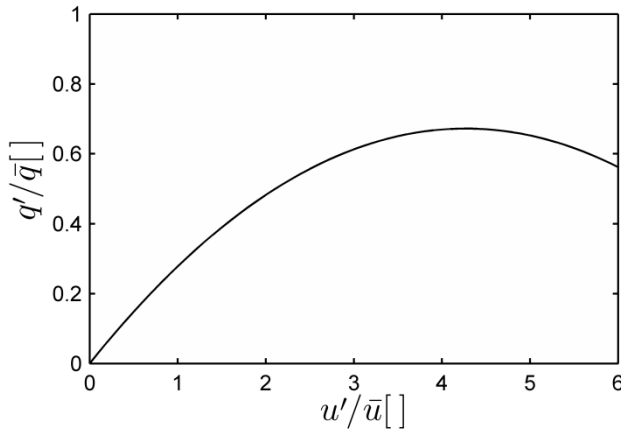


**Figure 6-7: Non-linear FTF for 40 kW and  $\lambda = 1.40$ .**



# Chapter 7 **Coupling with the Structure**

## **Introduction**

The previous chapters discussed the development of the thermoacoustic Limit Cycle Oscillation in the LIMOUSINE combustor based on relationships between the characteristic flame delays and the acoustic time period. This is a necessary but not sufficient condition, because LCO development also depends on the acoustic energy losses through the boundaries or to the structural elements. In most of thermoacoustic oscillations mentioned in the literature, the combustor wall/structure remains passive (figure 7-1) and does not play any role in the feedback loop. The liner or the walls can be excited by the acoustic field, but these vibrations are considered to have limited effects on the fluid domain. For that reason, they are not included in the Rayleigh criterion or standard the feedback loop.

The following chapter explores the interaction between structure and acoustics based on the measured data from the LIMOUSINE version 1 combustor. This version of the combustor is particularly well suited for this task, due to its particular construction. Large and thin walls encourage the coupling of wall vibrations to the sound field inside the domain to a much larger extent than other combustion setups.

## **Aero-Elastic Integration**

Opposite to the LIMOUSINE version 2 or the version 3, the LIMOUSINE version 1 combustor design features flexible liner walls with large aspect ratio (height/width) that results in reduced setup stiffness. The combustor reaction to the flame induced perturbations cannot be solely described by the acoustic field or the liner vibration. The measured response is in fact a combination of the two physics phenomena together, a multi-physics problem. In the next sections, the combustor acoustics and the structural response for this configuration are

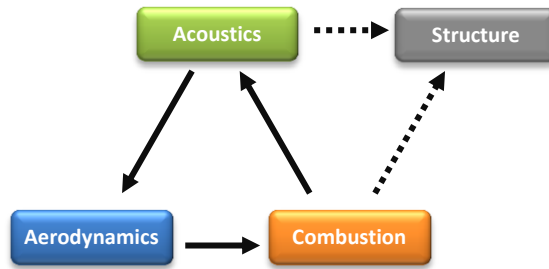


**Figure 7-1: Classical feedback loop including the structure. Solid arrows represent strong coupling and dashed arrows are weak coupling.**

characterized for non-reacting flows. Subsequently the measured data will be used to predict the system dynamics during the firing of the setup.

### Acoustic Boundary Condition

The acoustic boundaries of the combustor setup have an important role in the instability of the combustion-acoustic feedback loop. In combination with the temperature field, they set the frequencies in which the acoustic modes are in resonance. The flux of acoustic energy through the boundaries is also critical, because it is an important component of the acoustic losses. The reflection coefficient at the upstream and downstream ends can be measured with the *two microphone method* (figure 7-2 and figure 7-3), which was described in chapter 2.

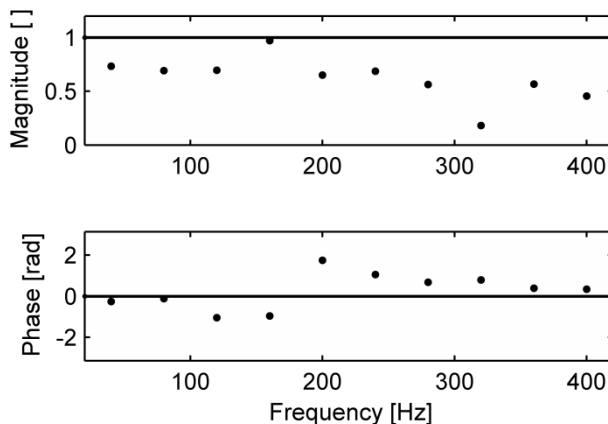


**Figure 7-2: LIMOUSINE version 1 upstream end reflection coefficient.**

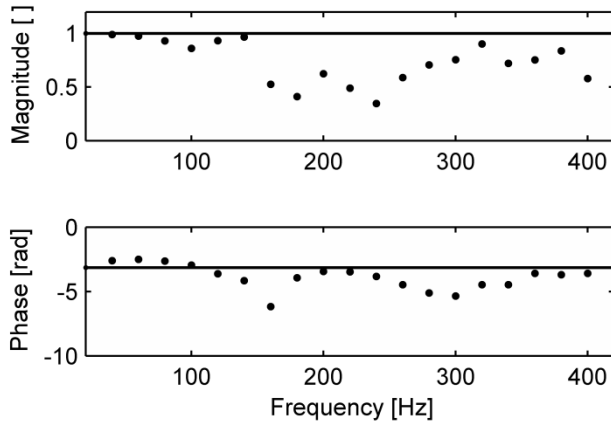


**Figure 7-3: LIMOUSINE version 1 downstream end reflection coefficient.**

Solid black lines indicate the anticipated reflection coefficient  $R$  of the termination and the points are the calculated values. The measured  $R$  coefficients at both ends loosely match with the predicted acoustic theory values. The main discrepancy is in the magnitude of the coefficient in the upstream end, due to the perforated plate located between the feeding air box and the combustor. In the downstream end, the agreement with the predicted values is good in the low (<200 Hz) and high (>300 Hz) frequency range. The values in the middle frequency range suffer low amplitude levels on the excitation signal, reducing the quality of the measured data. The fitted complex reflection coefficients are in table 7-1.

**Table 7-1: LIMOUSINE version 1 fitted reflection coefficients.**

R Coefficient	
Upstream end	Downstream end
$R = 0.6 e^{i0.2}$	$R = 0.8 e^{i2.8}$



## Acoustic Eigenfrequencies and Eigenmodes

With the chapter 2 analytical approach, the acoustic eigenfrequencies can be predicted with equation (2.17). The combustor was modeled with two 1D segments: one of them represents the plenum chamber and the other is the combustion chamber. Each segment has constant gas temperature and density. The measured reflection coefficients are used to adequately simulate the boundary conditions. For the cold case situation (25 °C in both elements), the first 3 modes are 63.5, 193.9 and 294.9 Hz. Even in the plenum chamber, the cut off frequency is well above 1000 Hz and the 1 dimensional approach is correct. The acoustic modes of the system were also measured with specific experiments.

The Frequency Response Function (FRF) is the relationship between the output and input signals of a system, considering it to behave like a black box. In an acoustic context, the excitation input signal is broadband noise fed into the system by a loudspeaker and the output signal is the recorded pressure oscillation at one particular microphone. The acoustic modes correspond to the main peaks of the magnitude of the FRF.

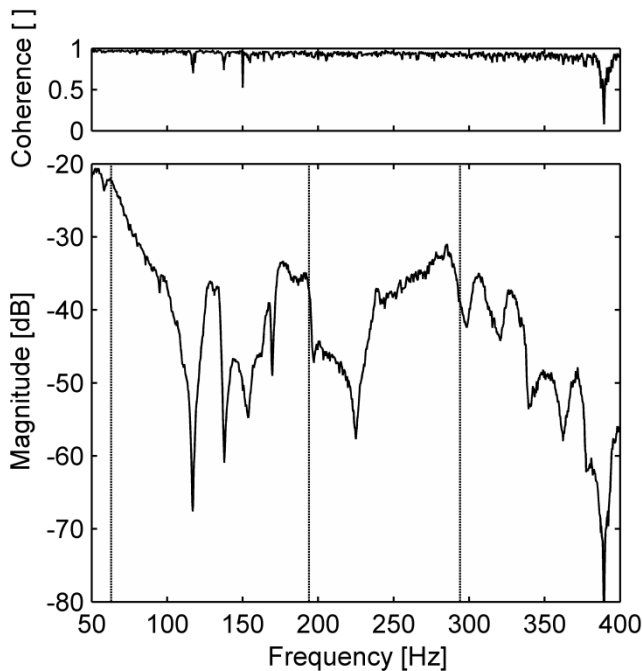


**Figure 7-4: LIMOUSINE version 1 acoustic dynamics coherence (top) and FRF (bottom). Vertical lines show the eigenmodes.**

The experimental results from these tests are plotted in figure 7-4. The FRF shows many dynamics and all associated of them have close to unity coherence values. The predicted acoustic eigenmodes with the equations are highlighted with vertical lines. The first acoustic peak frequency is overestimated by 17.1 % (52.2 Hz measured versus 63.5 Hz predicted) but the second and third peak frequencies are well predicted (190.6 Hz and 285.6 Hz). The other dynamics can be related to structural modes of the combustor.

## Structural Eigenfrequencies and Eigenmodes

Structural and acoustic perturbations have much in common. In fact, both are vibrational phenomena that are governed by similar equations and many of the tools developed for one field can be used with minor modifications in the other. The frequency of the different structural modes can be calculated with an analytical approach, but it is also possible to use empirical formulas [109]. For a rectangular plate with different sets of boundary conditions, the eigenfrequencies are given by equation (7.1).

$$f_{ij} = \frac{\lambda_{ij}^2}{2\pi a^2} \sqrt{\frac{Eh^3}{12m_p(1-\nu^2)}} \quad (7.1)$$

The parameter  $\lambda_{ij}^2$  depends on the boundary conditions and  $a$  is the characteristic width dimension of the plate. The thickness of the plate is  $h$ ,  $E$  is the Young's modulus of elasticity of the material,  $\nu$  is the Poisson ratio and  $m_p$  is the mass per unit of area. Torsional and bending modes do not change the volume inside the combustor and have a small effect in the acoustic field. Therefore, in the subsequent research, the only modes under consideration are plate vibrational modes. The structural eigenmodes (at room temperature) were also measured with the FRF of the structural field. The excitation signal may come from a mechanical shaker (analogous to the white noise audio excitation) or an impact hammer while the system response is recorded with single axis piezoelectric accelerometers. It is very important to locate the point of excitation and the accelerometers away from the expected location of the nodes, to capture the maximum number of eigenmodes. For that reason, both hammer impact point and the accelerometer were placed in the vertical symmetrical axis of the top liner and at  $\frac{1}{4}$  of the combustion chamber length downstream of the wedge's top face. The measured results from the experiment are given in figure 7-5. The first

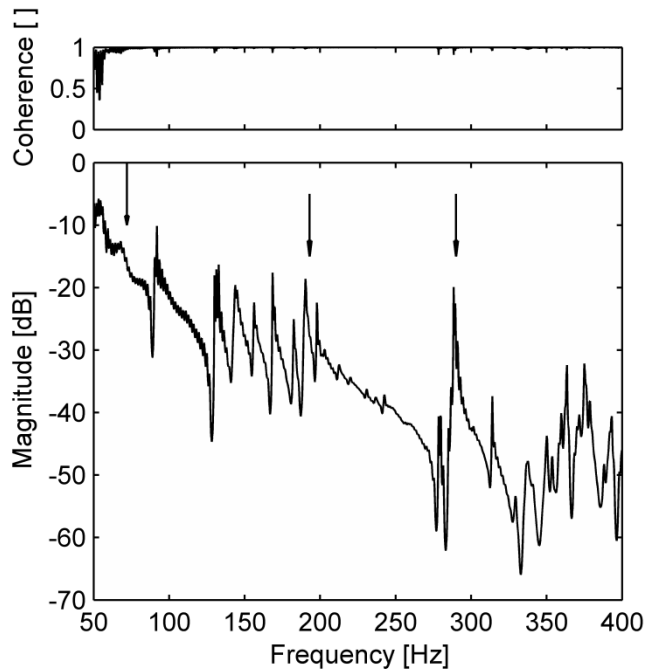


**Figure 7-5: LIMOUSINE version 1 structural dynamics coherence (top) and FRF (bottom). Arrows indicate the acoustic modes.**

characteristic of the measured values is the high coherence values in the studied range. The FRF magnitude shows many different dynamics, with the acoustic modes included among them (highlighted with arrows). The simultaneous study of structural and acoustic modes shows that many of FRF dynamics appear, with a small frequency shift, in both structural and acoustic spectra. The data was measured at two different moments, and the successive firings of the setup explain the discrepancies in the data and the frequency shift [129].

Table 7-2 on the top of the next page shows the predicted frequencies for a rectangular steel plate of the same dimensions of the liner wall and clamped at its four sides. It also shows the measured structural frequencies classified into two separate categories. The dynamics from the acoustic field (acoustic), or dynamics that come from structural vibrations. In the second case, modes can either come from the wall vibration (structural liner) or from the support frame of the setup (structural other).

**Table 7-2: Overview of the measured and predicted frequencies of vibration.**

Measured Frequency [Hz]	Analytical Frequency [Hz]	Origin (mode shape)
63		Acoustic
	80	Structural liner (1,1)
92	92	Structural liner (1,2)
132	142.7	Structural liner (1,3)
156	160	Structural liner (1,4)
168		Structural others
182	180	Structural liner (1,5)
193		Acoustic
201	206	Structural liner (2,1)
290		Acoustic

## Combustion Results

The following step is the characterization of the setup while it is in operation. The tests reveal two distinctive combustion regimes can be achieved. One presents high amplitude thermoacoustic pressure oscillations while the other stable shows dynamic. The unstable regime is present if the combustor operates with thermal larger than 40 kW and it is independent of the actual air factor  $\lambda$  of the mixture.

The main trait is the large and narrow dynamic in the 90 to 100 Hz range, which corresponds to the first acoustic eigenmode. The nonlinear effects appear at multiple times the main frequency in the pressure spectrum, in the typical fashion of the other LIMOUSINE setups. The effect of higher thermal power is the increase in magnitude of the main and the secondary dynamics. However, the spectrum also shows dynamics of structural nature in the range of 140 to 150 Hz. The results for a fixed air factor of  $\lambda = 1.60$  and 40, 50 and 60 kW thermal power are shown in figure 7-6. In general, the pressure spectrum characteristics are similar to the LIMOUSINE version 2 combustor.

The effect of the sensitivity to the air factor from richer to leaner mixtures is plotted in the three panes of figure 7-7. As the air and fuel mixture gets leaner for a fixed thermal power, the magnitude of the peaks decreases without ever reaching the stable combustion regime. Overall, the main characteristics of the spectra do change much for points with the same combustion regime.

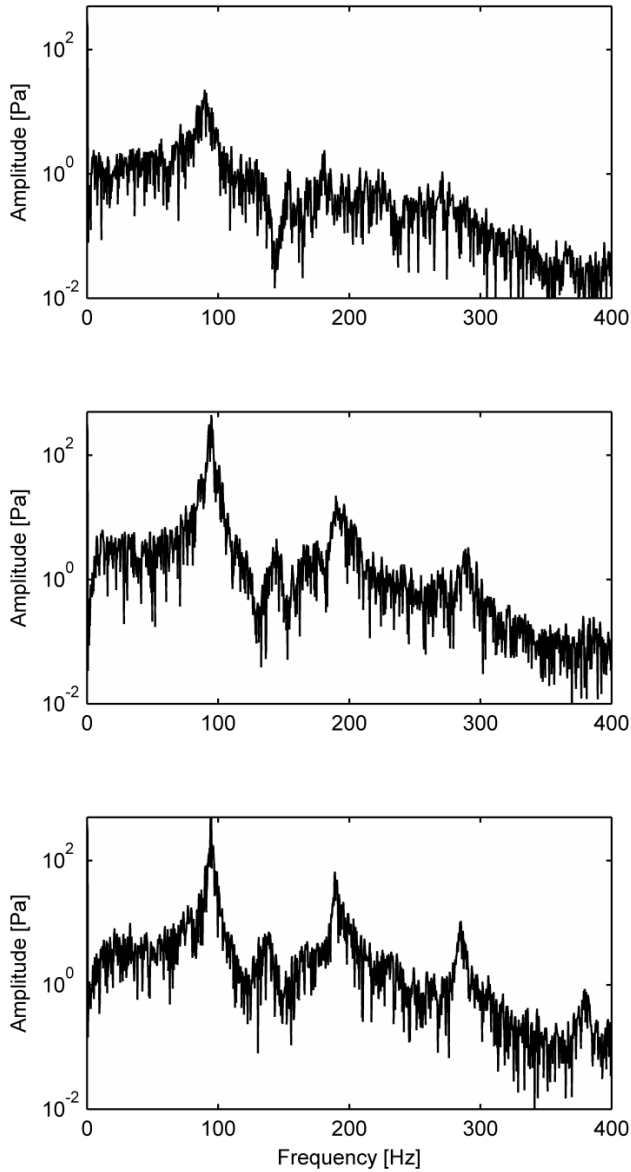


**Figure 7-6: LIMOUSINE version 1 PT 4 measured pressure spectra for  $\lambda = 1.60$  and 40 kW (top), 50 kW (middle) and 60 kW (bottom).**

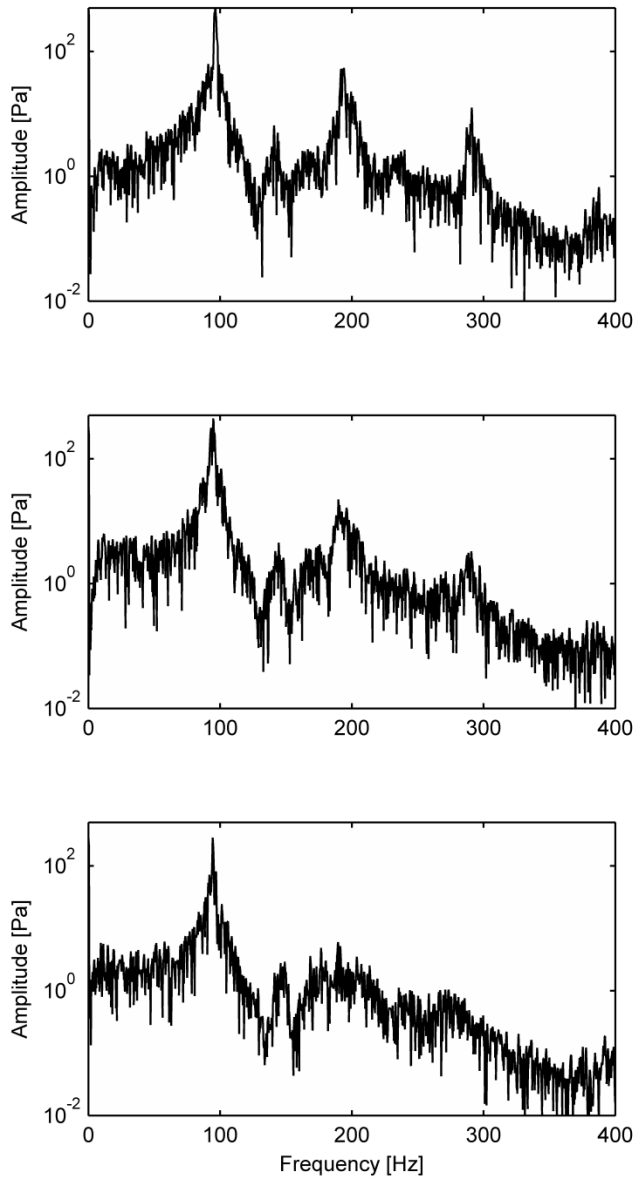


**Figure 7-7: LIMOUSINE version 1 PT 4 measured pressure spectra for 50 kW and  $\lambda = 1.20$  (top), 1.40 (middle) and 1.60 (bottom).**

Table 7-3 shows the measured values for the different cases under study. This table includes the flame burning conditions, the upstream Reynolds number, the measured oscillation frequencies and the temperature of the combustion chamber. The spontaneous emissions were recorded using a high speed intensified CCD camera aimed at the lateral window. The  $\text{CH}^*$  chemiluminescence pictures were obtained for one period of the flame perturbation and are shown in figure 7-8. The time interval between two consecutive frames is two milliseconds and corresponds to a  $72^\circ$  jump of the instability cycle. Despite the fact that only one perturbation cycle is presented, the motion of the flame repeats over and over during the full length of the clip. In these snapshots, the gases flow from bottom to top of the picture and the white areas indicate the zones of intense heat release. The flame rises symmetrically (and hence in synchronized flow) from each of the two sides of the bluff body. The maximum intensity level is reached in less than half of the period time, then decreases and remains at a low level until the beginning of the next cycle.

**Table 7-3: LIMOUSINE version 1 results.**

Power [kW]	Air factor $\lambda$ [-]	Re [-]	Peak Freq. [Hz]	Temp. in Comb. [°C]
40	1.20	7462	90.00	1081
40	1.40	8705	89.69	990
40	1.60	9949	89.00	939
40	1.80	11193	89.06	854
50	1.20	9327	96.25	1071
50	1.40	10882	94.69	1063
50	1.60	12436	94.38	962
50	1.80	13991	93.13	930
60	1.20	11193	98.75	1096
60	1.40	13058	94.38	1066
60	1.60	14924	92.5	1005
60	1.80	16789	89.38	907

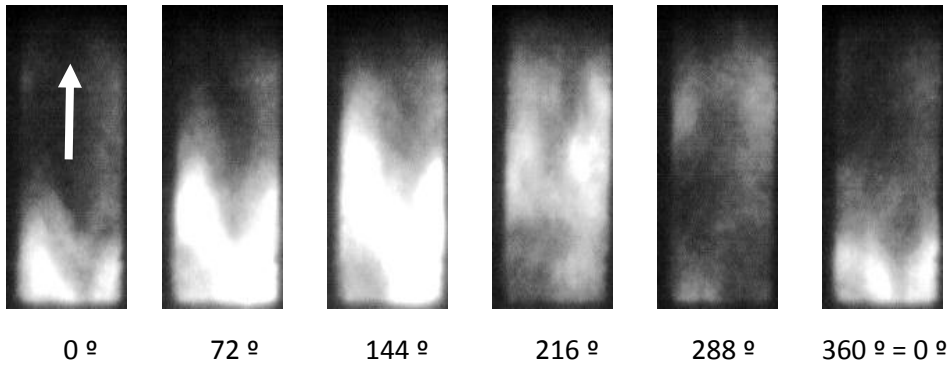


**Figure 7-8: LIMOUSINE version 1 CH\* flame emission.**

In figure 7-9 the heat release rate spectrum is plotted from the information of the movie frames. It shows a clear peak that coincides in frequency with the pressure perturbation and the frequency doubling effect.

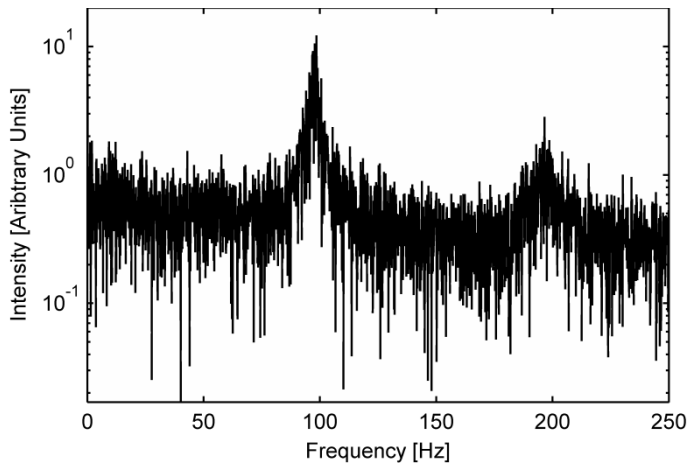


**Figure 7-9: LIMOUSINE version 1 CH\* emission for 50 kW and  $\lambda = 1.40$ .**

The presence of the unstable regime in the combustion process is indeed linked to the closure of the flame provided by the liner wall. In order to rule out the aerodynamic perturbations in the shear layers, the top part of the liner was removed and the CH\* spontaneous emission of the flame was measured. As confirmed by the experiments, none of the previously observed large amplitude dynamics are present; the perturbation has a clear thermoacoustic origin.



## Wall Vibration

One of the most important and interesting features of the combustion process in the LIMOUSINE version 1 combustor is the interaction of the pressure waves with the thin liner wall. Figure 7-10 shows the Laser Doppler Vibrometer (LDV) measured spectrum and it can be seen that shares many similarities with the pressure dynamics. The LDV sensor is able to pick up the thermoacoustic perturbations associated with the LCO, like the main and the secondary peaks and the structural motion perturbations. Nevertheless, the structural dynamics in the 140 Hz to 160 Hz range have a much larger magnitude in the LDV spectrum than the dynamics in the pressure spectrum counterparts. The results from multiple operating points are assembled in table 7-4.

**Table 7-4: LIMOUSINE version 1 measured wall vibration results.**

Power [kW]	Air factor $\lambda$ [-]	Re [-]	Peak Freq Structure [Hz]
40	1.20	7462	135.6
40	1.40	8705	154.8
40	1.60	9949	148.8
40	1.80	11193	147.5
50	1.20	9327	143.8
50	1.40	10882	144.4
50	1.60	12436	151.9
50	1.80	13991	145.3
60	1.20	11193	142.2
60	1.40	13058	134.4
60	1.60	14924	135.3
60	1.80	16789	135.0

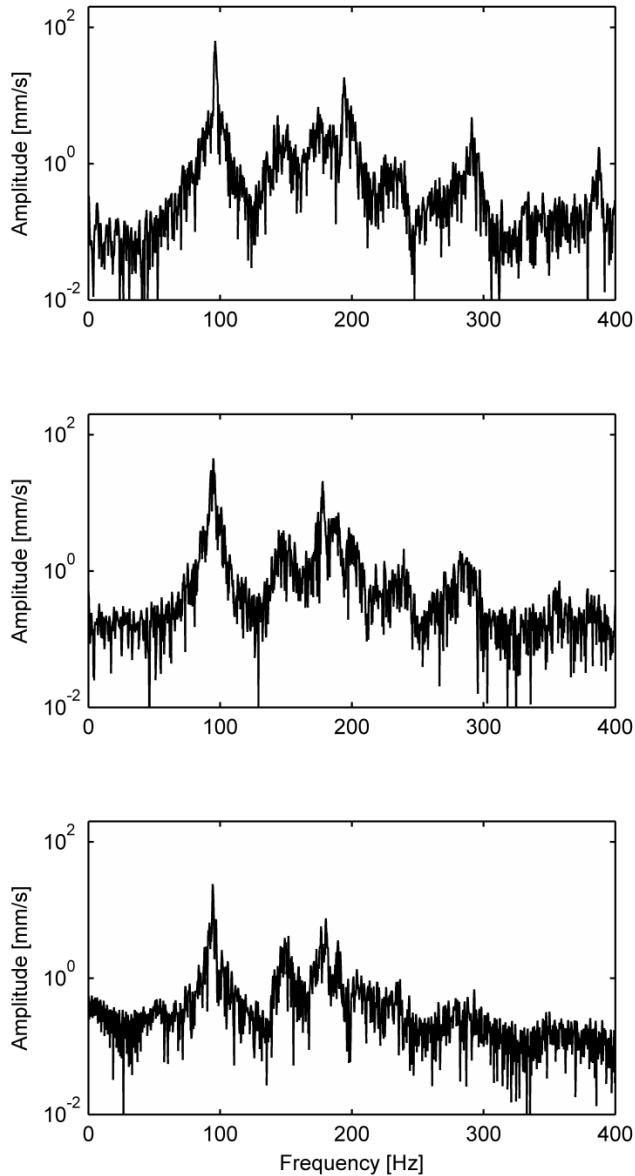


**Figure 7-10: LIMOUSINE version 1 wall vibration spectra for 50 kW and  $\lambda = 1.20$  (top),  $\lambda = 1.40$  (middle) and  $\lambda = 1.60$  (bottom).**

## Discussion

The flame dynamics analysis was performed with the study of the characteristic dimensionless numbers with the inlet flow Reynolds  $Re$  number, as was done in chapter 4. The trends of the Helmholtz  $He$  and Strouhal  $St$  number with inlet Reynolds number are plotted in figure 7-11. In this figure, the Helmholtz number has a value of 0.20 independent of the inlet velocity and considering the average speed of sound in the full combustor length. The Strouhal number of the follows a hyperbolic function  $St = 6772.8 Re^{-1.01}$  instead. The trends of both numbers point to the acoustic modes in the combustor as the driving physic of the flame instability, and in particular, the resonances of the 1/4 wave mode.

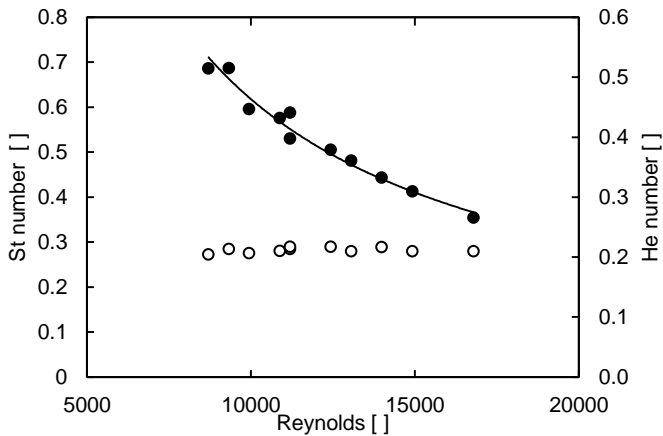


**Figure 7-11: LIMOUSINE version 1 dimensionless numbers. ● Strouhal number and ○ Helmholtz number.**

One of the most important characteristics of this combustor design is the interaction between flame and thin liner. The cross spectrum of the pressure, measured in the closest pressure transducer to the wedge in the downstream duct and the liner velocity is in figure 7-12. In this situation, the case 50 kW and air factor  $\lambda = 1.40$  is the point under study. The most important information of the cross spectrum is the peak location and their associated phase. If the phase of the peak is in the range between  $-\pi$  and  $\pi$ , both signals are in phase and they can easily exchange energy, which may lead to thermoacoustic oscillations. If the signals are not in phase, the energy transfer is not possible and the amplitude of the perturbation remains constant.

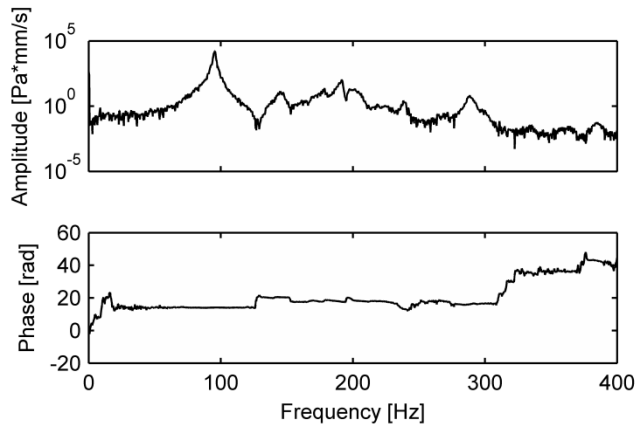


**Figure 7-12: LIMOUSINE version 1 cross spectrum of the pressure and wall velocity for 50 kW and  $\lambda = 1.40$ .**

The directly measured frequency and phase of the cross-spectrum are in table 7-5 for this flame conditions. The third column of this table is the corrected phase of the cross spectrum after the integration of measured wall velocity with LDV to wall displacement. The phase is presented in the  $-\pi$  to  $\pi$  range.

**Table 7-5: LIMOUSINE version 1 frequency and phase of the cross spectrum peaks for 50 kW and  $\lambda = 1.40$ .**

Peak	Frequency [Hz]	Phase [rad]	Corrected phase [rad]	Origin
1	95.6	14.11	0	Flame
2	145	20.45	0.02	Structural
3	191.6	17.61	-2.8	Flame double
4	288.4	16.06	1.92	Flame triple

The first (and most important) dynamic, as well as the second one in table 7-5 are in phase, while third and fourth dynamics are not in phase. The exchange of energy appears in the low frequency range and the third and fourth high frequency dynamics dissipate the energy. The prediction of the characteristic oscillation frequency of the liner in unstable combustion regime cases is not straightforward. Assuming a temperature of 450 °C in the liner, based in the emitted visible radiation, the first six structural frequencies predicted by the formula (7.1) are 72, 82, 128, 143, 162 and 185 Hz. It may seem unusual at first

sight that the excited structural eigenmode is not the first mode at 82.4 Hz. The reason for it is based on the displacement field of the structural eigenmodes and how they agree with the acoustic pressure profile.

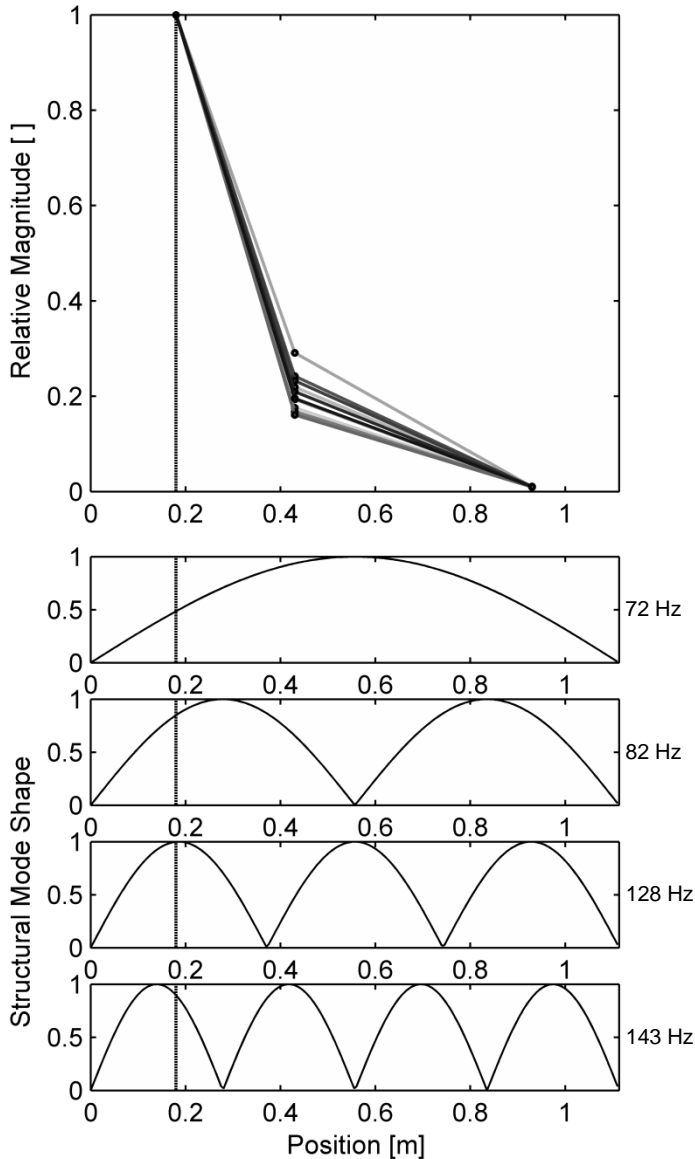


**Figure 7-13: LIMOUSINE version 1 pressure profile for different inlet Re number (top) and first four mode shape of the vertical centerline of the combustion chamber wall (bottom 4 panes). The wedge is the origin of the horizontal axis and the vertical line is the location of the maximum oscillation amplitude.**

The top pane of figure 7-13 shows the measured pressure profile in the combustion chamber of the LIMOUSINE version 1 on basis of the pressure amplitude recorded by the transducers PT 4 to PT 6. It shows that the studied cases (colored with a different gray shade for every upstream  $Re$  number), share identical profile, with a maximum of the pressure oscillations at the flame area and zero pressure at the exit end. The next four panes show the predicted displacement of the vertical centerline of the combustor chamber liner for the first four eigenmodes and clamp conditions at the four sides. The vertical line across all four panes indicates the maximum pressure oscillation amplitude. This maximum location does not coincide with a large wall displacement for the first two modes at 71 and 82 Hz, but it coincides with a maximum of displacement for the fourth 143 Hz predicted mode. Hence, this is the most likely eigenmode to be excited. This result also agrees with the information of table 7-5, that showed efficient energy transfer happens at 145 Hz.

### **Proposed Loop**

The recorded data from the pressure transducers and the Laser Doppler Vibrometer LDV together with the harvested data from the impact hammer test points to the necessity of a modification of the Limit Cycle feedback loop. In particular, it is necessary to change the role of the structure and the effects of the combustor walls vibration on the thermoacoustic flame dynamics. The loop modification is indispensable to explain why the structural dynamics are seen with moderate intensity in the pressure oscillations and why the fourth structural eigenmode appears as the most excited. The answer is because the two physics are linked to each other with strong ties (graph in figure 7-14 in the next page).

The two-way arrows between the structure and the acoustics in the new proposed loop mean that each field can interact and modify the other fields with 2 way interaction. Unlike the 1 way interaction of the original thermoacoustic loop, the combustion instability can couple with the eigenmodes of the structure that can interact well with it. This mode may not be the closest in frequency, but they can share a similar waveform profile that allows efficient energy exchange. The practical application of the new feedback loop is that can predict which additional frequencies will be excited in the event of Limit Cycle of pressure Oscillations and the designer can take action to improve the combustor design.

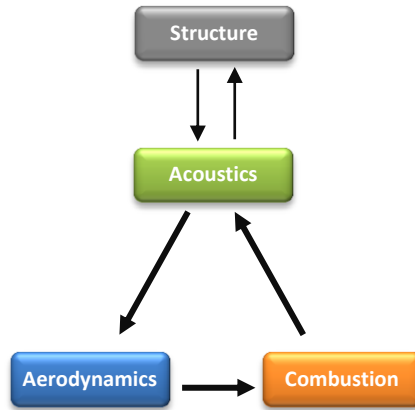


**Figure 7-14: Proposed feedback loop.**

LIMOUSINE version 1 and versions 2 and 3 share many geometric characteristics, combustion regimes and general behavior. The discussion about the dynamics for version 2 is carried in chapter 5. The results of the FSI in the LIMOUSINE version 3 are in appendix D.

# Chapter 8 Conclusions

This chapter summarizes all the findings over flame dynamics and thermoacoustic oscillations observed in the LIMOUSINE burners versions 2 and 3 in chapter 4, chapter 5, and chapter 6. Afterwards, the results about Fluid Structure Interaction in version 1 are presented (chapter 7).

## Observed Flame Instability Behavior

This dissertation is based on the observations of the flame dynamics in a laboratory-scale combustor. The combustor was custom made for this purpose and named after the project acronym LIMOUSINE. The combustor was designed and built by the University of Twente and twin copies were sent to the other fellow institutions. The burner can sustain bluff body stabilized flames from 30kW to 70 kW and large air factor. The LIMOUSINE combustor has a modular construction design that allows the modification of the burner type and combustion chamber length. The version 2 of the combustor has large passage ducts around the bluff body while the version 3 presents new re-designed lateral blocks that reduce the cross sectional burner area.

## LIMOUSINE Version 2 Flame Dynamics

The observed flames in LIMOUSINE version 2 single liner did not show any large amplitude thermoacoustics oscillation until an additional liner duct module was mounted on top of the combustion chamber. This change is sufficient to produce a Limit Cycle of pressure Oscillations for lean mixture ( $\lambda > 1.60$ ) that can reach thousands of Pascal in amplitude. The evolution of the dimensionless numbers, such  $He$  and  $St$  with respect to the inlet  $Re$  number suggests that the frequency of the oscillations is related to the volumetric acoustic eigenmodes. The stability of the combustion process is a function of the ratio of the flame convective time delay and the acoustic period. If both values are of the same magnitude, it is possible to develop a thermoacoustic feedback loop. The combustion of relatively near to stoichiometric mixtures ( $\lambda < 1.40$ ) decreases the convective time delay, which stops the feedback loop and transforms the characteristics compact flame of the LCO to two long and thin flamelets.



The combustion process on the single liner version 2 combustor have the same flame characteristic delays of its double liner counterpart, but a drop of almost 40% in the acoustic period due to the shorter combustion chamber is the reason that explains why this combustor does not develop thermoacoustic instabilities.

### **LIMOUSINE Version 3 Flame Dynamics**

The flame dynamics of the LIMOUSINE version 3 combustor (for single and double liner configuration), are opposite to the version 2. The unstable regime is now observed at close to stoichiometric air fuel mixtures while the stable regime is associated with lean flames. The main difference between the two versions are modified lateral blocks of the burner assembly, which reduce the available cross sectional area in the burner inlets. The increased jet speed generates stronger recirculation zones downstream of the wedge.

The measured frequency of the instability seems once more related to the acoustic eigenmodes of the combustion chamber, as pointed by the constant  $He$  numbers of the order of 0.4. The acoustic driving at this frequency is a consequence of the pressure profile discontinuity after and before the burner. The pressure profile shape points to an active region around the flame and to the rest of the combustor behaving as a resonator. This mechanism does not depend on the combustion chamber length, since it is observed as well in the double liner configuration. The main differences with the single liner are a less compact flame and, for certain fuel and air flow combinations, an intermediate flame regime that shows mixed characteristics from both regimes. The effectiveness of the energy exchange between released heat and pressure is related to the flame size.

The evaluation of the flame stability with the time delay model used in LIMOUSINE version 2 does not agree with the measured data in version 3. In this situation, the influence of the flow aerodynamics, and specially, the effects of the recirculation zone, are important and must be accounted for. The recirculation zone can either trap the flame in the wake of the bluff body and create a violent and sudden reaction or sustain two independent long and thin flames during the stable regime. The hypothesis is confirmed by the flame front temporal evolution recorded with high speed CCD cameras and the PIV images from Imperial College. Mathematically, the Aerodynamic/Acoustic (AA) ratio is used to evaluate this phenomenon. The AA ratio is a dimensionless number that relates frequency of instability, length of the recirculation zone and speed of the jets into the

combustion chamber, similar to the other dimensionless numbers  $St$  or  $He$ . Low values of this parameter (below 0.5) are characteristic of stable combustion, for both single and double liner configuration. On the contrary, large values result in thermoacoustics oscillations. The concept of the AA ratio may also be used in premixed swirl stabilized flames. Table 8-1 shows a quick overview of the studied cases.

**Table 8-1: Overview of LIMOUSINE combustor flame dynamics.**

Burner	Length	Limit cycle	Remarks
Version 2	Single liner	Not present	
	Double liner	For lean flames	<ul style="list-style-type: none"> <li>• Frequency is related to full combustor acoustics</li> <li>• Stability depends on flame/acoustic ratio</li> </ul>
Version 3	Single liner	For close to stoichiometric flames	<ul style="list-style-type: none"> <li>• Frequency is related to combustion chamber acoustics</li> <li>• Stability depends on aerodynamics (AA ratio)</li> </ul>
	Double liner		<ul style="list-style-type: none"> <li>• There is an intermediate regime</li> </ul>

## Nonlinear Dynamics

A large part of the dissertation has been focused on non-linear phenomena. The investigation includes the application of the chaos theory analysis to the measured time traces and the research of frequency doubling effects. The bifurcation of the combustion regime is not easy to predict, as it depends on the hysteresis of the combustor and sets the two different combustion regimes apart. The knowledge of the nonlinear effects helps to the development of more robust and efficient controllers for gas turbine engines. The differences between the stable and stable regimes also point to the idea of incorporating a different control strategy for each regime.

The unstable regime studied with chaos theory shows a relatively simple motion, with associated dimensions  $dE$  and  $dA$  between 2 and 3. This unstable motion is deterministic and may be controlled with traditional approaches, for example, feeding into the actuator the phase-delayed signal recorded in a sensor. On the other hand, the stable regime has significant higher dimensions  $dE$  and  $dA$  and much more complex behavior, which sometimes can even be chaotic. There is not any need for a control system in a stable regime, but it can be used to prevent the

rise of the thermoacoustic instability once the system reaches a bifurcation point. The practical control system implementation may require novel control strategies like neural networks. An additional advantage of controls systems is that the actuators can operate with low amplitudes, which results in simpler and cheaper solutions.

Analytical tools, such as the Rayleigh criterion and network models can predict the stable and unstable regimes based on prior knowledge of the system. However, these tools are insufficient to fully describe the effects of the limit cycle that are consequence of the large perturbations amplitude. Among these effects, frequency doubling is characteristic of the unstable regimes and it has been observed in every version of the LIMOUSINE combustor. Narrow band secondary peaks rise from the background of the pressure and heat release spectra at multiple times the frequency of the instability. Due to the complex geometry and the temperature gradients found along the version 3 of the LIMOUSINE combustor, the acoustic eigenfrequencies are not equally spaced in the frequency domain. Thus, the mentioned secondary peaks do not have an acoustic origin. Frequency doubling dynamics is the manifestation in the frequency domain of the asymmetrical temporal pressure waveform. The physical root cause of the nonlinearity lies on the flame dynamics and combustion kinetics.

In the unstable regime, the fuel in the bluff body wake does not burn steadily over the cycle. Due to acoustic velocity, the mixture accumulates in the recirculation zone and burns in a very short time at the beginning of every cycle. Only little fuel quantity is left for the rest of the cycle, which allows the flush of the product gases and the accumulation of fuel for the following cycle. The proposed model uses an expression that relates velocity perturbations and heat release in the time domain at the LCO frequency. This is very similar to a Flame Transfer Function, but valid only for the limit cycle conditions. The proposed model extends the well-known  $n - \tau$  linear model into a Taylor series, with the higher order terms describing the non-linear effects.

### **Fluid Structure Interaction**

Despite the Fluid Structure Interaction is visible in the three versions of the LIMOSINE combustor, it was studied more in detail in version 1. This combustor has a wider and longer liner made of 1 mm thick steel plate that reduces the overall stiffness and makes it more prone to couple with the thermoacoustic Limit

Cycle. This combustor was characterized by the acoustic reflection coefficient  $R$  of the upstream and downstream ends. After it, acoustic and structural eigenmodes were calculated from the measured data in the laboratory. The data showed that the two fields are interconnected to each other even without the combustion process.

The flame behavior presents similarities with the LIMOUSINE version 2 flame. The unstable regime corresponds to the operating parameters with large inlet flow velocity (large thermal power) independently of the air factor. The nonlinear frequency doubling dynamics were visible in the measured pressure spectrum during unstable combustion. Like in the other cases, the pressure profile has a maximum in the inlet of the combustor and a node at the exit plane. The largest FSI happens at limit cycle frequency, but the second largest interaction is related to the fourth structural mode. The reason is the shape of this particular eigenmode can interact well with the pressure field inside the combustor.

To be able to predict the coupling effects, the conventional feedback loop of the thermoacoustic instability has to be modified. In the original situation, the structural elements have a passive role between the combustion and the acoustics. In the proposed new loop the structure has a two way interaction with the sound field. With the structure being a principal player in the loop, the prediction of the Limit Cycle frequencies becomes an even more challenging task. One possible approach to this problem is the use of two way coupled simulations of the flame and liner wall.

## Final Remarks

Dear reader: If you have born with me for the full length of the dissertation, for all the successive chapters on flame dynamics and fluid structure interaction, then you must have grown a feeling inside your head. Worry not, I had the same experience while I was gathering the measured data and writing the dissertation. All presented results and their associated analyses share a common idea, the same key property. It may take you some time to realize, since in some chapters it is very obvious and in some is kind of subtle. I think this idea is so powerful and simple that I feel I can summarize the full extent of the PhD work in one single sentence: timing is everything.

The limit cycle phenomenon is the interaction between three and sometimes four different physics: acoustics, aerodynamics, chemical combustion and structural mechanics. Like everything else in nature, these physics are processes with their own associated times. You could also say that every process has its own eigenfrequencies, if you feel more comfortable in the frequency domain. The whole point of the dissertation is to understand those delays and how do they connect to each other. The LCO is the consequence of the acoustic period matching the chemical timescale and aerodynamic delay. The FSI is no more than the agreement of the previous delays with the vibration of the liner walls. That is all you need to know. Is it not beautiful?.

Allow me to finish with the expansion of this idea further than the boundaries of the dissertation. In physics, in nature and in life, timing is everything.

Juan Carlos

Enschede, May 2013.

# Bibliography

- [1] Pilavachi, P. A., 2002, "Mini- and micro-gas turbines for combined heat and power," *Applied Thermal Engineering*, 22(18), pp. 2003-2014.
- [2] 2012, "Siemens Energy," <http://www.energy.siemens.com/hq/en/power-generation/power-plants/gas-fired-power-plants/combined-cycle-power-plant-concept/scc5-8000h-1s.htm>.
- [3] 2001, "On the limitation of emissions of certain pollutants into the air from large combustion plants," DIRECTIVE 2001/80/EC, Official Journal of the European Communities, p. 21.
- [4] Pozarlik, A. K., 2010, "Vibro-acoustical instabilities induced by combustion dynamics in gas turbine combustors," Enschede.
- [5] Rea, S., James, S., Goy, C., and Colechin, M. J. F., 2003, "On-line combustion monitoring on dry low NO<sub>x</sub> industrial gas turbines," *Measurement Science and Technology*, 14(7), p. 1123.
- [6] Raun, R. L., Beckstead, M. W., Finlison, J. C., and Brooks, K. P., 1993, "A review of Rijke tubes, Rijke burners and related devices," *Prog. Energy Combust. Sci.*, 19(4), pp. 313-364.
- [7] Gelfand, S. A., 2004, *Hearing: An Introduction to Psychological and Physiological Acoustics*, Marcel Dekker Incorporated.
- [8] Leconte, J., 1858, "On the influence of musical sounds on the flame of a jet of coal-gas," *Philosophical Magazine Series 4*, 15(99), pp. 235-239.
- [9] Feldman, K. T., 1968, "Review of the literature on Sondhauss thermoacoustic phenomena," *Journal of Sound and Vibration*, 7(1), pp. 71-&.
- [10] Bisio, G., and Rubatto, G., 1999, "Sondhauss and Rijke oscillations—thermodynamic analysis, possible applications and analogies," *Energy*, 24(2), pp. 117-131.
- [11] Taconis, K. W., Beenakker, J. J. M., Nier, A. O. C., and Aldrich, L. T., 1949, "Measurements concerning the vapour-liquid equilibrium of solutions of He<sup>3</sup> in He<sup>4</sup> below 2.19°K," *Physica*, 15(8–9), pp. 733-739.
- [12] Rijke, P. L., 1859, "Notice of a new method of causing a vibration of the air contained in a tube open at both ends," *The London, Edinburgh and Dublin Philosophical Magazine and Journal of Science*, 17(62).
- [13] Noiray, N., Durox, D., Schuller, T., and Candel, S., 2008, "A unified framework for nonlinear combustion instability analysis based on the flame describing function," *Journal of Fluid Mechanics*, 615, pp. 139-167.
- [14] J.W. Strutt, L. R., 1894, *The series of sound*.
- [15] Crocco, L., Grey, J., and Matthews, G. B., 1955, "Preliminary measurements of the combustion time lag in a monopropellant rocket motor," *Symposium (International) on Combustion*, 5(1), pp. 164-170.

- [16] Blomshield, F. S., 2006, "Lessons Learned in Solid Rocket Combustion Instability," Proceedings of the 2006 AIAA Missile Sciences Conference Monterey, p. 20.
- [17] Putnam, A. A., 1971, Combustion-driven oscillations in industry, American Elsevier Pub. Co.
- [18] Lieuwen, T. C., and Yang, V., 2005, Combustion instabilities in gas turbine engines: operational experience, fundamental mechanisms and modeling American Institute of Aeronautics and Astronautics.
- [19] Lefebvre, A. H., and Ballal, D. R., 2010, Gas Turbine Combustion: Alternative Fuels and Emissions, Third Edition, Taylor & Francis.
- [20] Niederberger, A. S. P., Schuermans, B. B. H., and Guzzella, L., 2009, "Parameter identification for a low-order network model of combustion instabilities," International Journal of Spray and Combustion Dynamics, 1(1), pp. 113-142.
- [21] van Kampen, J. F., 2006, "Acoustic pressure oscillations induced by confined premixed natural gas flames," PhD thesis, University of Twente, Enschede.
- [22] Moureau, V., Domingo, P., and Vervisch, L., 2011, "From Large-Eddy Simulation to Direct Numerical Simulation of a lean premixed swirl flame: Filtered laminar flame-PDF modeling," Combustion and Flame, 158(7), pp. 1340-1357.
- [23] Hernández, I., Staffelbach, G., Poinot, T., Román Casado, J. C., and Kok, J. B. W., 2013, "LES and acoustic analysis of thermo-acoustic instabilities in a partially premixed model combustor," Comptes Rendus Mécanique, 341(1–2), pp. 121-130.
- [24] Hermeth, S., Staffelbach, G., Gicquel, L. Y. M., and Poinot, T., 2013, "LES evaluation of the effects of equivalence ratio fluctuations on the dynamic flame response in a real gas turbine combustion chamber," Proceedings of the Combustion Institute, 34(2), pp. 3165-3173.
- [25] Kelsall, G., and Troger, C., 2004, "Prediction and control of combustion instabilities in industrial gas turbines," Applied Thermal Engineering, 24(11–12), pp. 1571-1582.
- [26] Richards, G. A., Straub, D. L., and Robey, E. H., 2003, "Passive Control of Combustion Dynamics in Stationary Gas Turbines," Journal of Propulsion and Power, 19(5), pp. 795-810.
- [27] Schadow, K. C., and Gutmark, E., 1992, "Combustion instability related to vortex shedding in dump combustors and their passive control," Prog. Energy Combust. Sci., 18(2), pp. 117-132.
- [28] Gullaud, E., and Nicoud, F., 2012, "Effect of Perforated Plates on the Acoustics of Annular Combustors," Aiaa J., 50(12), pp. 2629-2642.
- [29] Peters, M., Hirschberg, A., Reijnen, A. J., and Wijnands, A. P. J., 1993, "Damping and reflection coefficient measurements for an open pipe at low Mach and low Helmholtz numbers," Journal of Fluid Mechanics, 256, pp. 499-534.
- [30] Hermann, J., Orthmann, A., Hoffmann, S., and Berenbrink, P., 2000, Active and passive control of combustion oscillations in a 260 MW heavy-duty gas turbine.
- [31] Blonbou, R., Laverdant, A., Zaleski, S., and Kuentzmann, P., 2000, "Active control of combustion instabilities on a rijke tube using neural networks," Proceedings of the Combustion Institute, 28(1), pp. 747-755.

- [32] Cosic, B., Bobusch, B. C., Moeck, J. P., and Paschereit, C. O., 2012, "Open-Loop Control of Combustion Instabilities and the Role of the Flame Response to Two-Frequency Forcing," *Journal of Engineering for Gas Turbines and Power-Transactions of the Asme*, 134(6).
- [33] Heckl, M. A., 1988, "Active control of the noise from a Rijke tube," *Journal of Sound and Vibration*, 124(1), pp. 117-133.
- [34] McManus, K. R., Poinso, T., and Candel, S. M., 1993, "A review of active control of combustion instabilities," *Prog. Energy Combust. Sci.*, 19(1), pp. 1-29.
- [35] Sato, H., Ikame, M., Harumi, K., Kishi, T., Hiraoka, K., Oka, H., Hayashi, A. K., and Ogawa, S., 2005, "Active instability control of thermoacoustic oscillation in premixed gas turbine combustors," *JSME Int. J. Ser. B-Fluids Therm. Eng.*, 48(2), pp. 328-333.
- [36] Seume, J. R., Vortmeyer, N., Krause, W., Hermann, J., Hantschk, C. C., Zangl, P., Gleis, S., Vortmeyer, D., and Orthmann, A., 1998, "Application of active combustion instability control to a heavy duty gas turbine," *Journal of Engineering for Gas Turbines and Power-Transactions of the Asme*, 120(4), pp. 721-726.
- [37] Tijani, M. E. H., and Spoelstra, S., 2008, "Study of a coaxial thermo acoustic-Stirling cooler," *Cryogenics*, 48(1-2), pp. 77-82.
- [38] Bothien, M. R., 2008, "Impedance tuning: A method for active control of the acoustic boundary conditions of combustion test rig," PhD, T U Berlin.
- [39] van der Eerden, F. J. M., de Bree, H. E., and Tjiedeman, H., 1998, "Experiments with a new acoustic particle velocity sensor in an impedance tube," *Sensors and Actuators A: Physical*, 69(2), pp. 126-133.
- [40] Ross, D. F., and Seybert, A. F., 1977, "Experimental-Determination Of Acoustic Properties Using A 2-Microphone Random-Excitation Technique," *Journal of the Acoustical Society of America*, 62, pp. S57-S57.
- [41] Chung, J. Y., and Blaser, D. A., 1980, "Transfer-Function Method Of Measuring In-Duct Acoustic Properties .2. Experiment," *Journal of the Acoustical Society of America*, 68(3), pp. 914-921.
- [42] Munjal, M. L., and Doige, A. G., 1990, "The two-microphone method incorporating the effects of mean flow and acoustic damping," *Journal of Sound and Vibration*, 137(1), pp. 135-138.
- [43] Fischer, A., Hirsch, C., and Sattelmayer, T., 2006, "Comparison of multi-microphone transfer matrix measurements with acoustic network models of swirl burners," *Journal of Sound and Vibration*, 298(1-2), pp. 73-83.
- [44] Fanaca, D., Alemela, P. R., Hirsch, C., and Sattelmayer, T., 2010, "Comparison of the Flow Field of a Swirl Stabilized Premixed Burner in an Annular and a Single Burner Combustion Chamber," *Journal of Engineering for Gas Turbines and Power-Transactions of the Asme*, 132(7).
- [45] Strahle, W. C., and Shivashankara, B. N., 1976, "Combustion Generated Noise In Gas-Turbine Combustors," *Journal of Engineering for Power-Transactions of the Asme*, 98(2), pp. 242-246.



- [46] Lieuwen, T., Torres, H., Johnson, C., and Zinn, B. T., 2001, "A mechanism of combustion instability in lean premixed gas turbine combustors," *Journal of Engineering for Gas Turbines and Power-Transactions of the Asme*, 123(1), pp. 182-189.
- [47] Sattelmayer, T., and Polifke, W., 2003, "Assessment of methods for the computation of the linear stability of combustors," *Combust. Sci. Technol.*, 175(3), pp. 453-476.
- [48] Ducruix, S., Schuller, T., Durox, D., and Candel, S., 2003, "Combustion dynamics and instabilities: Elementary coupling and driving mechanisms," *Journal of Propulsion and Power*, 19(5), pp. 722-734.
- [49] Nicoud, F., and Poinso, T., 2005, "Thermoacoustic instabilities: Should the Rayleigh criterion be extended to include entropy changes?," *Combustion and Flame*, 142(1-2), pp. 153-159.
- [50] Krediet, H. J., 2012, "Prediction of limit cycle pressure oscillations in gas turbine combustion systems using the flame describing function," University of Twente, Enschede.
- [51] Krediet, H. J., Beck, C. H., Krebs, W., Schimek, S., Paschereit, C. O., and Kok, J. B. W., 2012, "Identification of the Flame Describing Function of a premixed swirl flame from LES," *Combust. Sci. Technol.*, 184(7-8), pp. 888-900.
- [52] Bellows, B. D., Bobba, M. K., Seitzman, J. M., and Lieuwen, T., 2007, "Nonlinear flame transfer function characteristics in a swirl-stabilized combustor," *Journal of Engineering for Gas Turbines and Power-Transactions of the Asme*, 129(4), pp. 954-961.
- [53] Dowling, A. P., 1997, "Nonlinear self-excited oscillations of a ducted flame," *Journal of Fluid Mechanics*, 346, pp. 271-290.
- [54] Balachandran, R., Ayoola, B. O., Kaminski, C. F., Dowling, A. P., and Mastorakos, E., 2005, "Experimental investigation of the nonlinear response of turbulent premixed flames to imposed inlet velocity oscillations," *Combustion and Flame*, 143(1-2), pp. 37-55.
- [55] Bellows, B. D., Neumeier, Y., and Lieuwen, T., 2006, "Forced response of a swirling, premixed flame to flow disturbances," *Journal of Propulsion and Power*, 22(5), pp. 1075-1084.
- [56] Kim, K. T., Lee, J. G., Quay, B. D., and Santavicca, D. A., 2010, "Spatially distributed flame transfer functions for predicting combustion dynamics in lean premixed gas turbine combustors," *Combustion and Flame*, 157(9), pp. 1718-1730.
- [57] Schuller, T., Durox, D., and Candel, S., 2003, "A unified model for the prediction of laminar flame transfer functions: comparisons between conical and V-flame dynamics," *Combustion and Flame*, 134(1-2), pp. 21-34.
- [58] Armitage, C. A., Riley, A.J., Cant, R.S., Dowling, A.P. and Stow, S.R., 2004, "Flame transfer function for swirled LPP combustion from experiments and CFD," ASME Turbo Expo, ASME, Vienna, Austria.

- [59] Schimek, S., Moeck, J. P., and Paschereit, C. O., 2010, "An Experimental Investigation of the Nonlinear Response of an Atmospheric Swirl-Stabilized Premixed Flame," *ASME Conference Proceedings*, 2010(43970), pp. 665-675.
- [60] Kornilov, V. N., Schreel, K. R. A. M., and De Goey, L. P. H., 2007, "Experimental assessment of the acoustic response of laminar premixed Bunsen flames," *Proceedings of the Combustion Institute*, 31, pp. 1239-1246.
- [61] Lee, J. G., Kim, K., and Santavicca, D. A., 2000, "Measurement of equivalence ratio fluctuation and its effect on heat release during unstable combustion," *Proceedings of the Combustion Institute*, 28, pp. 415-421.
- [62] Kim, D., and Park, S. W., 2010, "Forced and self-excited oscillations in a natural gas fired lean premixed combustor," *Fuel Processing Technology*, 91(11), pp. 1670-1677.
- [63] Ax, H., Kutne, P., Meier, W., Koenig, K., Maas, U., Class, A., and Aigner, M., 2009, "Low pressure premixed CH<sub>4</sub>/air flames with forced periodic mixture fraction oscillations: experimental approach," *Applied Physics B-Lasers and Optics*, 94(4), pp. 705-714.
- [64] van Kampen, J. F., Kok, J. B. W., and van der Meer, T. H., 2007, "Efficient retrieval of the thermo-acoustic flame transfer function from a linearized CFD simulation of a turbulent flame," *International Journal for Numerical Methods in Fluids*, 54(9), pp. 1131-1149.
- [65] Polifke, W., Poncet, A., Paschereit, C. O., and Dobbeling, K., 2001, "Reconstruction of acoustic transfer matrices by instationary computational fluid dynamics," *Journal of Sound and Vibration*, 245(3), pp. 483-510.
- [66] Alemela, P. R., Fanaca, D., Hirsch, C., Sattelmayer, T., and Schuermans, B., 2010, "Determination and scaling of thermo acoustic characteristics of premixed flames," *International Journal of Spray and Combustion Dynamics*, 2(2), pp. 169-198.
- [67] Dowling, A. P., 1999, "A kinematic model of a ducted flame," *Journal of Fluid Mechanics*, 394, pp. 51-72.
- [68] Durox, D., Schuller, T., Noiray, N., and Candel, S., 2009, "Experimental analysis of nonlinear flame transfer functions for different flame geometries," *Proceedings of the Combustion Institute*, 32, pp. 1391-1398.
- [69] Palies, P., Durox, D., Schuller, T., and Candel, S., 2011, "Nonlinear combustion instability analysis based on the flame describing function applied to turbulent premixed swirling flames," *Combustion and Flame*, 158(10), pp. 1980-1991.
- [70] Palies, P., Durox, D., Schuller, T., Candel, S., and Asme, 2010, Swirling flame instability analysis based on the flame describing function methodology.
- [71] Karimi, N., Brear, M. J., Jin, S.-H., and Monty, J. P., 2009, "Linear and non-linear forced response of a conical, ducted, laminar premixed flame," *Combustion and Flame*, 156(11), pp. 2201-2212.
- [72] Balasubramanian, K., and Sujith, R., 2008, "Non-normality and nonlinearity in combustion-acoustic interaction in diffusion flames," *Journal of Fluid Mechanics*, 594, pp. 29-57.

- [73] Dhanuka, S. K., Temme, J. E., and Driscoll, J. F., 2011, "Lean-limit combustion instabilities of a lean premixed prevaporized gas turbine combustor," *Proceedings of the Combustion Institute*, 33(2), pp. 2961-2966.
- [74] Meier, W., Duan, X. R., and Weigand, P., 2005, "Reaction zone structures and mixing characteristics of partially premixed swirling CH<sub>4</sub>/air flames in a gas turbine model combustor," *Proceedings of the Combustion Institute*, 30(1), pp. 835-842.
- [75] Stöhr, M., Boxx, I., Carter, C., and Meier, W., 2011, "Dynamics of lean blowout of a swirl-stabilized flame in a gas turbine model combustor," *Proceedings of the Combustion Institute*, 33(2), pp. 2953-2960.
- [76] Soika, A., Dinkelacker, F., and Leipertz, A., 2003, "Pressure influence on the flame front curvature of turbulent premixed flames: comparison between experiment and theory," *Combustion and Flame*, 132(3), pp. 451-462.
- [77] Esquiva-Dano, I., Nguyen, H. T., and Escudie, D., 2001, "Influence of a bluff-body's shape on the stabilization regime of non-premixed flames," *Combustion and Flame*, 127(4), pp. 2167-2180.
- [78] Kariuki, J., Dawson, J. R., and Mastorakos, E., 2012, "Measurements in turbulent premixed bluff body flames close to blow-off," *Combustion and Flame*, 159(8), pp. 2589-2607.
- [79] Roman Casado, J. C., Alemela, P. R., and Kok, J. B. W., 2011, "Experimental and numerical study of the effect of acoustic time delays on combustion stability " *ICSVRio de Janeiro*.
- [80] Lipatnikov, A., and Sathiah, P., 2005, "Effects of turbulent flame development on thermoacoustic oscillations," *Combustion and Flame*, 142(1-2), pp. 130-139.
- [81] Nair, S., and Lieuwen, T., 2007, "Near-blowoff dynamics of a bluff-body stabilized flame," *Journal of Propulsion and Power*, 23(2), pp. 421-427.
- [82] Hield, P. A., Brear, M. J., and Jin, S. H., 2009, "Thermoacoustic limit cycles in a premixed laboratory combustor with open and choked exits," *Combustion and Flame*, 156(9), pp. 1683-1697.
- [83] Correa, S. M., and Gulati, A., 1992, "Measurements and modeling of a bluff body stabilized flame," *Combustion and Flame*, 89(2), pp. 195-213.
- [84] Henrikson, A. S., A., 1963, "CARS measurements and visualization of reacting flows in a bluff body stabilized flame," *Archive Set 474, American Institute of Aeronautics and Astronautics*.
- [85] Lysenko, D., Ertesvåg, I. S., and Rian, K. E., 2011, "Turbulent bluff body flows modeling using OpenFOAM technology," *MekIT*, pp. 189-208.
- [86] Giacomazzi, E., Battaglia, V., and Bruno, C., 2004, "The coupling of turbulence and chemistry in a premixed bluff-body flame as studied by LES," *Combustion and Flame*, 138(4), pp. 320-335.
- [87] Bai, X.-S., and Fuchs, L., 1994, "Modelling of turbulent reacting flows past a bluff body: assessment of accuracy and efficiency," *Computers & Fluids*, 23(3), pp. 507-521.

- [88] Nottin, C., Knikker, R., Boger, M., and Veynante, D., 2000, "Large eddy simulations of an acoustically excited turbulent premixed flame," *Proceedings of the Combustion Institute*, 28, pp. 67-73.
- [89] Shanbhogue, S. J., Husain, S., and Lieuwen, T., 2009, "Lean blowoff of bluff body stabilized flames: Scaling and dynamics," *Prog. Energy Combust. Sci.*, 35(1), pp. 98-120.
- [90] Erickson, R. R., and Soteriou, M. C., 2011, "The influence of reactant temperature on the dynamics of bluff body stabilized premixed flames," *Combustion and Flame*, 158(12), pp. 2441-2457.
- [91] Chaudhuri, S., Kostka, S., Renfro, M. W., and Cetegen, B. M., 2012, "Blowoff mechanism of harmonically forced bluff body stabilized turbulent premixed flames," *Combustion and Flame*, 159(2), pp. 638-640.
- [92] Broadwell, J. E., Dahm, W. J. A., and Mungal, M. G., 1985, "Blowout of turbulent diffusion flames," *Symposium (International) on Combustion*, 20(1), pp. 303-310.
- [93] Jackson, C. P., 1987, "A finite-element study of the onset of vortex shedding in flow past variously-shaped bodies," *Journal of Fluid Mechanics*, 182, pp. 23-45.
- [94] Nakagawa, T., 1989, "Vortex shedding mechanism from a triangular prism in a subsonic flow," *Fluid Dynamics Research*, 5(2), pp. 69-81.
- [95] Csiba, A. L., and Martinuzzi, R. J., 2008, "Investigation of bluff body asymmetry on the properties of vortex shedding," *Journal of Wind Engineering and Industrial Aerodynamics*, 96(6-7), pp. 1152-1163.
- [96] Prasad, A., and Williamson, C. H. K., 1997, "The instability of the shear layer separating from a bluff body," *Journal of Fluid Mechanics*, 333, pp. 375-402.
- [97] Sivasegaram, S., and Whitelaw, J. H., 1987, "Oscillations in confined disk-stabilized flames," *Combustion and Flame*, 68(2), pp. 121-129.
- [98] Hertzberg, J. R., Shepherd, I. G., and Talbot, L., 1991, "Vortex shedding behind rod stabilized flames," *Combustion and Flame*, 86(1-2), pp. 1-11.
- [99] Sivakumar, R., and Chakravarthy, S. R., 2008, "Experimental investigation of the acoustic field in a bluff-body combustor," *International Journal of Aeroacoustics*, 7(3-4), pp. 267-299.
- [100] Yu, K. H., Trouve, A., and Daily, J. W., 1991, "Low-frequency pressure oscillations in a model ramjet combustor," *Journal of Fluid Mechanics*, 232, pp. 47-72.
- [101] Rogers, D. E., and Marble, F. E., 1956, "A mechanism for high-frequency oscillation in ramjet combustors and afterburners," *Jet Propulsion*, 26(6), pp. 456-464.
- [102] Blackstock, D. T., 2000, *Fundamentals of physical acoustics*, Wiley, New York.
- [103] K lsheimer, C., and B chner, H., 2002, "Combustion dynamics of turbulent swirling flames," *Combustion and Flame*, 131(1-2), pp. 70-84.
- [104] de Jager, B., Kok, J. B. W., and Skevis, G., 2007, "The effects of water addition on pollutant formation from LPP gas turbine combustors," *Proceedings of the Combustion Institute*, 31(2), pp. 3123-3130.
- [105] Chakravarthy, S. R., Shreenivasan, O. J., Boehm, B., Dreizler, A., and Janicka, J., 2007, "Experimental characterization of onset of acoustic instability in a

- nonpremixed half-dump combustor," *Journal of the Acoustical Society of America*, 122(1), pp. 120-127.
- [106] Guthe, F., and Schuermans, B., 2007, "Phase-locking in post-processing for pulsating flames," *Meas. Sci. Tech.*, 18(9), pp. 3036-3042.
- [107] Shahi, M., Kok, J. B. W., Pozarlik, A. K., and Sponfeldner, T., 2013, "Thermal and fluid dynamic analysis of parpartially premixed turbulent combustion driven by thermo acoustic effects," ICSVBangkok.
- [108] Shahi, M., Kok, J. B. W., Roman Casado, J. C., and Sponfeldner, T., "Sensitivity of the numerical prediction of flow in the LIMOUSINE combustor on the chosen mesh and turbulent combustion model," *Proc. ASME Turbo Expo*.
- [109] Blevins, R. D., 1979, *Formulas for Natural Frequency and Mode Shape*, Krieger Publishing Company.
- [110] Kellert, S. H., 1993, *In the Wake of Chaos: Unpredictable Order in Dynamical Systems*, University of Chicago Press.
- [111] Gutmark, E., Parr, T. P., Hanson-Parr, D. M., and Schadow, K. C., 1991, "Use of chemiluminescence and neural networks in active combustion control," *Symposium (International) on Combustion*, 23(1), pp. 1101-1106.
- [112] Allen, M. G., Butler, C. T., Johnson, S. A., Lo, E. Y., and Russo, F., 1993, "An imaging neural network combustion control system for utility boiler applications," *Combustion and Flame*, 94(1-2), pp. 205-214.
- [113] Cammarata, L., Fichera, A., and Pagano, A., 2002, "Neural prediction of combustion instability," *Applied Energy*, 72(2), pp. 513-528.
- [114] Kadanoff, L. P., 1983, "Roads to chaos," *Phys. Today*, 36(12), pp. 46-53.
- [115] Abarbanel, H. D. I., 1996, *Analysis of observed chaotic data*, Springer, New York.
- [116] Kennel, M. B., Brown, R., and Abarbanel, H. D. I., 1992, "Determining embedding dimension for phase-space reconstruction using a geometrical construction," *Physical Review A*, 45(6), pp. 3403-3411.
- [117] Liebert, W., Pawelzik, K., and Schuster, H. G., 1991, "Optimal Embeddings of chaotic attractors from topological considerations," *Europhysics Letters*, 14(6), pp. 521-526.
- [118] Argyris, J., Faust, G., and Haase, M., 1991, "X-ALPHA-O-ZETA - An adventure in Chaos," *Comput. Meth. Appl. Mech. Eng.*, 91(1-3), pp. 997-1091.
- [119] Kabiraj, L., Sujith, R. I., and Wahi, P., 2012, "Bifurcations of Self-Excited Ducted Laminar Premixed Flames," *Journal of Engineering for Gas Turbines and Power-Transactions of the Asme*, 134(3).
- [120] Fichera, A., Losenno, C., and Pagano, A., 2001, "Experimental analysis of thermo-acoustic combustion instability," *Applied Energy*, 70(2), pp. 179-191.
- [121] Grassberger, P., and Procaccia, I., 1983, "Characterization of Strange Attractors," *Physical Review Letters*, 50(5), pp. 346-349.
- [122] Chatterjee, P., Vandsburger, U., Saunders, W. R., Khanna, V. K., and Baumann, W. T., 2005, "On the spectral characteristics of a self-excited Rijke tube combustor—

- numerical simulation and experimental measurements," *Journal of Sound and Vibration*, 283(3–5), pp. 573-588.
- [123] Tran, N., Ducruix, S., and Schuller, T., 2009, "Damping combustion instabilities with perforates at the premixer inlet of a swirled burner," *Proceedings of the Combustion Institute*, 32(2), pp. 2917-2924.
- [124] Bothien, M. R., Moeck, J. P., and Paschereit, C. O., 2008, "Active control of the acoustic boundary conditions of combustion test rigs," *Journal of Sound and Vibration*, 318(4-5), pp. 678-701.
- [125] Lacarelle, A., Luchtenburg, D. M., Bothien, M. R., Noack, B. R., and Paschereit, C. O., 2010, "Combination of Image Postprocessing Tools to Identify Coherent Structures of Premixed Flames," *Aiaa J.*, 48(8), pp. 1708-1720.
- [126] Moeck, J. P., Oevermann, M., Klein, R., Paschereit, C. O., and Schmidt, H., 2009, "A two-way coupling for modeling thermoacoustic instabilities in a flat flame Rijke tube," *Proceedings of the Combustion Institute*, 32(1), pp. 1199-1207.
- [127] Guethe, F., and Schuermans, B., 2007, "Phase-locking in post-processing for pulsating flames," *Measurement Science & Technology*, 18(9), pp. 3036-3042.
- [128] Crocco, L., Grey, J., and Harrje, D. T., 1960, "Theory of liquid propellant rocket combustion instability and its experimental verification" *Ars Journal*, 30(2), pp. 159-168.
- [129] Huls, R. A., 2006, "Acousto-elastic interaction in combustion chambers," *Enschede*.



# Appendix A **Semi-infinite hoses**

## **Introduction**

Pressure transducers are delicate sensors that can be damaged by the harsh conditions and high temperatures usually found in combustion experiments. Therefore, they need to be cooled to allow long life and precise measurements. One possible solution is the installation of water cooled jackets around the sensor. The jacket allows the transducer to be directly installed in the liner of the combustor, but they need a complex plumbing system.

One alternative solution to the tube cooled collars are the semi-infinite hoses. The transducer is not placed on the combustor wall, but in a side branch tube. The pressure transducer is far from the heat sources, where it can be easily cooled by an external air jet. There is no mean flow of hot gas through the hose, because the pipe is closed at the other end. Viscous effects and damping at the end pipe termination diminish the reflected amplitude pressure waves, effectively creating an anechoic end that does not radiate sound into the principal domain.

In the early stages of the research, the hoses used for the LIMOUSINE combustor were inherited from the DESIRE setup, also at the University of Twente Thermal Laboratory. These hoses were  $\frac{1}{2}$  inch in diameter and the length was between 6 and 10 m.

## **Proposed Design Changes**

However, due to their relatively large cross sectional area, these hoses dissipate a significant amount of acoustic energy from the main domain and thereby effectively change the acoustic behavior. For example, the measured reflection coefficient of the downstream end of the combustor using multi microphone technique gave poor results that did not agree with the expected theoretical response when the large diameter hoses were used.





**Figure A-1: Old (LHS) and new (RHS) semi-infinite hose holders.**

To reduce the acoustic losses and their impact in the main acoustic field, the size of the hoses is reduced to 4 mm internal diameter. The side branches pieces were modified for the new diameter and instead of the reinforced PVC pipe, semi-flexible polyurethane tubing is chosen. The pipe length is also increased to 33 meters.

To compare the old and new hoses, the absorption coefficient at the beginning of the hoses is calculated with the two microphone method. The results in figure A-2 show that the reflection coefficient is much higher and regular in the new design as compared to the old design for studied frequency the range.

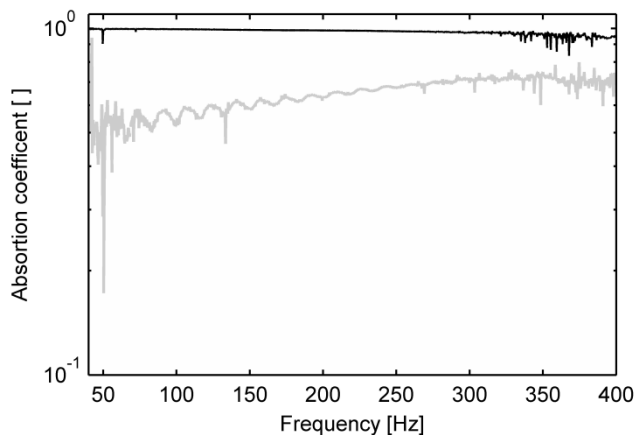


**Figure A-2: Absorption coefficient for the new semi-infinite hose configuration (black) and the old configuration (gray).**

The introduction of the hoses resulted in changes in the combustion stability behavior, increasing the range of the unstable flame. With the old hoses, the marginal unstable air factor was  $\lambda = 1.60$ . With the new hose design, it was possible to achieve limit cycle at even leaner conditions. The combustion regime changes for LIMOUSINE version 3 are in table A-1.

**Table A-1: LIMOUSINE version 3 single liner combustion regime as a function of the semi infinite hoses design: Unstable for new and old (light gray), stable for both designs(white), stable for the old design and unstable for the new design (dark gray).**

Air factor [ ]	Power [kW]			
	30	40	50	60
1.20				
1.40				
1.60				
1.80				



# Appendix B Impedance Tube

## Introduction

The impedance tube is a device that can measure the acoustic properties of a material or a geometrical configuration placed at one of its ends. In this research this device is used as a benchmark to check the performance of the two microphones and the multi-microphone method for 1D acoustic field characterization. The impedance tube is also very a valuable tool for the training on acoustic and data acquisition.

The setup is a thick wall tube that can be built from metal or plastic. Best results are obtained in thicker wall pipes. At one of its sides there is a speaker and the other is the sample under study. It has ports for the installation of at least 2 pressure transducers. The pipe has usually more than two installation ports, to allow the characterization of samples in wider frequency ranges. The data acquisition system records the signals from the transducers and generates the sound signal sent to the speaker.

The tube in the laboratory of Twente is made from PVC pipe, with an internal diameter of 125 mm and 3.5 mm wall thickness. There are pressure transducers ports at 100, 300, 400, 600, 800 and 900 mm from the sample end. Figure B-1 shows the results of an open ended tube and closed ended tube pointing to the adequate behavior of the multi microphone technique.

The LIMOUSINE combustor can be considered as an impedance tube when characterizing its acoustic boundary conditions.

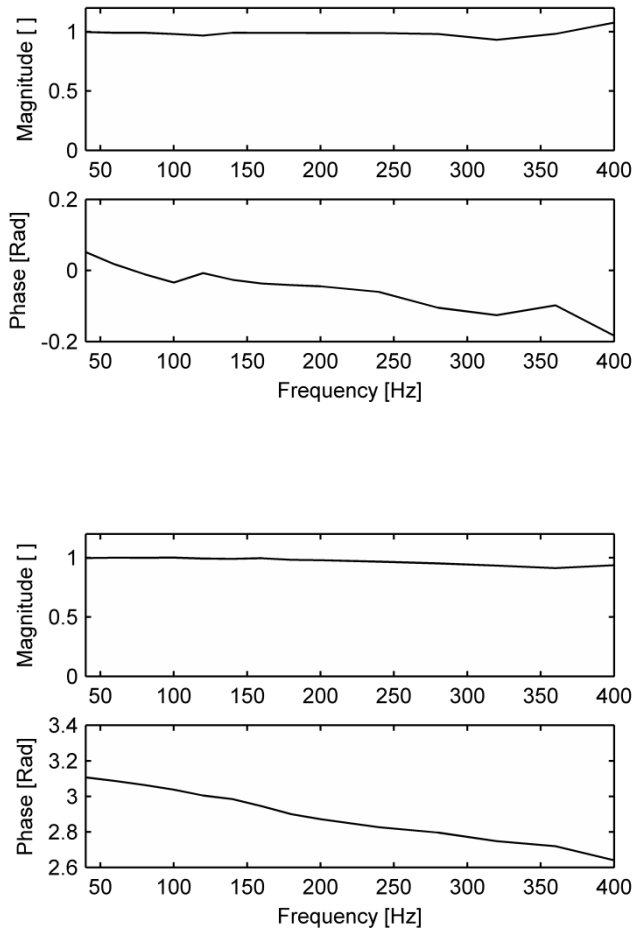


Figure B-1: Impedance tube results for a closed end (top) and open end (bottom).

# Appendix C **Green's Function Approach**

## **Introduction**

In addition to the analytical and experimental methods, there is yet another approach to calculate the acoustic eigenmodes: the Green's function of the pressure field. The Green function describes the temporal response  $t$  of a system, as seen by an observer in position  $x$  to an impulse excitation located in the point  $y$  at time  $\tau$ :  $G(x, y, t, \tau)$ . The governing equation is therefore:

$$\frac{1}{c^2} \frac{\partial^2 G}{\partial t^2} - \nabla^2 G = \delta(x - y) \delta(t - \tau) \quad (\text{C-1})$$

And any solution has to verify causality and reciprocity to be physical relevant.

$$G(x, y, t, \tau) = 0 \text{ for } t < \tau \quad (\text{C-2})$$

$$G(x, y, t, \tau) = G(y, x, t, \tau) \quad (\text{C-3})$$

The Green's function is used to solve the acoustic wave equation with a general source term,

$$\frac{\partial^2 p(\omega, x)'}{\partial x^2} + k^2 p(\omega, x)' = \delta(x - y) \delta(t - \tau) \quad (\text{C-4})$$

By integrating it over time and space. The Green's function can also be simplified to a 1 dimension function or transformed from the frequency domain to the time domain with some mathematical manipulation.

There is a scientific field in which the use of impulse excitation signals to unveil the system characteristics is very common: structural analysis. In the structural case, an instrumented hammer is used to deliver a short pulse of energy to the system, exciting all the frequencies simultaneously. Sensors such as accelerometers, velocity and displacement detectors or deformation gauges are

used to record the system response and calculate the eigenfrequencies and damping coefficients.

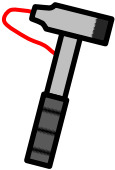
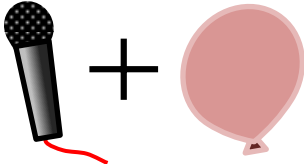
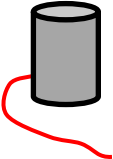
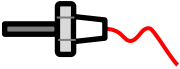




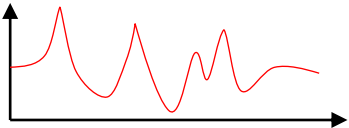
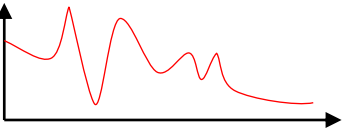
The idea presented here is to mimic the procedure of the structural analysis to calculate the acoustic eigenmodes of the combustor. All the signal conditioning and processing techniques developed for the structural system can be used in this approach, saving developing time. Moreover, most the equipment can also be directly adapted to this technique, making it possible to measure the modes in existing installations with available material.

## **Experimental Implementation**

The employed experimental procedure is a copy of to the structural method. The excitation source signal is provided by an exploding latex balloon instead of the instrumented hammer. The hammer uses a force cell to measure the delivered impact force, while an open field microphone located close to the combustor open end registers the pressure pulse. This signal also triggers the data acquisition system. The response of the combustor is recorded with pressure transducers, in the same way the accelerometer measures the vibration level. The measured signals are windowed using an exponential function to reduce the spectral leakage and noise levels. To improve the measurements accuracy, the final result is the average of several independent measurements.

A fast Fourier transform algorithm computes the spectrum of the signals, to calculate the auto spectrum and frequency response functions. The auto spectrum is the product of the signal spectrum by its complex conjugate, resulting in real valued function. The physical meaning of the autospectrum is the description of the energy content of each frequency component. The auto spectrum of the input signal (hammer force or pressure of the bust) should be flat and powerful to adequately excite all the frequencies in the range of interest. The Frequency Response Function, defined as the quotient of the structural response and the applied force, is linked to the eigenfrequencies and eigenmodes. Eigenfrequencies of the system will appear as peaks in the magnitude of the FRF spectrum. Moreover, the eigenmodes shape can be re-constructed with several FRF measurements at different positions. The parallelism is shown in table C-1, where the only differences are the employed sensors. Data acquisition cards and signal processing software are the same for both cases.

**Table C-1: Comparison between Green’s function of the structural and acoustic domains.**

Structural domain		Acoustic domain
 <p>Instrumented impact hammer</p>	<p>Stimulus signal and transducer</p>	 <p>Open field microphone and bursting balloon</p>
 <p>accelerometer</p>	<p>Response transducer</p>	 <p>Pressure transducer</p>
 <p>Signal conditioner, amplifier and data acquisition system</p>	<p>Signal Processing</p>	 <p>Signal conditioner, amplifier and data acquisition system</p>
 <p>Personal Computer</p>	<p>Data processing</p>	 <p>Personal Computer</p>
 <p>Structural FRF</p>	<p>Result</p>	 <p>Acoustic FRF</p>



## Results

The investigation of the Greens function was carried out in LIMOUSINE version 3 single liner burner and the results are plotted in figure C-1. The latex balloon was located on the outlet of the combustor and the response was measured with the pressure transducers PT 4 to PT 6, which are located on the combustion chamber side tubes. The magnitude of the Green function for each channel is shown for the 50 to 400 Hz range. The black line is the pressure transducer 4 (closest to the burner), pressure transducer 5 in the middle of the combustion chamber is the thin gray line and the thick gray line is the pressure transducer closest to the combustor exit (PT 6). The vertical axis is the magnitude of the sound expressed in decibels dB. The principal dynamics are located at 89, 253 and 357 Hz, which agree well with the measured acoustic modes with other methods. (See table 4-1).

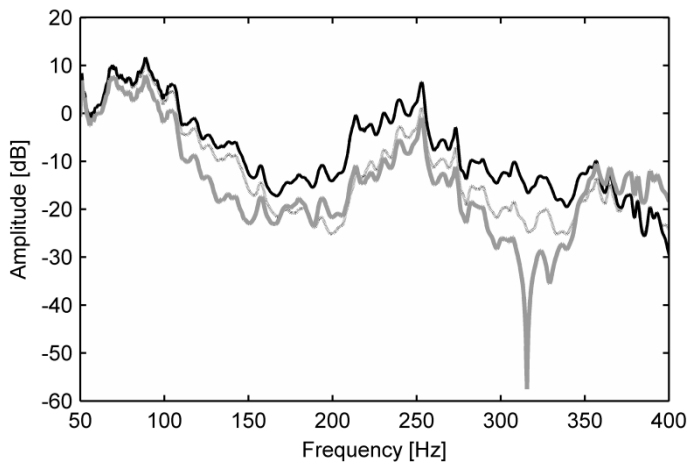


**Figure C-1: Response function for PT 1 (black), PT 3 (thin gray), PT 2 (thick gray).**

# Appendix D **FSI In A Thin Liner Combustor**

## **Introduction**

One of the phenomena studied within the framework of the LIMOUSINE project is the interaction between the fluid domain and the constructive elements. During stable combustion regime, the acoustic perturbations do not have large amplitudes, so the intensity of the interaction is small. However, during the occurrence of a Limit Cycle, the large amplitude of the pressure oscillations produces considerable stresses in the material, which reduce the lifetime of the elements.

The special geometry of the combustor provides a good platform for the study of the Fluid Structure Interaction or FSI. The flame dynamics are known and repeatable, which is important for the correlation of the results from different operative cases. Moreover the LIMOUSINE modular design allows for readily exchange of liners with different characteristics. The FSI reference case was the version 3 burner with the single liner. The liner is made from stainless steel 310 and has a thickness of 4 mm. More results related to this case particular are in chapter 4 and chapter 5.

## **Experimental Investigation**

The effect of the fluid structure interaction was tested for three different modifications of the reference case. The first modification is in the boundary conditions of the liner, with the addition of extra supports to the downstream flange of the combustion chamber. The second modification replaced the 4 mm thick liner by a 1 mm thick liner. The flame conditions of this study were 40 kW power and air factor  $\lambda = 1.20$ . The results are plotted in figure D-1. The two panes of this figure show the pressure and heat release rate spectra for the three cases. The results are identical for the three structural conditions, which mean that the acoustic field in the combustor and the flame dynamics are independent of the kind of installed liner.

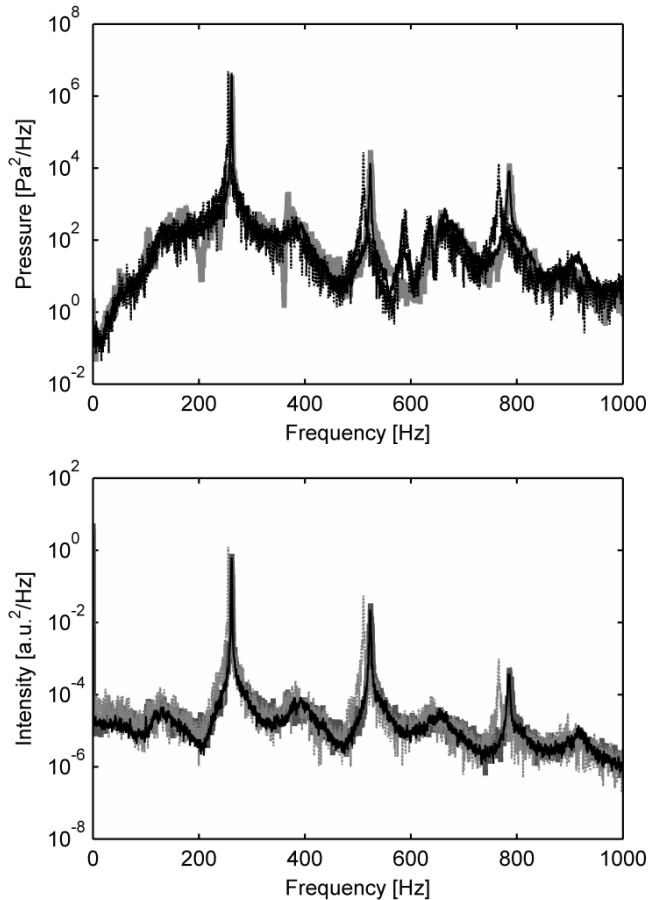


**Figure D-1: LIMOUSINE version 3 single liner pressure spectrum PT 4 (top) and heat release spectrum (bottom) for 40 kW and  $\lambda = 1.20$  for 4 mm free liner (black), 1 mm liner (thin gray) and 4 mm and clamp liner (thick gray).**

## Results

The wall vibration spectrum was measured on the vertical centerline of the liner and at the PT 4 pressure transducer height (figure D-2). The reference case with clamp-free conditions shows the structural modes previously explained in the body of the dissertation. If the thick liner is clamped at the top end, the main modes remain at the same frequency values, but with lower amplitude. The top flange of the liner already limits the motion of the side walls and the additional support only reinforces the effect. However, the 1 mm thick liner modes are different. The level of the structural vibrations in the thin liner is higher than the thick liner and so is the vibration at the flame instability. There are some dynamics

around 600 Hz, but then there are some new modes close to 700 Hz that are unique to this configuration. This agrees with the higher structural eigenfrequencies expected in a lighter liner with higher natural modes.

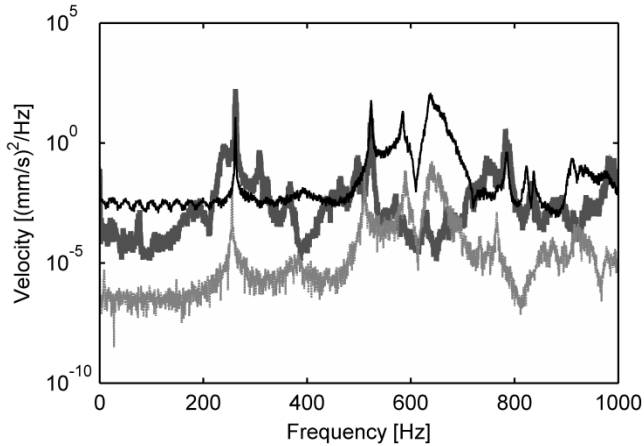


**Figure D-2: LIMOUSINE version 3 single liner LDV spectra for 40 kW and  $\lambda = 1.20$  for 4 mm free liner (black), 1 mm liner (thin gray) and 4 mm and clamp liner (thick gray).**



# Appendix E Measurement Accuracy

## Introduction

This appendix presents the measurements errors of the sensors and data acquisition card.

For the measurement of the pressure, the transducer has a maximum non linearity error of 0.1% of FSO, the amplifier has a maximum error of 0.003 % and the inaccuracy of the data acquisition card is 0.19% in the selected measuring range (-10 V to 10 V). Therefore, for pressure measurements of the order of 4000 Pascal, the error for a single sample 12%. However, the data acquisition system combines the results of several samples (20) to reduce this margin to values of the order of 2.6 %.

$$error\ noise = \frac{1}{\sqrt{number\ of\ samples}} \quad (E-1)$$

The error in the PSD, which is a squared value, is two times this value.

## Relative Calibration

To reduce the relative error between the pressure transducers, they are calibrated against each other. The produces is done in a special setup that consists of a hollow pipe with thick walls and large flanges at each end. One of its sides has a speaker and the other presents 4 drilled holes to install the pressure transducers. The speaker is used to produce a 1 dimensional acoustic field inside the pipe, which is recorded by the sensors. Because the sensitive elements of the transducers are co-planar, the pressure oscillations are identical in the four of them. The sketch of this setup is in figure E-1.

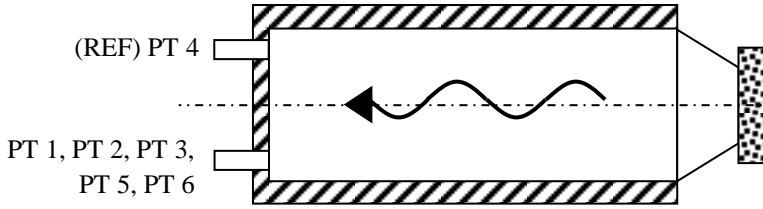


**Figure E-1: Skecht of the calibration device.**

This device is able to measure the phase delays between the pressure transducers and the differences magnitudes relative to a single reference sensor, which is PT 4. These results allow the correction of the measured pressure values.

Figure E-2 shows the results of sensors PT 1, PT 2, PT 3, PT 5 and PT 6 with respect to PT 4. Sensors 2 to 6 have the same output magnitude wise as the reference. Sensor PT 1 underperforms, measuring a magnitude around 78% of the reference value. Phase differences between the transducers are very small, of the order of 0.005 radians. Hence, a phase correction was not applied in the post processing.

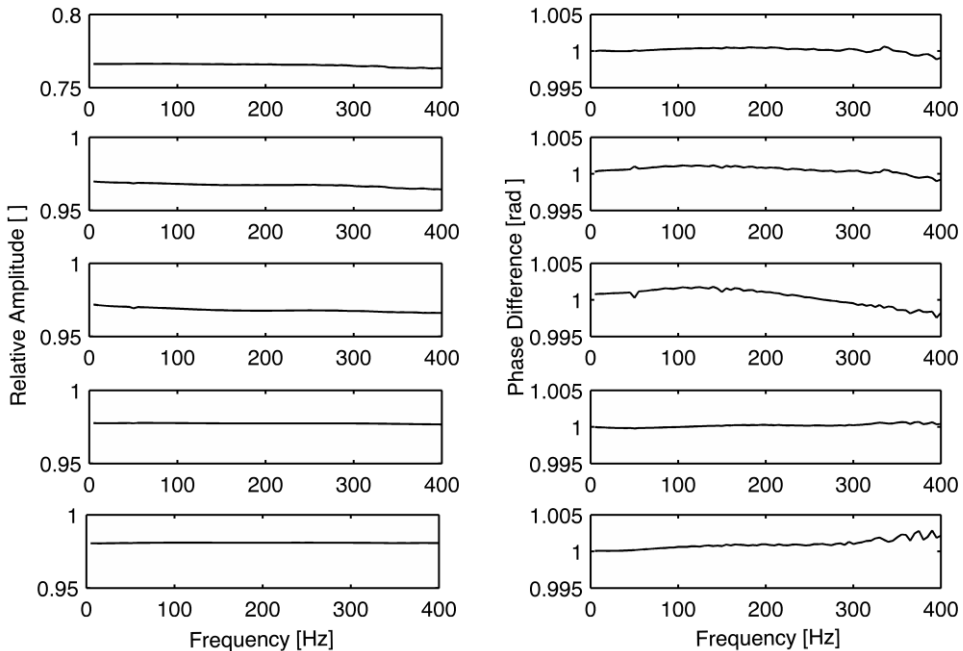


**Figure E-2: Left column is the relative magnitude of PT 1 (top), PT 2, PT 3, PT 5 and PT 6 (bottom) with respect PT 4. Right column is the phase difference of PT 1 (top), PT 2, PT 3, PT 5 and PT 6 (bottom) with PT 4.**

The accuracy of the internal clock of the data acquisition card is 50 ppm, which result in frequency errors of 0.0005 Hz.

The K type thermocouple used for the temperature measurements has error of 5 °C at 1000 °C. The gas analyzer has 5% tolerance for all the measured species and resolution of 0.1% in percentages or 1 ppm.

The Laser Doppler Vibrometer uses the Doppler shift of the laser beam to measure the structural vibration frequency. Because both vales are directly correlated, LDV sensors do not need calibration. The only source of error in this measurement is the data acquisition card. Meanwhile, the main target of the PMT measurements is the frequency of the flame oscillations and the relative comparison between two different cases. Therefore, this sensor was not calibrated.





**UNIVERSITY OF TWENTE.**

*ISBN 978-90-365-3554-0*